

**DESIGN AND SYNTHESIS OF QUINOXALINE
DERIVATIVES FOR MEDICINAL APPLICATION
AGAINST BREAST CANCER CELLS**

MASTER OF SCIENCE

in

CHEMISTRY

K Lekgau

2021

**DESIGN AND SYNTHESIS OF QUINOXALINE DERIVATIVES
FOR MEDICINAL APPLICATION AGAINST BREAST
CANCER CELLS**

BY

Lekgau Karabo

DISSERTATION

Submitted in fulfilment of the requirements for the degree of

MASTER OF SCIENCE

in

CHEMISTRY

in the

FACULTY OF SCIENCE AND AGRICULTURE

(School of Physical and Mineral Science)

At the

UNIVERSITY OF LIMPOPO

Supervisor: Prof W Nxumalo

Co-supervisors: Dr TC Leboho

: Dr NJ Gumede (Mangosuthu University of Technology)

2021

Declaration

I declare that the “Design and synthesis of quinoxaline derivatives for medicinal application against breast cancer cells” (dissertation / thesis) hereby submitted to the University of Limpopo, for the degree of master of science in chemistry (degree & field of research) has not previously been submitted by me for a degree at this or any other university; that it is my work in design and in execution, and that all material contained herein has been duly acknowledged.



.....

Lekgau K (Mr)

12 April 2021

.....

Date

Dedication

This thesis is dedicated to my Family,
my late mother Martha Lekgau,
my late grandmother Rebecca Lekgau,
my Aunt Edith Lekgau,
my sister Rebotile Lekgau and
my brothers Ntheteng and Tiego

Acknowledgements

The author wishes to express his sincere gratitude to:

- ❖ the supervisors, Prof W Nxumalo, Dr TC Leboho and Dr NJ Gumede for their dedicated support, guidance and constant encouragement. Their supervision and guidance throughout my research project were quite inspirational and excellent.
- ❖ the NMR technician, Ms TG Ramakadi for training and assistance in running and processing of the nuclear magnetic resonance spectra.
- ❖ his friend, Mr CT Selepe and colleagues, Miss LA Raphoko, Mr KB Dilebo, Mr TD Rikhotso, Miss MM Mashilo, Miss PB Maifo and, Mr NR Moroane for their great influence and support academically.
- ❖ the members of the Medicinal Chemistry Group at UL for all the encouragement and support.
- ❖ the former Head of Chemistry Department, Dr Mary S Thomas and the Head of Chemistry Department, Prof RM Mampa as well as the leadership under faculty of science and agriculture at University of Limpopo for providing the necessary equipments and facilities for my project.
- ❖ the Centre for High Performance Computing for allowing access to their resources for molecular modeling.
- ❖ Prof TM Matsebatlela and Ms MC Lebepe for the anticancer and cytotoxicity assay experimental data.
- ❖ University of Stellenbosch and University of Venda for high resolution mass spectrometry analysis.
- ❖ University of Cape Town H3D Centre for Drug Discovery for testing compounds against Mtb.
- ❖ National Research Foundation and Sasol Inzalo Foundation for financial support.

Scientific contributions

Conference attended: FSA, Frank Warren Conference and SACI.

Oral presentation at:

10th Faculty of Sciences and Agriculture, University of Limpopo Research day-

Date: 19-20 September 2019 (see appendix)

Frank Warren Conference 2019- Date: 7 – 11 July 2019 (see appendix)

Poster presentation at:

SACI Young chemists Symposium 2019- Date: 31st October 2019 (see appendix)

Submitted for publication:

Synthesis of novel quinoxaline-alkynyl derivatives and their anti-*Mycobacterium tuberculosis* activity (see appendix)

Table of Contents

Declaration	iii
Dedication	iv
Acknowledgements	v
Scientific contributions.....	vi
List of abbreviations	xii
Abstract	1
Chapter 1	3
Introduction	3
1. Cancer	4
1.1. Types of breast cancer	4
1.2. Causes of cancer	5
1.3. Therapy	5
1.3.1 Systemic treatments.....	6
1.3.2. Aromatase (CYP19A1).....	8
1.3.2 Cyclin-dependent kinases2 (CDK2)	11
1.4. Heterocyclic compounds	13
1.4.1. Nitrogen-containing heterocyclic compounds.....	14
1.4.1.1. Quinoxaline derivatives.....	15
1.4.1.2. Quinoxaline derivatives as anticancer agents against breast cancer	16
1.5. Molecular modeling	18
1.5.1. Molecular docking programs	18
1.5.2. Molecular docking	19
1.5.2.1. Schrodinger modules applied in the present study	20
1.5.2.1.1. Ligprep.....	20

1.5.2.1.2.	Protein Preparation Wizard.....	20
1.5.2.1.3.	Virtual screening workflow	20
1.5.2.1.4.	Induced Fit docking	21
1.5.2.1.5.	QikProp.....	21
1.6.	Aim.....	22
1.7.	Objectives.....	22
1.8.	References	23
Chapter 2	31
Results and discussion.....		31
2.1.	Molecular modelling.....	32
2.1.1.	Cross docking against aromatase (PDB code: 3EQM)	32
2.1.2.	Structure based virtual screening against aromatase (PDB code: 3EQM)	34
2.1.3.	Induced fit docking and binding mode analysis	36
2.1.4.	Cross docking against CDK2 (PDB code: 3QQJ).....	44
2.1.5.	Structure based virtual screening against CDK2 (PDB code: 3QQJ)	46
2.1.6.	Induced fit docking and binding mode analysis	47
2.1.7.	Physicochemical properties and ADME prediction.....	53
2.2.	Chemistry	55
2.3.	Biological evaluation.....	74
2.3.1.	Evaluation of synthesised compounds against breast cancer (MCF-7)	74
2.3.2.	Evaluation of synthesised compounds against <i>M tuberculosis</i>	76
2.4.	References	81
Chapter 3	83
3.1.	Conclusion.....	84
3.2.	Future work	85
Chapter 4	86

Methodology.....	86
4.1. Molecular modelling.....	87
4.2. Chemistry	87
General information.....	87
4.2.1. Preparation of quinoxalin-2-ol (48) ³	88
4.2.2. Preparation of 6-nitroquinoxalin-2-ol (49) ⁴	89
4.2.3. Preparation of 6-nitroquinoxalin-2-yl benzenesulfonate (50) ³	89
4.2.4. General procedure for the Sonogashira coupling reaction on 6-nitroquinoxalin-2-yl benzenesulfonate	90
4.2.4.1. Synthesis of 3-(6-nitroquinoxalin-2-yl) prop-2-yl-1-ol (45)	90
4.2.4.2. Synthesis of 1-(6-nitroquinoxalin-2-yl)hex-1-yn-3-ol (51)	91
4.2.4.3. Synthesis of 2-methyl-4-(6-nitroquinoxalin-2-yl)but-3-yn-2-ol (52)	91
4.2.4.4. Synthesis of 2-methyl-4-(6-nitroquinoxalin-2-yl)but-3-yn-2-amine (53)	92
4.2.4.5. Synthesis of 2-(2-cyclopropylethynyl)-6-nitroquinoxaline (54).....	92
4.2.4.6. Synthesis of 2-(hex-1-ynyl)-6-nitroquinoxaline (55).....	93
4.2.4.7. Synthesis of 6-nitro-2-(oct-1-ynyl) quinoxaline (56)	94
4.2.5. General esterification reaction at alcohol group	94
4.2.5.1. Synthesis of 3-(6-nitroquinoxalin-2-yl)prop-2-ynyl acetate (57).....	94
4.2.5.2. Synthesis of 1-(6-nitroquinoxalin-2-yl)hex-1-yn-3-yl acetate (58).....	95
4.2.5.3. Synthesis of 3-(6-nitroquinoxalin-2-yl)prop-2-ynyl benzoate (59).....	96
4.2.5.4. Synthesis of 1-(6-nitroquinoxalin-2-yl)hex-1-yn-3-yl benzoate (60).....	96
4.2.5.5. Synthesis of 3-(6-nitroquinoxalin-2-yl)prop-2-ynyl thiophene-2-carboxylate (61)	97
4.2.5.6. Synthesis of 1-(6-nitroquinoxalin-2-yl)hex-1-yn-3-yl thiophene-2-carboxylate (62)	98
4.2.5.7. Synthesis of 3-(6-nitroquinoxalin-2-yl)prop-2-ynyl methane sulfonate (63)	98

4.2.6.	Oxidation reaction	99
4.2.6.1.	Synthesis of 1-(6-nitroquinoxalin-2-yl)hex-1-yn-3-one (64)	99
4.2.7.	General reduction reaction at nitro group	100
4.2.7.1.	Synthesis of 3-(6-aminoquinoxalin-2-yl)prop-2-ynyl thiophene-2-carboxylate (31)	100
4.2.7.2.	Synthesis of 1-(6-aminoquinoxalin-2-yl)hex-1-yn-3-yl thiophene-2-carboxylate (32)	101
4.2.7.3.	Synthesis of 2-(oct-1-ynyl)quinoxalin-6-amine (33).....	101
4.2.7.4.	Synthesis of 3-(6-aminoquinoxalin-2-yl)prop-2-ynyl benzoate (34)	102
4.2.7.5.	Synthesis of 2-(3-amino-3-methylbut-1-ynyl)quinoxalin-6-amine (35)	10
2		
4.2.7.6.	Synthesis of 2-(2-cyclopropylethynyl)quinoxalin-6-amine (37).....	103
4.2.7.7.	Synthesis of 2-(hex-1-ynyl)quinoxalin-6-amine (38).....	104
4.2.7.8.	Synthesis of 1-(6-aminoquinoxalin-2-yl)hex-1-yn-3-yl benzoate (40)	104
4.2.7.9.	Synthesis of 3-(6-aminoquinoxalin-2-yl)prop-2-ynyl acetate (41).....	105
4.2.7.10.	Synthesis of 1-(6-aminoquinoxalin-2-yl)hex-1-yn-3-yl acetate (43)	105
4.2.7.11.	Synthesis of 1-(6-aminoquinoxalin-2-yl)hexan-3-one (65)	106
4.2.8.	General hydrolysis reaction of ester	106
4.2.8.1.	Synthesis of 1-(6-aminoquinoxalin-2-yl)hex-1-yn-3-ol (36)	107
3.2.8.1.	Synthesis of 3-(6-aminoquinoxalin-2-yl)prop-2-yn-1-ol (39)	107
4.3.	Biological evaluation.....	108
4.3.1.	MTT Assay	108
4.3.2.	Broth micro-dilution method	108
4.4.	References	110
Chapter 5	112

APPENDIX	112
The spectral analysis of all compounds identified from molecular docking.	113
Scientific contributions.....	139
10th Faculty of Sciences and Agriculture, University of Limpopo Research day	139
Frank Warren Conference 2019.....	140
SACI Young chemists Symposium 2019.....	141
Publication: Synthesis of novel quinoxaline-alkynyl derivatives and their anti- Mycobacterium tuberculosis activity.	142

List of abbreviations

A

ADME Absorption, distribution, metabolism, excretion

Ala Alanine

CYP19A1 Aromatase

Arg Arginine

Asn Asparagine

Asp Aspartic acid

B

MCF-7 Breast cancer cell lines

brs Broad singlet

C

CADD Computer Aided Drug Design

CuI Copper Iodide

δ Chemical shift

CDCl₃ Deuterated Chloroform

CHCl₃ Chloroform

3EQM Crystal structure of human placental aromatase cytochrome P450 in complex with androstenedione

CDKs Cyclin-dependent kinases

3QQJ Crystal structure of CDK2 in complex with inhibitor

D

°C Degree Celsius

DNA Deoxyribonucleic acid

DCM Dichloromethane

DMAP	4-Dimethylamino pyridine
DMF	N,N-Dimethylformamide
DMSO-d ₆	Deuterated Dimethyl sulfoxide
DMSO	Dimethyl sulfoxide
MTT	3-(4, 5-dimethylthiazol-2-yl)-2, 5-diphenyltetrazolium bromide
d	Doublet
dd	Doublet of doublets
H3D	Drug Discovery and Development Centre
E	
EtOAc	Ethyl acetate
EtOH	Ethanol
Et ₃ N	Triethylamine
Eq.	Equivalence
F	
FDA	Food and drug administration
FGI	Functional group interconversion
FTIR	Fourier-transformation infrared spectroscopy
G	
GLIDE	Grid based Ligand Docking with Energetics
Gln	Glutamine
Glu	Glutamic acid
Gly	Glycine
H	
Hem	Haemoglobin

HIV	Human immunodeficiency virus
HRMS	High resolution mass spectroscopy
Hz	Hertz
HTVS	High-Throughput Virtual Screening
H ₂ O	Water
H ₃₇ Rv	Mycobacterium tuberculosis strain

I

IC ₅₀	Half Maximal Inhibitory Concentration
IDC	Invasive ductal carcinomas
ILC	Invasive lobular carcinoma
IFD	Induced Fit Docking
Ile	Isoleucine

J

<i>J</i>	Coupling constant
----------	-------------------

K

KOH	Potassium hydroxide
-----	---------------------

L

Leu	Leucine
LigPrep	Ligand Preparation
Lys	Lysine

M

MeOD	Deuterated methanol
MeOH	Methanol
Met	Methionine
Mtb	Mycobacterium tuberculosis

MIC Minimum inhibitory concentration

MHz Megahertz

min Minutes

Mp. Melting point

m Multiplet

MS Mass spectrometry

N

NaHCO₃ sodium hydrogen carbonate

Na₂SO₄ Sodium sulfate

N₂ Nitrogen molecule (g)

NMR Nuclear magnetic resonance

O

OPLS Optimized Potentials for Liquid Simulations

P

PdCl₂(PPh₃)₂ Bis(triphenylphosphine)palladium(II) dichloride

PDB Protein Database Bank

pH Power of hydrogen

Phe Phenylalanine

ppm part per million

% Percentage

R

rmsd Root-mean-square deviation

S

SERMs Selective Estrogen Receptor Modulators

SnCl₂ Tin(II) chloride

T

TB Tuberculosis

THF Tetrahydrofuran

TLC Thin Layer Chromatography

t Triplet

Thr Threonine

Trp Tryptophan

V

Val Valine

VSW Virtual Screening Workflow

W

WHO World Health Organization

Abstract

Breast cancer is a malignant tumour that starts in the cells of the breast. Many studies revealed aromatase (CYP19A1) and cyclin-dependent kinase 2 (CDK2) as possible therapeutic targets regarding breast cancer treatment, because they play crucial roles in anti-apoptotic processes during cell proliferation. Quinoxaline derivatives have attracted a great deal of attention due to their biological activities against fungi, virus, bacteria and cancer. Computer modelling was employed in order to reduce time and cost by searching the library of molecules and identifying those which are likely to bind to the drug target.

A library of new one hundred (100) nitro and amino quinoxaline alkyne derivatives were successfully designed and screened against target proteins (CYP19A1 and CDK2) using virtual screening technique and thirteen (13) molecules were identified to be hit compounds against both targets with the docking score ranging from -6.143 to -8.372 kcal/mol as a measure of binding affinity. The hit compounds were subjected to IFD in order to identify tight binding through intermolecular interactions with active site residues of the binding pocket of the target proteins.

All identified nitro and amino quinoxaline alkyne derivatives were successfully synthesised in a multi-step reaction sequence and their spectroscopic analysis (NMR, FTIR and MS) were in good agreement with the proposed structures in a good to moderate yield. The newly synthesised novel amino and nitro-quinoxaline derivatives were evaluated for anti-proliferative activity against breast cancer (MCF-7). Compound **59** showed to possess good inhibition against MCF-7 with an IC_{50} of 9.102 μ M, whereas compounds **34**, **54**, **56** and **61** showed promising activity against MCF-7 with an IC_{50} value of < 50 μ M. However, the MTT assay results showed that **59** was found to be toxic with an IC_{50} value of 0.205 μ M against Raw 264.7 cell line. The dose response investigations showed that **31** and **34** have the promising anti-cancer activity against CYP19A and the correlation between molecular modelling (*in-silico*) and CYP19A inhibition activities (*in-*

vitro), was established as compounds **31** and **34** were identified to bind to the drug target (CYP19A) with the docking score of -8.372 and 7.630 kcal/mol respectively.

All the synthesized compounds were evaluated for the antitubercular activity against Mtb H37Rv strain as a secondary study. Compounds **57-62** with nitro-quinoxaline derivatives exhibited stronger inhibitory effects on Mtb H37Rv strain. In addition, compounds **60** and **62** were found to be most active against Mtb H37Rv with the high activity at MIC₉₀ of <0.65 and <0.64 μ M respectively. All active compounds are currently investigated for their cytotoxicity which have not been investigated before.

Chapter 1

Introduction

1. Cancer

Cancer is a deadly disease caused by asymmetrically unregulated cell growth resulting in a tumour.¹ Cancer cells have lost the ability to follow the normal control that the body exerts on all cells during the cell cycle. Cancer can occur everywhere in the body because there are cells everywhere in the body.² Cancer cells have been reported to be more metabolically active than normal cells and this results in cancer cells replicating faster than normal cells. If left untreated, tumour can grow and invade or spread into the surrounding normal tissues or over a large area in the body i.e malignant tumour.³

According to World Health Organisation (WHO), cancer is a major cause of morbidity (26 %) and mortality (13 %).⁴ Most of the cancers are labelled based on the organ where they originated from, namely: breast cancer, cervical cancer, prostate cancer, liver cancer, lung cancer, brain cancer, and many others refer to where the abnormal cells started to develop.² However, the present study will focus on breast cancer which is the most common malignancy and the leading cancer in women, with 30 % estimated new cases of all cancer types and 14 % estimated deaths annually.⁴

1.1. Types of breast cancer

Breast cancer is more likely to occur either in the ducts and lobules of the breast. Ductal breast cancer refers to cancer that starts at the cells of ducts, and lobular breast cancer starts at the wall of the lobules.⁵ It is also classified as non-invasive (does not spread) and invasive (spread). Invasive breast cancer is much more common, and it can spread to the lymph nodes and even other parts of the body. About 80% of all breast cancers are invasive ductal carcinomas (IDC). Invasive lobular carcinoma (ILC) is the second most common type of breast cancer (approximately 10%) after invasive ductal carcinoma.⁶

1.2. Causes of cancer

A small mutation can interfere with genes, causing the loss of control during cell division. A genetic mutation is the main cause of uncontrolled cell growth which leads to the carcinoma condition.² Common factors that causes cancer includes life-style choices such as use of tobacco, alcohol abuse, lack of physical exercise, ultraviolet radiation from the sun and unhealthy diet.⁷ Not only acquired or somatic mutation leads to cancer, but an individual can also inherit damaged genes from parents. The standard procedure is to develop drugs that aim on the specific therapeutic targets in order to kill or inhibit cancer cells. Once mutations begin to change the cells, treatment requires new therapy.²

1.3. Therapy

There are various primary therapies for cancer treatment, namely: surgery, radiation, systematic treatments (chemotherapy and hormonal therapy) and combination therapy.⁸ Surgery works by directly removing the tumour. Radiation therapy provides high energy X-ray to kill tumour cells. Systemic treatments provide medicines that can kill those individual cells or inhibit their cell division. Modern breast cancer treatment uses a combination or sequence of different treatments (surgery, radiation, and systemic treatments) according to each patient's requirements and preferences. The complexity of the disease at every stage and each individual's different genes, makes the process difficult to point one universal treatment.⁹

There are two main types of surgery treatment to remove breast cancer: lumpectomy, where only a portion of the breast comprising the cancer is removed, and mastectomy where the entire breast is removed, including all of the breast tissues and sometimes other adjacent tissues. The treatment depends on the location of cancer cells and there are risk factors which include the development of tenacious pain¹⁰ and slightly elevated probabilities of recurrences over a relatively long time.⁹ Radiation therapy has an advantage of accessing localised cancer cells in a very confined space, however the radiation may also damage the healthy cells and that may cause severe heart diseases.¹¹

1.3.1 Systemic treatments

Systemic treatments are the most preferred methods, because drugs can travel through the bloodstream and reach cancer cells anywhere in the body.⁹ Breast cancer cells need hormones in order to grow. Hormone therapy works by blocking cancer cells from receiving natural hormones that they need to survive.¹² Many studies revealed several possible therapeutic targets such as aromatase (CYP19A1) and cyclin-dependent kinases2 (CDK2) regarding breast cancer treatment because they play crucial roles in anti-apoptotic processes during cell proliferation.^{13,3}

Nakata and co-workers¹⁴ reported that most of postmenopausal women have higher chances of developing breast cancer. In postmenopausal women, estrogen hormones are produced in non-ovarian tissue such as breast tissue or are synthesized incidentally by aromatase. Breast cancer in postmenopausal women is due to local formation of estrogen which fuel their own growth. The estrogen blockage is clinically important in treatment of hormone-dependent breast cancer.¹⁵ The study demonstrated two significant ways of interfering with endogenous hormone production in an attempt to treat hormone-dependent breast cancer. One is to use anti-estrogen which act by binding on the estrogen-receptor and another way is to use anti-enzyme (anti-aromatase) to prevent breast cancer from making more estrogen to sustain its survival.¹⁴

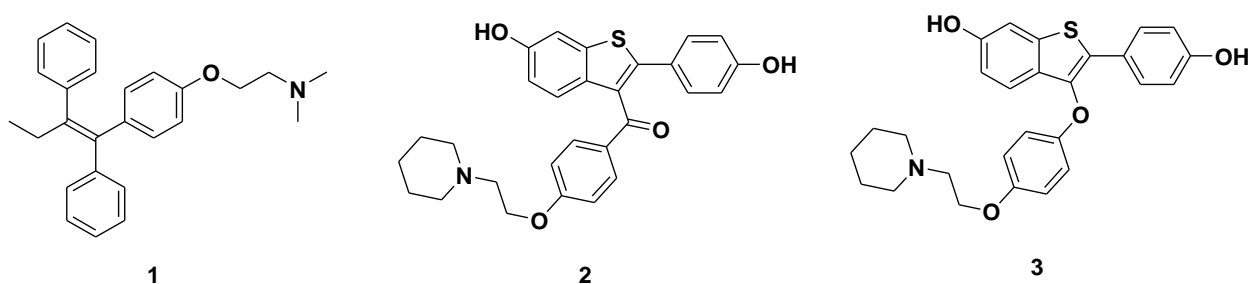


Figure 1.1: Clinically used anti-estrogen drugs.

Non-steroidal estrogen receptor inhibitors such as tamoxifen **1**, raloxifene **2** or arzoxifene **3** are used to block the actions of estrogen during treatment of hormone dependent breast cancer as depicted in **figure 1.1**.¹⁶

Tamoxifen **1** was initially synthesised in 1962 by Dora Richardson and was originally designed as a contraceptive drug. Later, tamoxifen was developed as anti-estrogen for the treatment of breast cancer because of its ability to suppress ovulation in women. When the clinical trials revealed that the drug could also be useful in preventing re-occurrence of breast cancer or occurrence in women at high risk of breast cancer, the drug became the best-selling anti-estrogen medicine in the 1980s.¹⁷ However, it was later realised that it caused uterine cancer in some women and it may also increase the possibilities of blood clots and stroke.¹⁶

A benzothiophene derivative, raloxifene **2** was approved for remedial use in the United States in 1997 as a selective estrogen receptor modulator used for the treatment of breast cancer. Furthermore, **2** was used to reduce the occurrence of invasive breast cancer in postmenopausal women, who are at high risk for developing the disease.¹⁸ However, raloxifene **2** may cause serious blood clots leading to the increased risk for deep vein thrombosis, pulmonary embolism and stroke.¹⁹

Arzoxifene **3** is another benzothiophene derivative which is structurally similar to raloxifene **2**, except that it has an ether functional group at 3 position of benzothiophene instead of ketone functional group on raloxifene **2**.²⁰ Arzoxifene **3** is also a selective estrogen receptor modulator which possesses superior anti-tumour activity to both raloxifene **2** and tamoxifen **1** in an *in-vitro* studies against MCF-7 human breast cancer cells.¹⁹ Compound **3** never completed all of the clinical trial phases. The clinical results of phase III trial showed that arzoxifene **3** possessed side effects such as deep vein thrombosis, pulmonary embolism similar to raloxifene **2**, thus **3** was relegated from further investigations.²⁰

1.3.2. Aromatase (CYP19A1)

Selective estrogen receptor modulators (SERMs) may act as incomplete agonists or exercise some estrogenic action in other tissues, leading to an increased risk of endometrial cancer or stroke. Aromatase inhibitor was used as an alternative for treatment of hormone dependent breast cancer, which lack estrogenic effects and cause fewer side effects.¹⁵ As a matter of fact, down-regulation of estrogen biosynthesis by aromatase inhibition signifies an effective approach for the treatment of hormone-sensitive breast cancer. This approach has already yielded several molecules with significant clinical activity.⁸

Several aromatase inhibitors possessing either steroidal or nonsteroidal scaffolds have been developed as competitive or mechanism-based inhibitors. Steroidal aromatase inhibitors have a similar appearance with androstenedione **4** (**figure 1.2**), a molecular structures of the natural substrate of aromatase which is a common precursor of estrogen.²¹ CYP19A1 enzyme is a metal-containing enzyme, which has an iron atom at the heme moiety in its active site i.e. Ferric heme porphyrin which is important for metal coordination and other intermolecular interactions with inhibitors.⁸ The aromatase inhibitors compete with natural substrate inside an active site of an enzyme and form interaction through intermolecular forces and metal coordination.²¹

Aromatase (CYP19A1) is an enzyme that catalyses the metabolism of androgens (androstenedione **4** and testosterone) into estrogens such as estrone and estradiol.⁸ Aromatase catalyses the final and limiting step in estrogen biosynthesis. Its inhibition will only affect estrogen biosynthesis without affecting the production of the other significant steroids needed by the body.²² Estrogen is a hormone responsible for development and regulation of female reproductive system. Estrogen plays a key role in the development of hormone-dependent breast cancer.²³ Recent studies reported high expression of aromatase in or near breast tumour spots, therefore, aromatase is marked as a suitable therapeutic target in hormone therapy for breast cancer.¹³

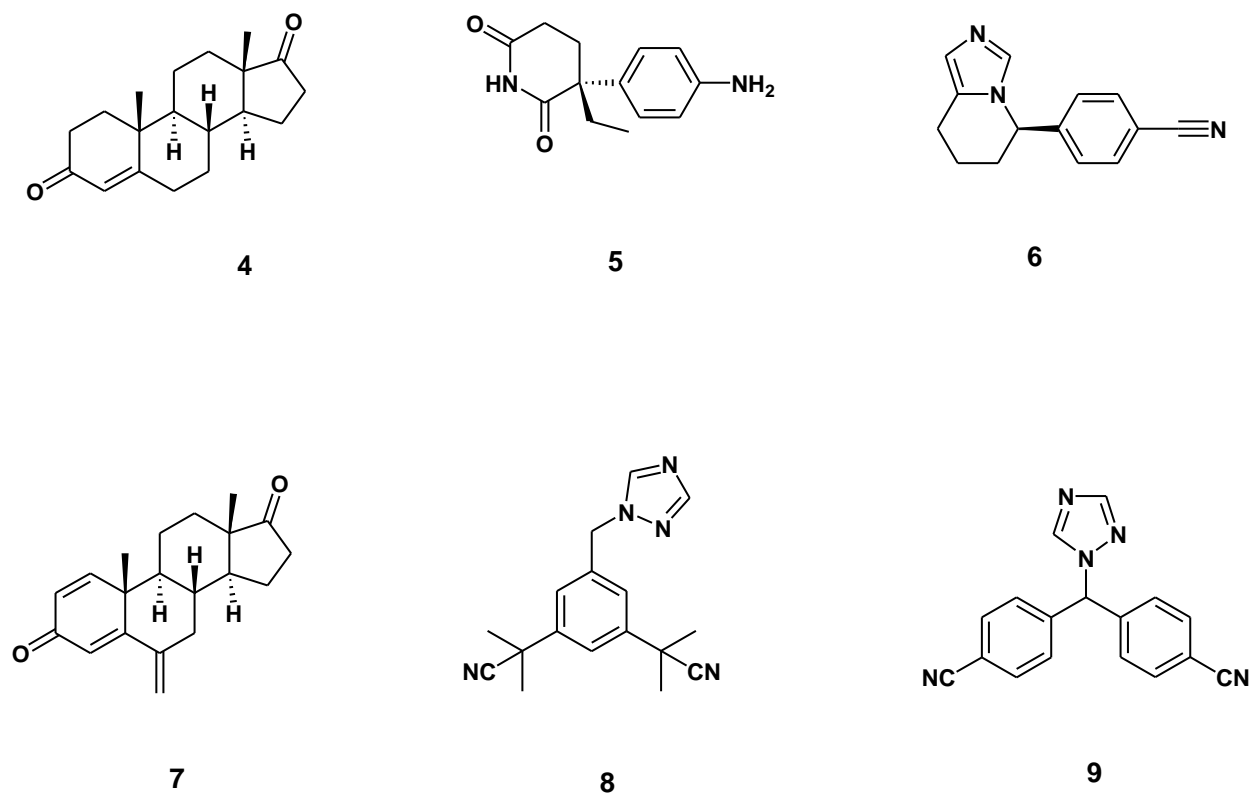


Figure 1.2: Molecular structures of the aromatase natural substrate, androstenedione **4** and commonly used aromatase inhibitors for the treatment of breast cancer.

The medical use of aminoglutethimide **5** was discovered in 1960 as an anticonvulsant drug. Aminoglutethimide is one of the derivatives of hypnotic sedative agent, glutethimide. Aminoglutethimide **5** was the first nonsteroidal aromatase inhibitor to be approved in 1969 by the Food and Drug Administration (FDA) and has been used in the treatment of breast cancer in postmenopausal women. However, its use was terminated due to its toxicity which caused severe side effects such as hypertension, liver damage and adrenal insufficiency, among others.²⁴

Fadrozole **6** is a second-generation nonsteroidal aromatase inhibitor to reach the clinical stage. It has higher specificity for aromatase than aminoglutethimide **5** and it has been used in many countries for the treatment of both early stage and advanced hormone-

depended breast cancer in postmenopausal women as one of the standard chemotherapies. However, fadrozole **6** possess some severe side effects such as vomiting of blood, hot flashes and somnolence, and that prompted the development of the next generation of aromatase inhibitors.²⁵

The third generation of aromatase inhibitors used clinically includes the steroid, exemestane **7** and the non-steroidal triazole derivatives, anastrozole **8** and letrozole **9** which are very potent, specific and selective aromatase inhibitors that allow almost complete estrogen suppression. They have been approved for the treatment of estrogen-dependent breast cancer in postmenopausal women.^{26,27}

Exemestane **7** works by lowering the estrogen level in postmenopausal women, which may slow down the growth of estrogen-dependent breast tumour that require estrogen to grow. It binds irreversibly to aromatase, inactivating it through suicide aromatase inhibition. Exemestane **7** reduces the amount of estrogen in the body which can result in osteoporosis, which is one of the side effects, together with vaginal bleeding and fatigue.²¹

Anastrozole **8** was approved for medical use in 1995 and it has been used in the treatment and prevention of breast cancer in postmenopausal women. However, the severe side effects which include an increased risk of heart disease and osteoporosis limited further clinical application of anastrozole **8**.²⁶ Letrozole **9** was approved for medical use in 1996 and it has been used as an aromatase inhibitor for the treatment of either local or metastatic breast cancer in postmenopausal women. However, the most common side effects associated with letrozole **9** are sweating, hot flashes, arthralgia (joint pain), and fatigue. Therefore, the development of resistance to the above-mentioned aromatase inhibitors and their related side effects prompted the need to develop novel and improved alternative aromatase inhibitors.²⁷ Furthermore, the occurrence of significant side effects accompanying the prolonged clinical use of current available aromatase inhibitors

demands for the exploration of new, potent, more selective, and less toxic aromatase inhibitors.²⁸

1.3.2 Cyclin-dependent kinases2 (CDK2)

Cells grow and divide as part of the normal cell cycle. The cell cycle is regulated by small signalling molecules that control cell division and growth at a molecular level. There are checkpoints during the cell cycle where the cell must receive a specific signal to proceed through G1 (pre-synthetic growth, or gap 1), S (DNA synthesis), G2 (pre-mitotic growth, or gap 2), and M (mitotic) phases in a normal physiological cell division.²⁹ The cell cycle progression is regulated by specific proteins called CDKs. CDK4/6 and CDK2 regulate the restriction point at the boundary of the G1/S phase. CDK2, a crucial target that may offer a therapeutic advantage based on potential CDK4/6 inhibitor resistance, has been a hot subject for research in drug discovery.³⁰

CDK2 plays a key role in the progression of the cell cycle, where it is supremely active during the G1 phase and G1/S transition.³¹ If the cell failed its checkpoint, it undergoes apoptosis but if the genetic mutation occur which lead to loss or the relative down regulation of apoptotic pathway, the cell divide in an uncontrollable manner and results in the formation of cancer. Loss of cell cycle control as the results of dysregulation is one of the hallmarks of cancer as highlighted by Hanahan and Weinberg in a classical review of the Hallmarks of cancer.³² Proliferation of breast cancer cells through the deregulation of cell cycle control such as CDK2 (which is one of the important therapeutic targets in cancer treatment) has prompted the development of CDK2 inhibitors as one of the cancer therapeutic targets.³³ The competitive CDK2 inhibitors in breast cancer works by blocking the cyclin E-CDK2 complex, thereby preventing the phosphorylation of retinoblastoma (RB) protein to stop the cell cycle from progressing to S phase in order to prevent proliferation of cancer.²⁹

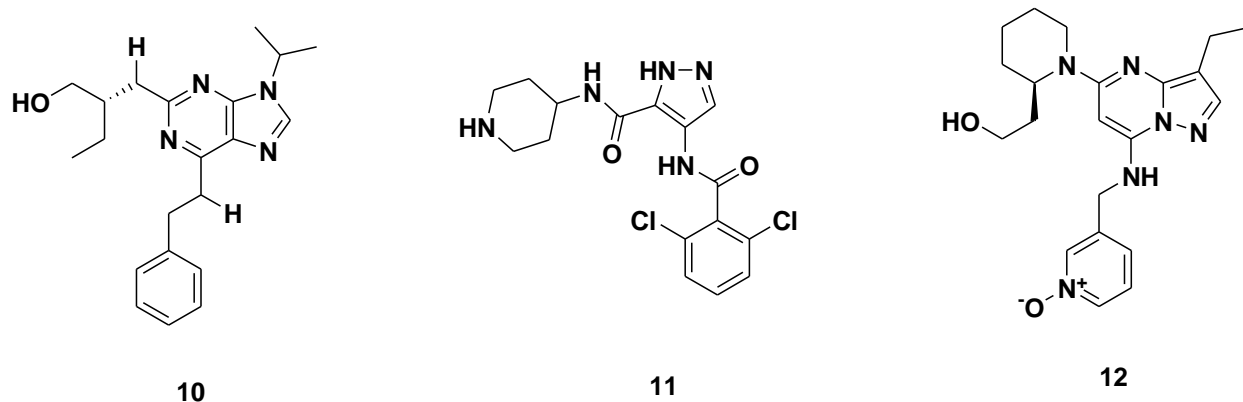


Figure 1.3: Common cyclin-dependent kinase2 (CDK2) inhibitors that are currently in clinical trials as an anticancer agent.

Figure 1.3 shows drugs that are currently in clinical investigation for the treatment of breast cancer as CDK2 inhibitors. Seliciclib **10** is a novel trisubstituted purine derivative which exerted some anti-tumour activity. The compound inhibited multiple enzyme targets such as CDK2, CDK7 and CDK9 enzymes that are essential in the process of cell division and cell cycle control. CDK7 and CDK9 enzymes are responsible for the regulation of transcription. The drugs distract the transcription and expression of the genes that are very important for maintaining cells in oncogenic state.²⁹ The phase I clinical trials results of seliciclib **10** demonstrated its potential to inhibit CDK2 in cancer cells through the down regulation of the enzyme. Tourneau *et al*,³⁴ reported that based on pharmacokinetic data and dose–intensity analyses, seliciclib **10** was taken forward to phase II trials.³⁴ The side-effects reported in Phase I trials associated with seliciclib **10** included asthenia, anorexia, nausea, vomiting, liver function abnormalities, hypokalaemia and serum creatinine increase.^{29,34} Because of the absence of significant antitumor responses and the level of toxicity, seliciclib **10** did not gain FDA approval.²⁹

AT7519 **11** is a small-molecule inhibitor of numerous cyclin-dependent kinases (CDK1, CDK2, CDK4, CDK5, CDK6 and CDK9) showed a strong anti-proliferative activity against a wide range of human cancer cell lines, including breast cancer. AT7519 **11** is currently

in early stage clinical development as an anti-cancer agent and it showed encouraging anti-cancer activity by inducing tumour cell apoptosis at very low concentration.³⁵ Dose-limiting toxicities included fatigue and electrocardiographic prolongation, nausea, vomiting, anorexia, constipation, peripheral edema, pyrexia, and hypotension occurred in approximately half of the patients. Roskoski³⁶ stated in the review that “it is unlikely that AT7519 will gain FDA approval unless better clinical outcomes are observed”.³⁶

Pyrazolopyrimidine derivative, dinaciclib **12** is a novel, potent, small-molecule inhibitor of numerous cyclin-dependent kinases (CDKs) including CDK2 in breast cancer cell lines. Based on many studies, dinaciclib **12** has proven to be a potent inducer of apoptosis in tumour cell lines.^{37,38} In addition, Mita and co-workers³⁹ reported that the results from phase II clinical trials showed dinaciclib **12** had good antitumor activity in breast cancer patients.³⁹ The most common side effects associated with dinaciclib **12** are leukopenia, thrombocytopenia, gastrointestinal symptoms, alopecia, and fatigue.³⁸ Based on the results of numerous clinical trials, dinaciclib **12** appears to be safe and generally tolerated as monotherapy in patients with advanced breast cancer and is currently under clinical evaluation in combination studies with other anticancer agents.³⁹

Even though both clinical and advanced research for breast cancer has been improved, the overall survival of patients has, however, not been significantly improved regarding late diagnosis, resistance and early metastasis. The development of more effective, selective, and less toxic anticancer agents remains a major challenge.³

1.4. Heterocyclic compounds

There is a need for development of new drugs for breast cancer treatment that are more effective with minimum side effects. Chemistry of heterocyclic compounds is one of the most complex and growing branches in medicinal chemistry for drug discovery. Heterocyclic chemistry deals with heterocyclic organic compounds containing one or

more atoms other than hydrogen and carbon in the ring structure, such as nitrogen (N), sulfur (S) and oxygen (O).⁴⁰

Ferlin and colleagues⁴¹ reported several pyrroloquinoline incorporated with imidazole and triazole derivatives which showed potency against aromatase similar to that of letrozole. Functional groups such as imidazole, triazole, phenol, thiophene and pyridine are able to form nitrogen heme iron coordination. The active site of aromatase is dominated by aliphatic amino acid residues such as Met 374, Val 373, Val 370, Ile 305, Ala 306, Ile 133, Trp 224, Leu 372, Leu 477, Phe 134 and Thr 310. Hence, inhibitors with aromatic scaffolds are expected to bind with high affinity.⁸ Ibrahim and colleagues⁴² reported several 4-aminopyrido[2,3-d]pyrimidine derivatives as anti-proliferative CDK2 inhibitors. The presence of lone-electron pairs on heteroatoms may also contribute to the formation of hydrogen bonding, which increases the solubility, and binding affinity of the molecule to its potential targets.⁴⁰

1.4.1. Nitrogen-containing heterocyclic compounds

Nitrogen-containing heterocyclic compounds is a huge class of compounds containing nitrogen atoms along with carbon atoms in the rings.⁴³ Nitrogen-containing heterocyclic compounds have attracted a great deal of attention due to their biological activities against various diseases such as leishmania, tuberculosis, malaria, cancer, depression, and neurological problems.⁴⁴ Many pharmacologically important molecules consist of nitrogen-containing heterocyclic compounds as a core scaffold. Some examples of nitrogen-containing heterocyclic compounds are illustrated in **Figure 1.4**. Compounds with aryl moieties often exhibit improved solubility and stability.⁴³

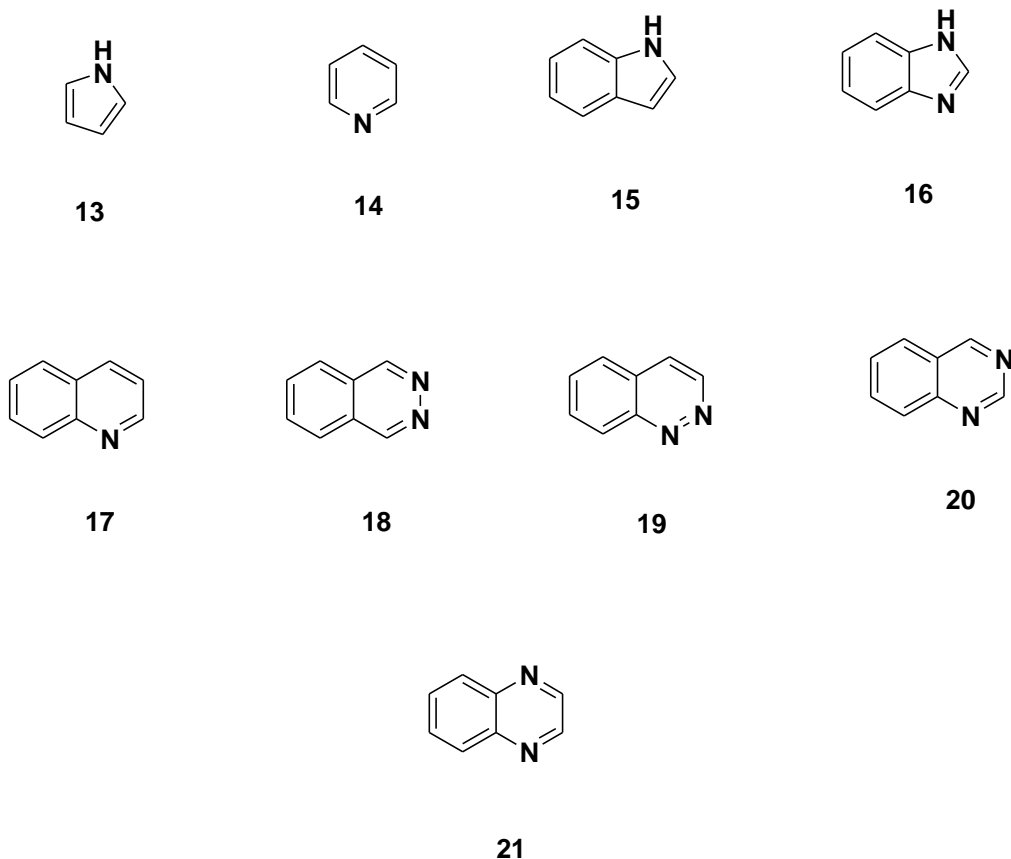


Figure 1.4: Examples of heterocyclic compounds: (a) Pyrrole **13**, (b) Pyridine **14**, (c) Indole **15**, (d) Benzimidazole **16**, (e) Quinoline **17**, (f) Phthalazine **18**, (g) Cinnoline **19**, (h) Quinazoline **20** and (i) Quinoxaline **21**.

1.4.1.1. Quinoxaline derivatives

Quinoxaline **21** nucleus is one of the most popular class of nitrogen-containing heterocyclic compounds in medicinal chemistry. The nucleus consists of a benzene ring and a pyrazine ring fused together.^{45,46} Quinoxaline derivatives are rare in nature and most of them are synthetic.⁴⁴ Quinoxaline derivatives have attracted much interest due to the versatility in their biological properties such as antitumor, anti-inflammatory, antimicrobial and antiviral.^{46,47} Quinoxaline nucleus serves as a scaffold to assemble a large number of compounds in an effort to obtain better derivatives with diverse medicinal applications.⁴⁴ Examples of drugs containing quinoxaline currently on the market are brimonidine **22** used to treat glaucoma, quinacillin **23** that has antibacterial properties,

varenicline **24** as a smoking cessation agent,⁴⁸ and erdafitinib (balversa) **25** which is one of the small molecule drugs approved recently as anti-cancer agent to treat bladder cancer.³⁶

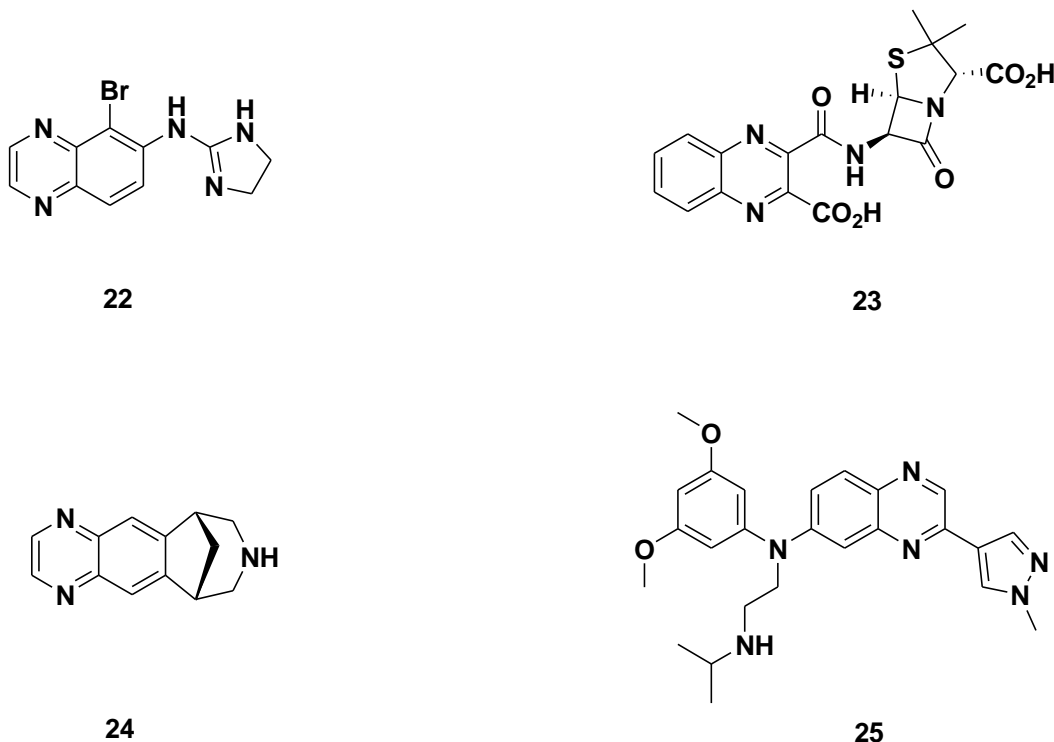


Figure 1.5: Examples of clinically approved drugs which comprise quinoxaline scaffold.

1.4.1.2. Quinoxaline derivatives as anticancer agents against breast cancer

There are many potential drugs consisting of quinoxaline scaffolds that are currently being investigated as potential anticancer agents. Galal *et al*,⁴⁹ synthesized a series of novel quinoxaline derivatives and evaluated them for their *in vitro* antiproliferative activity against breast cancer cell line (MCF-7) and discovered that 1-allyl-3-(2-(4-(dimethylamino)benzylidene)hydrazinyl)quinoxalin-2(1H)-one **26** showed good activity, with the IC₅₀ value of 2.90 ± 0.04 pmol/ml compared to doxorubicin **29** (3.20 ± 0.02 pmol/ml) which was used as a standard and the compound was subjected to *in vivo* study (**Figure 1.6**).⁴⁹

Figure 1.6 shows some examples of compounds containing quinoxaline scaffold that showed promising results against breast cancer cell line (MCF-7) in an *in vitro* study. Abbas and colleagues⁵⁰ also reported 2-(6-bromo-3-methyl-2-oxoquinoxalin-1(2*H*)-yl)acetohydrazide **27** and 2-(7-bromo-2-methylquinoxalin-3-yloxy)benzenamine **28** with the IC₅₀ values of 0.01 ± 0.001 and 0.02 ± 0.001 ug/L, respectively against breast cancer cell line (MCF-7). Compounds **27** and **28** showed more effective inhibition activity than doxorubicin **29** (0.04 ± 0.008 ug/L) which is a well-known chemotherapy medication used to treat cancer.⁵⁰ Sibiya and co-workers⁴⁵ reported 3-(quinoxaline-3-yl) prop-2-yn-1-ol **30** with a good anti-cancer property against MCF-7 breast cancer cells in an *in vitro* study.⁴⁵

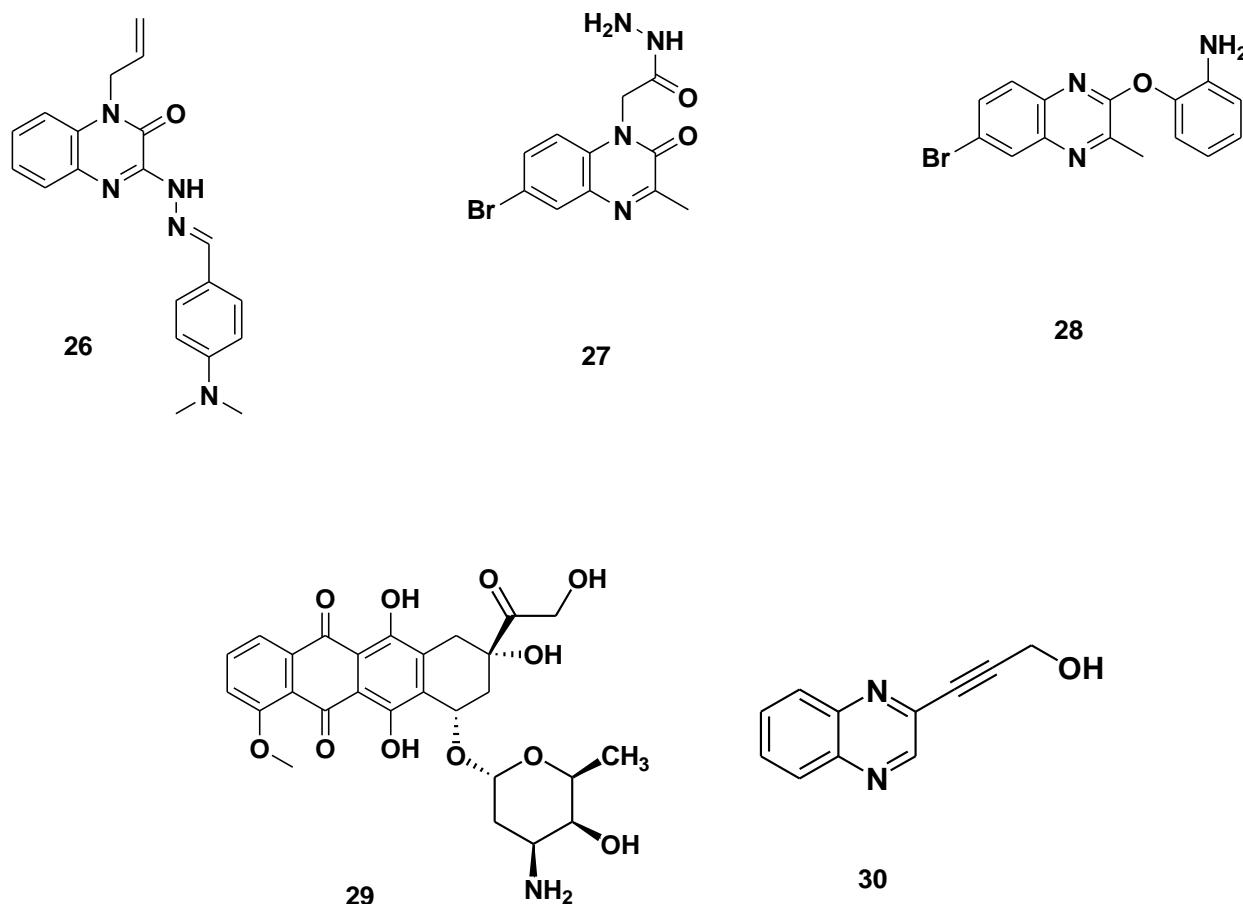


Figure 1.6: Examples of compounds containing quinoxaline scaffold that showed promising results against breast cancer and doxorubicin **29** (which was used as reference).

1.5. Molecular modeling

The development of new drugs is extremely important in medicinal chemistry, but the process is expensive, time-consuming and with low rate of success.^{51,52} Computer-aided drug design (CADD) offers an *in silico* (computer-based) approach which shortens time and expenses by searching potential novel drugs before synthesis.⁵³ The integration of computational and experimental approaches has been of great value in drug design and synthesis.⁵⁴ Several approved drugs such as HIV protease inhibitors,⁵⁵ saquinavir, ritonavir, indinavir and tirofiban have benefited a lot from the use of this particular technique.⁵³ CADD tool is classified into structure-based drug design and ligand-based drug design. Ligand-based design uses only knowledge about the ligands, for example in cases where the structure of the target protein is not known.⁵⁶

Computational methods involve “docking” of small molecules into the active site of the receptor (enzyme) in a variety of positions, orientations and conformations. Then the computer model predicts the best pose and the binding affinity or score which represent the strength of binding. The method mimics the binding of ligand to a protein and it has some remarkable successes in drug discovery.⁵⁵ Molecular docking can be undertaken by employing a rigid body docking (lock and key), rigid receptor-flexible ligand approach, and flexible receptor and ligand approach (induced fit docking).⁵³

1.5.1. Molecular docking programs

A variety of commercial software programs are available for personal computer-based systems as well as supercomputer-based systems. Currently, there are many molecular modeling software programs that are available for commercial and academic molecular modeling functions.⁵⁷ These include molecular docking programs such as DOCK, AutoDock, Gold, FlexX, GLIDE, ICM, PhDOCK and Surflex that are currently available. New programs are continuously being developed and many existing programs are frequently being upgraded with new technology. The performance of numerous molecular docking programs was studied intensively and the general conclusion drawn from the

studies was that no docking program is consistently superior to all other programs, and that the success or failure was dependent on the combination of ligand and receptor characteristics.^{56,58}

1.5.2. Molecular docking

In order to design a drug for a particular disease, scientists must understand the disease they wish to treat at a molecular level, so that they can predict the structure of a target enzyme. The 3D structure of the target can be obtained either from X-ray crystallography, multidimensional NMR spectroscopy or homology modeling to do docking. Homology modeling can produce practical protein structures by providing a three dimensional model from a template protein sequence based on the structure of one or more homologous proteins of which the structures have been reported before.⁵⁴

Computer docking is a vital tool in understanding the binding mode between small molecules and a receptor, which is a driving force in the field of computer-aided drug design. Hydrogen bonding and metal coordination keeps molecules tightly bound to the enzyme. Hydrophobic protein atoms enclose hydrophobic ligand atoms. Other special interactions that attract ligands to proteins include pi-cation and pi-pi stacking interactions between aromatic groups of the ligand and protein. Potent ligands fit tightly inside the binding site of a protein while avoiding steric conflict. Molecular docking is used for both exploring possible positions, orientations and conformations of a small molecule inside the binding site of a protein as well as estimation of the binding affinity which represent the strength of ligand-protein interactions.⁵⁴

1.5.2.1. Schrodinger modules applied in the present study

1.5.2.1.1. Ligprep

Ligand preparation is an important step for the preparation of chemical compounds before performing screening. The concept involves converting two-dimensional structure into three-dimensional structure with the option to expand each import structure by generating variation on minimization, optimization, low energy conformers, enantiomers tautomer, ring conformers and also generate possible ionization states at target pH using Epik to not only predict the ionization states but also the energetic penalty associated with them.^{59,60}

1.5.2.1.2. Protein Preparation Wizard

The protein structure from protein data bank (PDB) is not suitable for immediate use in molecular modeling calculations. They usually consist of heavy atoms and may include co-crystallised ligands, water molecules, metal ions and cofactors. Some structures are multimeric and may need to be reduced to a single unit. PDB structures may also be missing atoms and connectivity information, which must be assigned along with bond order and formal charges. Therefore, targeted protein must be pre-processed using Protein Preparation Wizard of the Schrödinger Suite to assign bond orders, filling missing hydrogens, side chains and loops, capping termini using prime, and deleting unnecessary water molecules.⁵⁹ The refine tab/panel involves optimization of hydrogen bonding network and minimization in which heavy atoms can be restrained with the OPLS3e force field until a final root mean square deviation (rmsd) of 0.030 Å to eliminate steric clashes and relaxing side chains.^{15,60}

1.5.2.1.3. Virtual screening workflow

Virtual screening is a computational technique used in drug discovery to search the library of chemical compounds in order to screen and identify structures which are most likely to

bind to the drug target with high affinity. This experiment is performed using rigid receptor - flexible ligand.⁵⁵

1.5.2.1.4. Induced Fit docking

Induced-fit docking (IFD) accounts for protein flexibility in the entire protein and the ligand, in order to capture the real binding event. The flexibility allows the receptor to alter its binding site so that it can accommodate the shape and binding mode of the ligand, since in reality many proteins undergo sidechain or backbone movements, upon ligand binding.⁶¹ The induced-fit docking process involves the prediction of ligand conformation and orientation (or posing) within a targeted binding site and measure the glide score in order to identify the energetically most favourable pose, each pose is evaluated or scored based on its fit to the target in terms of shape and properties such as hydrogen bonding, pi-pi bonding and electrostatic interactions as well as metal coordination.⁵⁵

1.5.2.1.5. QikProp

QikProp module on the Schrodinger suit is used to predict the suitable physicochemical and pharmacokinetic properties (ADME: absorption, distribution, metabolism, excretion) of the ligands. It provides the detailed analysis of significant pharmaceutical and drug-like properties, including percentage of human oral absorption, aqueous solubility, octanol/water partition coefficient, central nervous system activity, brain/blood partition coefficient, molecular weight, number of hydrogen bond donors and acceptors. In addition, a drug-like molecule should satisfy Lipinski rule of five which state that a compound to be drug-like need to satisfy the following parameters which include: molecular weight \leq 500 daltons, hydrogen bond donor \leq 5, hydrogen bond acceptor \leq 10 and predicted octanol/water partition coefficient $<$ 5.⁵⁹

The present study aims to design a large library of small molecules (amino and nitro quinoxaline with functionally substituted alkyne derivatives) and perform virtual screening workflow (VSW) for hits identifications to reduce the number of false negatives in the subset of compounds. Once the hits are identified, they are subjected to Induced Fit Docking (IFD) for the optimization of their binding affinity and ADME prediction for pharmacokinetics studies. The identified hit compounds will then be synthesised in the hope of obtaining new potential anticancer agents.

1.6. Aim

The aim of the study was to design and synthesise *de novo* the quinoxaline derivatives and evaluate their biological activity against breast cancer cells.

1.7. Objectives

The objectives of the study were to:

- I. design library of compounds determined by our research group, using structure based virtual screening workflow (VSW) to filter all compounds and perform Induced Fit Docking (IFD) to predicting ligand-receptor binding modes.
- II. synthesise ligand inhibitors which were predicted by VSW to have high negative docking score value against various enzymes such as CYP19A1 and CDK2.
- III. evaluate the synthesised compounds against breast cancer cells and recombinant enzymes.

1.8. References

1. Campbell, M., K. and Farrell, S., O. Biochemistry. 6th edition. Australia. Thomson., 425-434 (2006).
2. De, A., Kuppusamy, G. and Karri, V. V. S. R. Affibody molecules for molecular imaging and targeted drug delivery in the management of breast cancer. *Int. J. Biol. Macromol.*, **107**, 906–919 (2018).
3. Brackstone, M., Townson, J. L. and Chambers, A. F. Tumour dormancy in breast cancer: An update. *Breast Cancer Res.*, **9**, 1–7 (2007).
4. Siegel, R. L., Miller, K. D. and Jemal, A. Cancer Statistics , *J. Clin.*, **67**, 7–30 (2017).
5. van de Water, W., Fontein, D. B. Y, van Nes, J. G. H., Bartlett, J. M. S., Hille, E. T. M., Putter, H., Robson, T., Liefers, G., Roumen, R. M. H., Seynaeve, C., Dirix, L. Y., Paridaens, R., Kranenbarg, E. M., Nortier, J. W. R., van de Velde, C. J. H. Influence of semi-quantitative oestrogen receptor expression on adjuvant endocrine therapy efficacy in ductal and lobular breast cancer – A TEAM study analysis. *Eur. J. Cancer*, **49**, 297–304 (2013).
6. Arpino, G., Bardou, V. J., Clark, G. M. and Elledge, R. M. Infiltrating lobular carcinoma of the breast : tumor characteristics and clinical outcome. *Breast Cancer Res.*, **6**, 7–11 (2004).
7. Youlden, D. R., Cramb, S. M., Dunn, N. A. M., Muller, J. M., Pyke, C. M., Baade, P. D. The descriptive epidemiology of female breast cancer : An international comparison of screening , incidence , survival and mortality. *Cancer Epidemiol.*, **36**, 237–248 (2012).
8. Bonfield, K., Amato, E., Bankemper, T., Agard, H., Steller, J., Keeler, J. M., Roy, D., McCallum, A., Paula, S. and Ma, L. Development of a new class of aromatase inhibitors: Design, synthesis and inhibitory activity of 3-phenylchroman-4-one (isoflavanone) derivatives. *Bioorg Med Chem.*, **20**, 1–7 (2012).
9. Heil, J., Kuerer, H. M., Pfob, A., Rauch, G., Sinn, H. P., Golatta, M., Liefers, G. J.

- and Peeters, M. J. V. Eliminating the breast cancer surgery paradigm after neoadjuvant systemic therapy : current evidence and future challenges. *Ann. Oncol.*, **31**, 61–71 (2020).
10. Miaskowski, C., Cooper, B., Paul, S. M., West, C., Langford, D., Levine, J. D., Abrams, G., Hamolsky, D., Dunn, L., Dodd, M., Neuhaus, J., Baggott, C., Dhruva, A., Schmidt, B., Cataldo, J., Merriman, J. and Aouizerat, B. E. Identification of Patient Subgroups and Risk Factors for Persistent Breast Pain Following Breast Cancer Surgery. *J. Pain*, **13**, 1172–1187 (2012).
 11. Chang, J. S., Shin, J., Park, E. and Kim, Y. B. Risk of cardiac disease after adjuvant radiation therapy among breast cancer survivors. *The Breast*, **43**, 48–54 (2019).
 12. Shah, C. H., Balkrishnan, R., Diaby, V. and Xiao, H. Examining factors associated with adherence to hormonal therapy in breast cancer patients. *Res. Soc. Adm. Pharm.*, 1–9 (2019).
 13. Suvannang, N., Nantasenamat, C., Isarankura-Na-Ayudhya, C. and Prachayasittikul, V. Molecular Docking of Aromatase Inhibitors. *Molecules*, **16**, 3597–3617 (2011).
 14. Nakata, T., Takashima, S., Shiotsu, Y., Murakata, C., Ishida, H., Akinagad, S., Li, P., Sasano, H., Suzuki, T. and Saeki, T. Role of steroid sulfatase in local formation of estrogen in post-menopausal breast cancer patients. *J. Steroid Biochem. Mol. Biol.*, **86**, 455–460 (2003).
 15. Caporuscio, F., Rastelli, G., Imbriano, C. and Del Rio, A. Structure-based design of potent aromatase inhibitors by high-throughput docking. *J. Med. Chem.*, **54**, 4006–4017 (2011).
 16. Park, W. and Jordan, V. C. Selective estrogen receptor modulators (SERMS) and their roles in breast cancer prevention. *Trends. Mol. Med.*, **8**, 82–88 (2002).
 17. Quirke, V. M. Tamoxifen from Failed Contraceptive Pill to Best-Selling Breast Cancer Medicine : A Case-Study in Pharmaceutical Innovation. *Front. Pharmacol.*,

- 8**, 1–16 (2017).
18. Lippman, M. E., Cummings, S. R., Disch, D. T., Mershon, J. L., Dowsett, S. A., Cauley, J. A. and Martino, S. Effect of Raloxifene on the Incidence of Invasive Breast Cancer in Postmenopausal Women with Osteoporosis Categorized by Breast Cancer Risk. *Clin. Cancer Res.*, **12**, 5242–5248 (2006).
 19. Morello, K. C., Wurz, G. T. and DeGregorio, M. W. Pharmacokinetics of Selective Estrogen Receptor Modulators. *Clin. Pharmacokinet.*, **42**, 361–372 (2003).
 20. Jackson, L. R., Cheung, K. L., Buzdar, A. U. and Robertson, J. F. R. Arzoxifene : the evidence for its development in the management of breast cancer. *Core Evid.*, **2**. 251–258 (2008).
 21. Varela, C. L., Amaral, C., da Silva, E. T., Lopes, A., Correia-da-Silva, G., Carvalho, R. A., Costa, S. C. P., Fernanda M.F. Roleira, F. M. F., Teixeira, N. Exemestane metabolites : Synthesis , stereochemical elucidation , biochemical activity and anti-proliferative effects in a hormone- dependent breast cancer cell line. *Eur. J. Med. Chem.*, **87**, 336–345 (2014).
 22. Ahmad, I. Recent developments in steroidal and nonsteroidal aromatase inhibitors for the chemoprevention of estrogen-dependent breast cancer. *Eur. J. Med. Chem.*, **102**, 375–386 (2015).
 23. Brueggemeier, R. W., Richards, J. A. and Petrel, T. A. Aromatase and cyclooxygenases: Enzymes in breast cancer. *J. Steroid Biochem. Mol. Biol.*, **86**, 501–507 (2003).
 24. Avendaño, C. and Menéndez, J. C. Medicinal Chemistry of Anticancer Drugs. 2nd edition. Madrid. Elsevier Health Sciences., 53–91 (2008).
 25. Falkson, C. I. and Falkson, H. C. A randomised study of CGS 16949A (fadrozole) versus tamoxifen in previously untreated postmenopausal patients with metastatic breast cancer. *Ann. Oncol.*, **7**, 465–469 (1996).
 26. Sestak, I., Blake, G. M., Patelc, R., Colemand, R. E., Cuzicka, J. and Eastell, R. Comparison of risedronate versus placebo in preventing anastrozole-induced

- bone loss in women at high risk of developing breast cancer with osteopenia. *Bone*, **124**, 83–88 (2019).
27. Zwiefelhofer, E. M., Davis, B. M. and Adams, G. P. Research and development of a silicone letrozole-releasing device to control reproduction in cattle. *Theriogenology*, **146**, 104–110 (2020).
 28. Castellano, S., Stefancich, G., Ragno, R., Schewe, K., Santoriello, M., Caroli, A., Hartmann, R. W. and Sbardella, G. CYP19 (aromatase): Exploring the scaffold flexibility for novel selective inhibitors. *Bioorg. Med. Chem.*, **16**, 8349–8358 (2008).
 29. Roskoski, R. J. Cyclin-dependent protein kinase inhibitors including palbociclib as anticancer drugs. *Pharmacol. Res.*, **107**, 249–275 (2016).
 30. Sánchez-Martínez, C., Lallena, M. J., Sanfeliciano, S. G. and de Dios, A. Cyclin dependent kinase (CDK) inhibitors as anticancer drugs: Recent advances (2015–2019). *Bioorg. Med. Chem. Lett.*, **29**, 1–18 (2019).
 31. Tripathi, S. K., Muttineni, R. and Singh, S. K. Extra precision docking, free energy calculation and molecular dynamics simulation studies of CDK2 inhibitors. *J. Theor. Biol.*, **334**, 87–100 (2013).
 32. Hanahan, D. and Weinberg, R. A. The Hallmarks of Cancer. *Cell*, **100**, 57–70 (2000).
 33. Whittaker, S. R., Mallinger, A., Workman, P. and Clarke, P. A. Inhibitors of cyclin-dependent kinases as cancer therapeutics. *Pharmacol. Ther.*, **173**, 83–105 (2017).
 34. Le Tourneau, C., Faivre, S., Laurence, V., Delbaldo, C., Vera, K., Girre, V., Chiao, J., Armour, S., Frame, S., Green, S. R., Gianella-Borradori, A., Dieras, V. and Raymond, E. Phase I evaluation of seliciclib (R -roscovitine), a novel oral cyclin-dependent kinase inhibitor , in patients with advanced malignancies. *Eur. J. Cancer*, **46**, 3243 –3250 (2010).
 35. Squires, M. S., Cooke, L., Lock, V., Qi, W., Lewis, E. J., Thompson, N. T., Lyons,

- J. F. and Mahadevan, D. AT7519 , a Cyclin-Dependent Kinase Inhibitor , Exerts Its Effects by Transcriptional Inhibition in Leukemia Cell Lines and Patient Samples. *Mol. Cancer Ther.*, **9**, 920–929 (2010).
36. Roskoski, R. J. The role of fibroblast growth factor receptor (FGFR) protein-tyrosine kinase inhibitors in the treatment of cancers including those of the urinary bladder. *Pharmacol. Res.*, **151**, 1–22 (2020).
37. Parry, D., Guzi, T., Shanahan, F., Davis, N., Prabhavalkar, D., Derek Wiswell, D., Seghezzi, W., Paruch, K., Dwyer, M. P., Doll, R., Nomeir, A., Windsor, W., Fischmann, T., Wang, Y., Oft, M., Chen, T., Kirschmeier, P., and Lees, E. M. Dinaciclib (SCH 727965), a Novel and Potent Cyclin-Dependent Kinase Inhibitor. *Mol. Cancer Ther.*, **9**, 2344–2354 (2010).
38. Kumar, S. K., LaPlant, B., Chng, W. J., Zonder, J., Callander, N., Fonseca, R., Fruth, B., Roy, V., Erlichman, C. and Stewart, A. K. Dinaciclib , a novel CDK inhibitor , demonstrates encouraging single-agent activity in patients with relapsed multiple myeloma. *Blood*, **125**, 443–448 (2015).
39. Mita, M. M., Anil A. Joy, A. A., Mita, A., Sankhala, K., Jou, Y., Zhang, D., Statkevich, P., Zhu, Y., Yao, S., Small, K., Bannerji, R. and Shapiro, C. L. Randomized Phase II Trial of the in Patients With Advanced Breast Cancer. *Clin. Breast Cancer*, **14**, 169–176 (2014).
40. Sribalan, R., Banupriya, G., Kirubavathi, M. and Padmini, V. Synthesis , biological evaluation and in silico studies of tetrazole- heterocycle hybrids. *J. Mol. Struct.*, **1175**, 577–586 (2019).
41. Ferlin, M. G., Carta, D., Bortolozzi, R., Ghodsi, R., Chimento, A., Pezzi, V., Moro, S., Hanke, N., Hartmann, R. W., Basso, G., and Viola, G. Design, synthesis and structure-activity relationships of azolymethylpyrroloquinolines as nonsteroidal aromatase inhibitors. *J. Med. Chem.*, **56**, 7536–7551 (2013).
42. Ibrahim, D. A. and Ismail, N. S. M. Design, synthesis and biological study of novel pyrido[2,3-d]pyrimidine as anti-proliferative CDK2 inhibitors. *Eur. J. Med. Chem.*,

- 46**, 5825–5832 (2011).
43. Arora, P., Arora, V., Lamba, H. S. and Wadhwa, D. Importance of heterocyclic chemistry: A review. *Int. J. Pharm. Sci. Res.*, **3**, 2947–2954 (2012).
 44. Pereira, J. A., Pessoa, A. M., Cordeiro, M. N. D. S., Rúben Fernandes, R., Cristina Prudencio, C., Noronha, J. P. and Vieira, M. Quinoxaline, its derivatives and applications: A State of the Art review. *Eur. J. Med. Chem.*, **97**, 664–672 (2015).
 45. Sibiyi, M. A., Raphoko, L., Mangokoana, D., Makola, R., Nxumalo, W. and Matsebatlela, T. M. Induction of Cell Death in Human A549 Cells Using 3-(Quinoxaline-3-yl) Prop-2-ynyl Methanosulphonate and 3-(Quinoxaline-3-yl) Prop-2-yn-1-ol. *Molecules*, **24**, 1-16 (2019).
 46. Kaushal, T., Srivastava, G., Sharma, A. & Negi, A. S. Bioorganic & Medicinal Chemistry An insight into medicinal chemistry of anticancer quinoxalines. *Bioorg. Med. Chem.*, **27**, 16–35 (2019).
 47. Ndlovu, N. T. and Nxumalo, W. Nucleophilic Substitution on 2-Monosubstituted Quinoxalines Giving 2,3-Disubstituted Quinoxalines: Investigating the Effect of the 2-Substituent. *Molecules*, **21**, 1–11 (2016).
 48. Rajule, R., Bryant, V. C., Lopez, H., Luo, X. and Natarajan, A. Perturbing pro-survival proteins using quinoxaline derivatives : A structure – activity relationship study. *Bioorg. Med. Chem.*, **20**, 2227–2234 (2012).
 49. Galal, S. A., Abdelsamie, A. S., Soliman, S. M., Mortier, J., Wolber, G., Ali, M. M., Tokuda, H., Suzuki, N., Lida, A., Ramadan, R. A. and Diwani, H. I. Design, synthesis and structure-activity relationship of novel quinoxaline derivatives as cancer chemopreventive agent by inhibition of tyrosine kinase receptor. *Eur. J. Med. Chem.*, **69**, 115–124 (2013).
 50. Abbas, H. S., Al-marhabi, A. R., Eissa, S. I. and Ammar, Y. A. Molecular modeling studies and synthesis of novel quinoxaline derivatives with potential anticancer activity as inhibitors of c-Met kinase. *Bioorg. Med. Chem.*, **23**, 6560–6572 (2015).

51. Tang, Y., Zhu, W., Chen, K. & Jiang, H. New technologies in computer-aided drug design: Toward target identification and new chemical entity discovery. *Drug Discov. Today Technol.* **3**, 307–313 (2006).
52. Huang, H., Yu, H. W., Chen, C., Hsu, C., Chen, H., Lee, K., Tsai, F. and Chen, C. Y. Current developments of computer-aided drug design. *J. Taiwan Inst. Chem. Eng.*, **41**, 623–635 (2010).
53. Śledź, P. and Caflisch, A. Protein structure-based drug design: from docking to molecular dynamics. *Curr. Opin. Struct. Biol.*, **48**, 93–102 (2018).
54. Honarparvar, B., Govender, T., Maguire, G. E. M., Soliman, M. E. S. and Kruger, H. G. Integrated Approach to Structure-Based Enzymatic Drug Design : Molecular Modeling , Spectroscopy , and Experimental Bioactivity. *Chem. Rev.*, **114**, 493–537 (2014).
55. Kitchen, D. B., Decornez, H., Furr, J. R. and Bajorath, J. Docking and scoring in virtual screening for drug discovery: Methods and applications. *Nat. Rev. Drug Discov.*, **3**, 935–949 (2004).
56. Ferreira, L. G., Santos, R. N., Oliva, G. and Andricopulo, A. D. Molecular Docking and Structure-Based Drug Design Strategies. *Molecules*, **20**, 13384–13421 (2015).
57. Nadendla, R. R. Molecular Modeling : A Powerful Tool for Drug Design and Molecular Docking. *Resonance*, 51–60 (2004).
58. Cross, J. B., Thompson, D. C., Rai, B. K., Baber, J. C., Fan, K. Y., Hu, Y. and Humblet, C. Comparison of Several Molecular Docking Programs : Pose Prediction and Virtual Screening Accuracy. *J. Chem. Inf. Model*, **49**, 1455–1474 (2009).
59. Panwar, U. and Singh, S. K. Structure-based virtual screening toward the discovery of novel inhibitors for impeding the protein-protein interaction between HIV-1 integrase and human lens epithelium-derived growth factor (LEDGF / p75).

- J. Biomol. Struct. Dyn.*, **1102**, 1–19 (2017).
60. Gumede, N. J., Nxumalo, W., Bisetty, K., Gilabert, L. E. and Medina-hernandez, M. J. Prospective computational design and in vitro bio-analytical tests of new chemical entities as potential selective CYP17A1 lyase inhibitors. *Bioorg. Chem.*, 1–20 (2019).
 61. Wang, H., Aslanian, R. and Madison, V. S. Induced-fit docking of mometasone furoate and further evidence for glucocorticoid receptor 17 a pocket flexibility. *J. Mol. Graphics and Modelling*, **27**, 512–521 (2015).

Chapter 2

Results and discussions

2.1. Molecular modelling

Computational strategies for structure-based visual screening grants a crucial opportunity to the expensive and time taking process of random screening. Docking is used to describe the enzyme-drug candidate recognition profile at molecular level. In order to explain the binding affinity obtained experimentally. In some cases, docking is used to predict the binding affinities of new compounds prior to synthesis. The end goal is to prioritize active compounds for synthesis, prior to bioanalysis.^{1,2} In the presents study, a highly advantageous visual screening approach was applied to identifying a novel inhibitor against target enzymes (aromatase and CDK2).

2.1.1. Cross docking against aromatase (PDB code: 3EQM)

For validation of the docking process, the investigation began with re-docking of a known co-crystallized structure, androstenedione **4** (natural substrate) into the active site of the crystal structure of aromatase in order to relate analysis of ligand binding confirmation with interactive residue, total number of interactive bonds, docking score and glide energy, and verify the performance of the docking process as well. In cross-docking, the co-crystalized ligand of the receptor is removed from the protein-ligand complex and then re-docked into the native receptor using cross-docking script.¹

In breast cancer the binding of a drug to the CYP19A1 follows type I and type II interaction. Type I interaction follows a binding mode of the natural substrate to the enzyme. Where two amino acid residues are involved in binding, which are ASP309 and MET374. On the other hand, type II interaction involves the metal coordination of the inhibitor to ferric heme, as well as the involvement of ASP309 and MET374 in binding.² Androstenedione **4** (natural substrate) follows a type I interaction, with the carbonyl group of the steroid showing a hydrogen bond with MET374.

Table 2.1: Re-docking result of 3EQM co-crystallized structure, androstenedione **4**.

Compound ID	Docking score (kcal/mol)	Glide E model (kcal/mol)	Glide energy (kcal/mol)	Total no. of Interactive bond	Interactive Residues-distance (Å)	IFD score (kcal/mol)
	-5.205	-82.329	-54.370	01	Met 374 - 1.88	-939.90

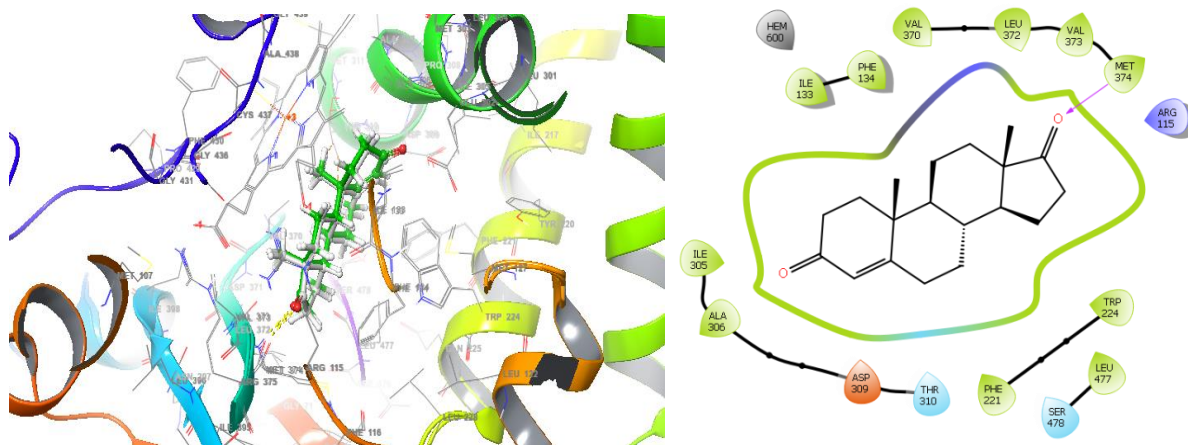


Figure 2.1: Model representation of molecular interaction analysis of both native (carbon in green colour) and docked (carbon in grey colour) structures of **4** (androstenedione) in the active site of aromatase (3EQM) and its 2D interaction profile respectively, the hydrogen bond is shown by the purple line.

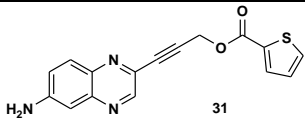
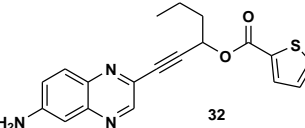
The highest docking score of Compound **4** was found to be -5.205 kcal/mol, glide energy -54.370 kcal/mol, glide Emodel -82.329 kcal/mol, and IFD score -939.90 kcal/mol as depicted in **Table 2.1**. Only one interaction was observed through hydrogen bond between the amino group of Met 374 and the oxygen on one of the carbonyl group on both native and docked structures of **4** with a distance of 1.88 Å. A degree of alignment was observed between native and docked structure with the RMSD value of 1.2433, indicating a successful docking procedure (**fig. 2.1**).

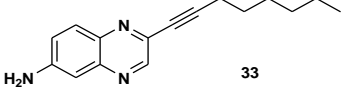
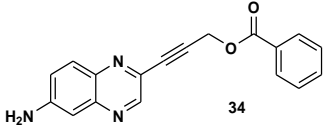
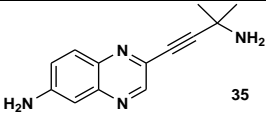
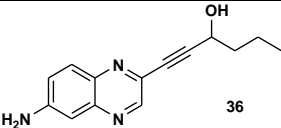
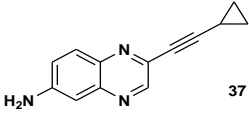
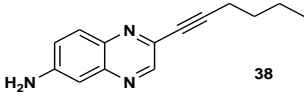
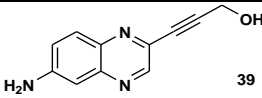
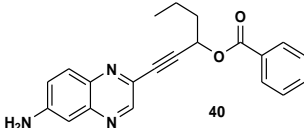
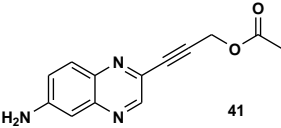
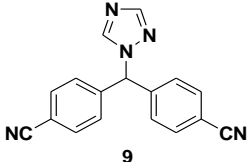
2.1.2. Structure based virtual screening against aromatase (PDB code: 3EQM)

Virtual screening is a computational technique used in drug discovery to search the library of chemical compounds in order to identify structures which are most likely to bind to the drug target.²

Virtual screening workflow was applied on a new chemical library of one hundred (100) different quinoxaline derivatives which were designed based on the chemical we have in our laboratory catalogue and eleven (11) were identified to be those structures which are most likely to bind to the therapeutic target, aromatase (3EQM). The docking score and glide energy of top 11 hit compounds are shown in **Table 2.2**. Docking results revealed the strong binding of hit compounds with active site residues of binding pocket in the crystal structure of human placental aromatase. The values such as the Glide energy scores are used to rank-order compounds. However, one usually uses a criteria to select the candidate compounds based on the interactive amino acids, metal coordination and the docking score.

Table 2.2: Docking results of 11 hit compounds identified from virtual screening as well as letrozole **9** as a positive control inhibitor against crystal structure of aromatase.

Compound ID	Docking score (kcal/mol)	Glide Evdw (kcal/mol)	Glide Ecoul (kcal/mol)	Glide energy (kcal/mol)	Total no. of Interactive bond	Interactive residues
 31	-8.372	-38.092	-5.213	-43.305	02	Leu 372 Leu 477
 32	-7.918	-41.565	-4.742	-46.307	02	Leu 372 Leu 477

 33	-7.762	-30.851	-3.117	-33.968	01	Ala 375
 34	-7.630	-38.801	-4.647	-43.448	02	Leu 477 Gly 614
 35	-7.628	-24.617	-3.449	-28.065	03	Leu 372 Trp 224 Ala 306
 36	-7.536	-34.381	-5.103	-39.848	01	Asp 378
 37	-7.137	-25.988	0.119	-25.869	01	Leu 372
 38	-6.489	-29.950	-1.940	-31.980	01	Leu 372
 39	-6.457	-28.193	-2.759	-30.952	01	Ala 306
 40	-6.421	-44.687	-1.018	-45.705	02	Leu 372 Arg 115
 41	-6.143	-35.303	-6.586	-41.889	03	Leu 372 Arg 115 Arg 115
 9	-6.502	-32.510	0.118	-32.392	03	Met 374 Trp 224 Hem 600

2.1.3. Induced fit docking and binding mode analysis

The identified 11 compounds were subsequently subjected to the flexible docking process through induced fit docking (IFD) in order to identify tight binding and also to establish whether protein flexibility improves the docking scores of the molecules that were prioritized for synthesis. All compounds as well as the known ligand **9** interact with different amino acids in different mode of interactions and a distance, hence different docking scores are observed.

Table 2.3: Induced fit docking result of the 11 hit compounds identified from virtual screening as well as letrozole as a positive control inhibitor.

Compound ID	Docking score (kcal /mol)	Glide E model (kcal /mol)	Glide energy (kcal /mol)	Total no. of Interactive bond	Interactive Residues-distance (Å)	IFD score (kcal /mol)
36	-8.814	-63.528	-44.990	03	Leu 477 - 1.98 Leu 372 -1.84 Glu 302 - 2.22	-943.16
41	-8.749	-40.779	-40.286	02	Leu 477 - 1 .98 Leu 372 - 1.92	-944.89
37	-8.438	-43.622	-37.037	02	Leu 477 - 2.04 Leu 372 – 1.87	-942.66
35	-7.709	-47.916	-40.619	03	Leu 477 - 1.87 Leu 372 - 2.04 Glu 302 - 2.00	-945.56
39	-7.684	-56.115	-40.216	01	Asp 309 - 1.70	-942.54
38	-7.511	-34.329	-34.351	01	Asp 309 - 2.08	-942.85
33	-7.160	-49.642	-43.332	02	Leu 477 - 1.87 Leu 372 - 2.05	-941.18

31	-6.934	-58.226	-40.241	05	Ile 305 - 2.54 Met 374 - 1.93 Trp 224 - 4.14 Trp 224 - 3.77 Hem 600	-942.13
40	-6.455	-74.460	-55.232	03	Glu 302 - 2.77 Hem 600 Hem 600	-942.43
32	-	-	-	-	-	-
34	-	-	-	-	-	-
Letrozole 9	-8.018	-91.501	-55.542	032	Met 374 - 2.03 Hem 600- 5.48 Hem 600- 4.41	-941.16

The binding mode of different compounds will be discussed in the following sections in order of the best to the poorest docking score.

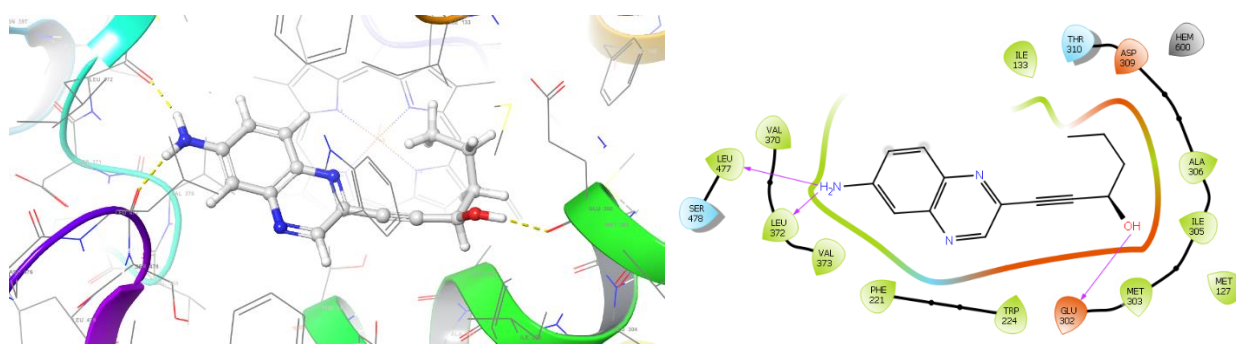


Figure 2.2: Model representation of molecular interaction analysis of **36** in the active site of aromatase (3EQM) and its 2D interaction profile respectively, the hydrogen bond is shown by the purple line.

2.1.3.21. Binding mode of 36 in the active site of aromatase enzyme.

The highest docking score of compound **36** was found to be -8.814 kcal/mol, glide energy -44.990 kcal/mol, glide Emodel -63.523 kcal/mol, and IFD score -943.16 kcal/mol as depicted in **Table 2.3**. A total of three interactions were observed, two interactions were through hydrogen bonding between amino group from **36** and the carboxyl group of Leu 477 as well as of Leu 372 with a distance of 2.08 and 1.84 Å respectively. Another interaction was through hydrogen bond between hydroxyl group of **36** and the oxygen on carboxyl group of Glu 302 with a distance of 2.22 Å (**fig. 2.2**).

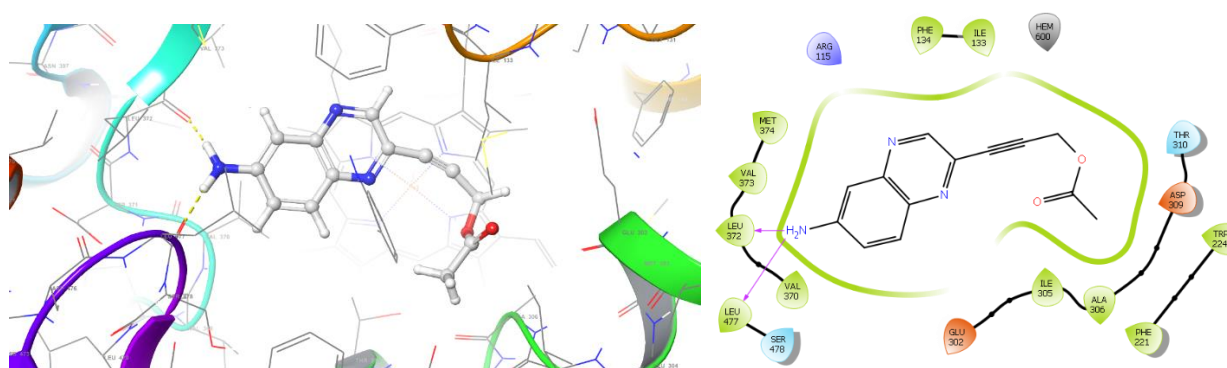


Figure 2.3: Model representation of molecular interaction analysis of **41** in the active site of aromatase (3EQM) and its 2D interaction profile respectively, the hydrogen bond is shown by the purple line.

2.1.3.2. Binding mode of 41 in the active site of aromatase enzyme.

The highest docking score of compound **41** was found to be -8.749 kcal/mol, glide energy -40286 kcal/mol, glide Emodel -40.779 kcal/mol, and IFD score -944.89 kcal/mol as depicted in **Table 2.3**. A total of two interactions were observed, both interactions were through hydrogen bonding between amino group from **41** and the carboxyl group of Leu 477 as well as of Leu 372 with a distance of 1.98 and 1.92 Å respectively (**fig. 2.3**).

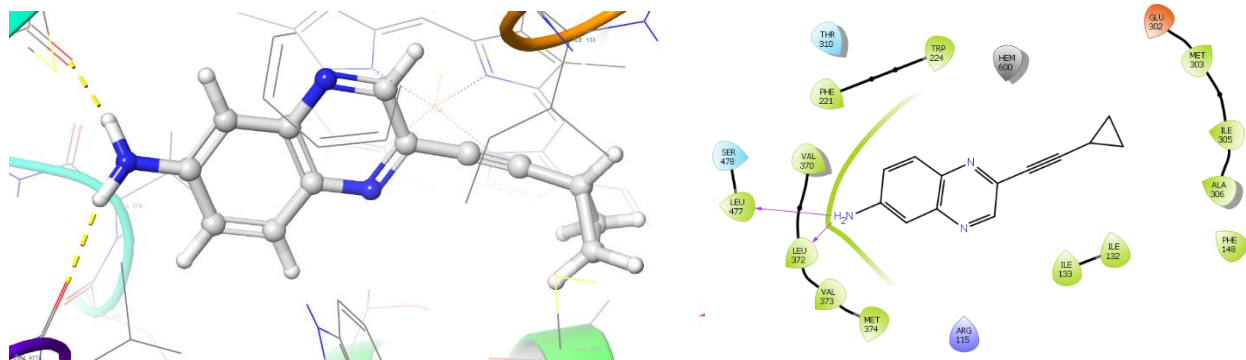


Figure 2.4: Model representation of molecular interaction analysis of **37** in the active site of aromatase (3EQM) and its 2D interaction profile respectively, the hydrogen bond is shown by the purple line.

Binding mode of **37** in the active site of aromatase enzyme.

The highest docking score of compound **33** was found to be -8.438 kcal/mol, glide energy -37.037 kcal/mol, glide Emodel -43.622 kcal/mol, and IFD score -942.66 kcal/mol. A total of two interactions were observed, both interactions were through hydrogen bonding between amino group from **33** and the carboxyl group of Leu 477 as well as of Leu 372 with a distance of 2.04 and 1.87 Å respectively (**fig. 2.4**).

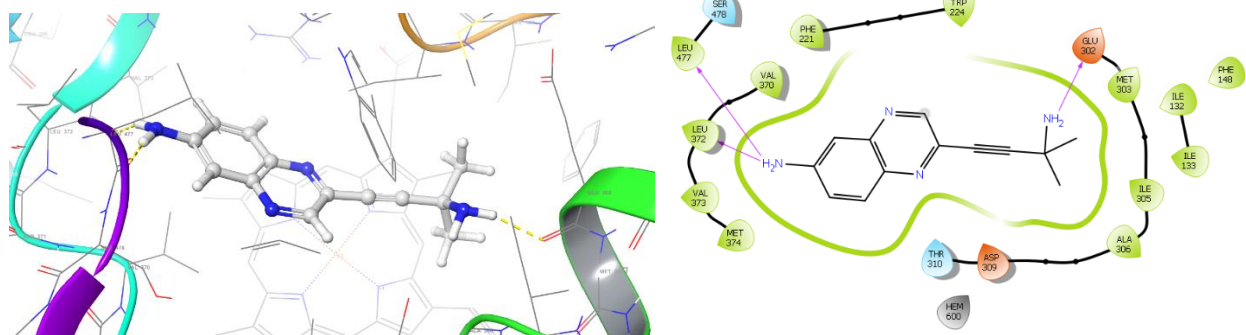


Figure 2.5: Model representation of molecular interaction analysis of **35** in the active site of aromatase (3EQM) and its 2D interaction profile respectively, the hydrogen bond is shown by the purple line.

2.1.3.3. Binding mode of 35 in the active site of aromatase enzyme.

The highest docking score of compound **35** was found to be -7.709 kcal/mol, glide energy -40.619 kcal/mol, glide Emodel -17.916 kcal/mol, and IFD score -945.56 kcal/mol as depicted in **Table 2.3**. A total of three interactions were observed, two interactions were through hydrogen bonding between amino group from **35** with the oxygen on carboxyl group of Leu 477 and Leu 372 with a distance of 2.04 and 1.87 Å respectively, and the other interactions was also through hydrogen bond between amino group at the propargylic position on **35** with the carboxyl group of Glu 302 with a distance of 2.00 Å (**fig. 2.5**).

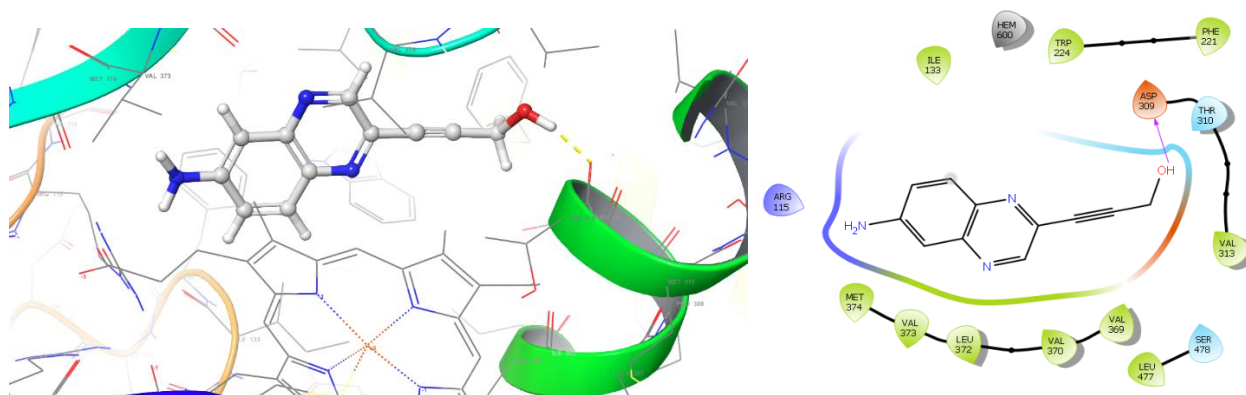


Figure 2.6: Model representation of molecular interaction analysis of **39** in the active site of aromatase (3EQM) and its 2D interaction profile, the hydrogen bond is shown by the purple line.

2.1.3.4. Binding mode of 39 in the active site of aromatase enzyme.

The highest docking score of compound **39** was found to be -7.684 kcal/mol, glide energy -40.216 kcal/mol, glide Emodel -56.115 kcal/mol, and IFD score -942.54 kcal/mol as depicted in **Table 2.3**. Only one interaction was observed which was hydrogen bond between hydroxyl group of **39** and the oxygen on carboxyl group of Asp 309 with a distance of 1.70 Å (**fig. 2.6**).

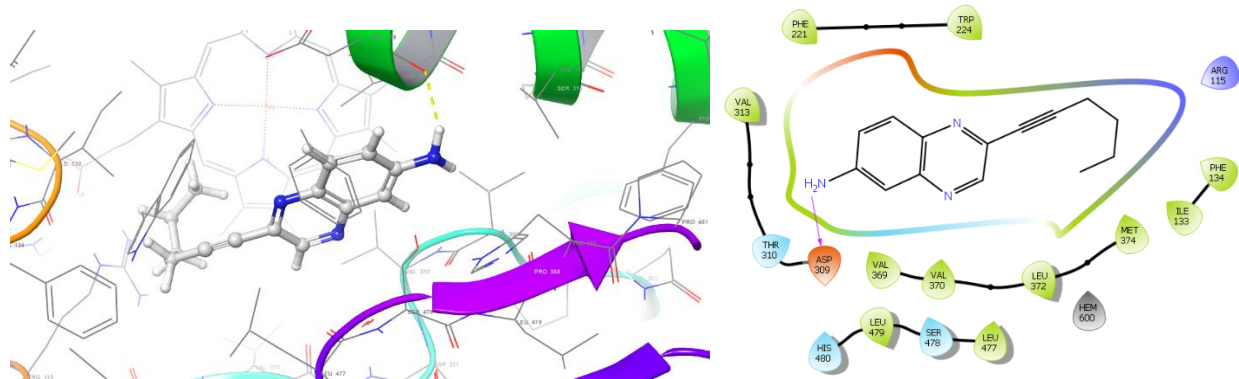


Figure 2.7: Model representation of molecular interaction analysis of **38** in the active site of aromatase (3EQM) and its 2D interaction profile respectively, the hydrogen bond is shown by the purple line.

2.1.3.5. Binding mode of **38** in the active site of aromatase enzyme.

The highest docking score of compound **38** was found to be -7.511 kcal/mol, glide energy -34.351 kcal/mol, glide Emodel -34.329 kcal/mol, and IFD score -942.85 kcal/mol as depicted in **Table 2.3**. Only one interaction was observed which was through hydrogen bond between amino group from **38** and the carboxyl group of Asp 309 with a distance of 2.11 Å (**fig. 2.7**).

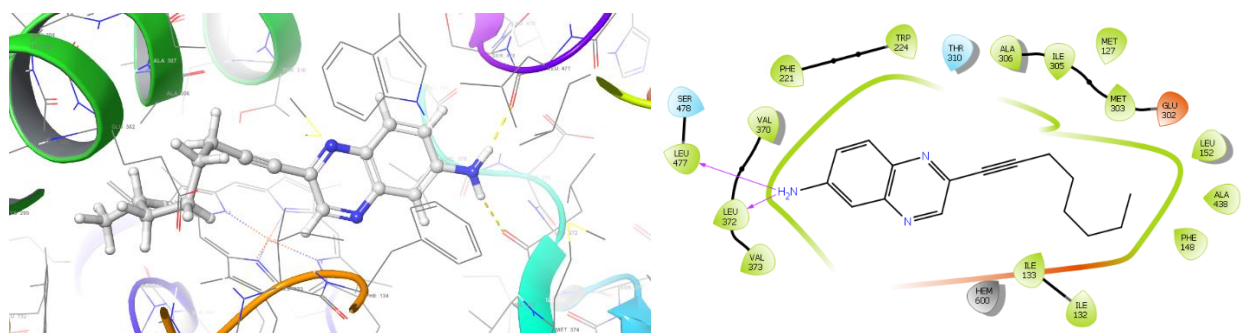


Figure 2.8: Model representation of molecular interaction analysis of **33** in the active site of aromatase (3EQM) and its 2D interaction profile respectively, the hydrogen bond is shown by the purple line.

2.1.3.6. Binding mode of 33 in the active site of aromatase enzyme.

The highest docking score of compound **33** was found to be -7.160 kcal/mol, glide energy -43.642 kcal/mol, glide Emodel -49.642 kcal/mol, and IFD score -941.18 kcal/mol as depicted in **Table 2.3**. A total of two interactions were observed, both interactions were through hydrogen bonding between amino group from **33** and the carboxyl group of Leu 477 as well as of Leu 372 with a distance of 2.04 and 1.87 Å respectively (**fig. 2.8**).

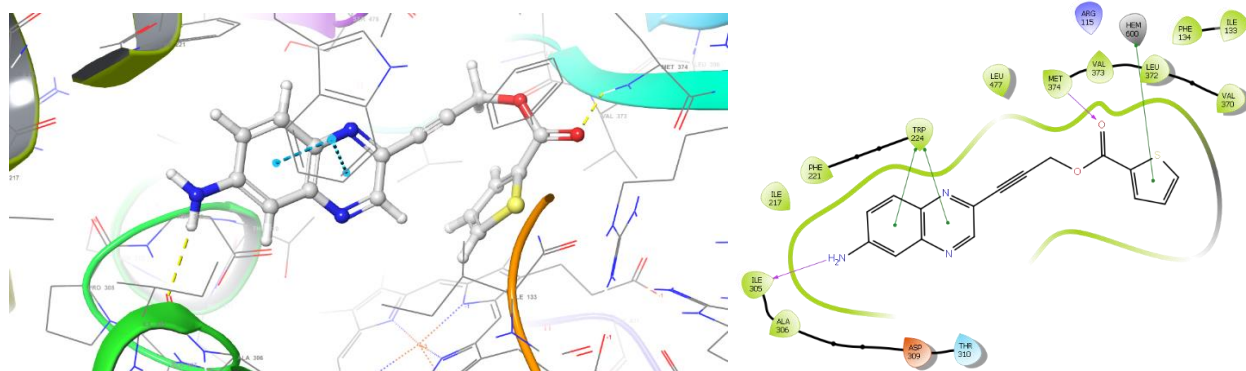


Figure 2.9: Model representation of molecular interaction analysis of **31** in the active site of aromatase (3EQM) and its 2D interaction profile respectively, pi-pi stacking is shown by green line and the hydrogen bond is shown by the purple line.

2.1.3.7. Binding mode of 31 in the active site of aromatase enzyme.

The highest docking score of compound **31** was found to be -6.934 kcal/mol, glide energy -40.241 kcal/mol, glide Emodel -58.226 kcal/mol, and IFD score -942.13 kcal/mol as depicted in **Table 2.3**. A total of five interactions were observed, two hydrophobic interactions were also observed through pi-pi stacking between phenyl group and pyrazine group of **31** with the indole side chain of Trp 224 with a distance of 4.14 and 3.77 Å respectively. One pi-pi stacking between thiophenyl group of **31** and ferric heme moiety. Another interaction was through hydrogen bond between amino group from **31** and the carboxyl group of Ile 305 with a distance of 2.54 Å and the other interaction was

through hydrogen bond between the amino group of Met 374 and the oxygen on the carbonyl group of **31** with a distance of 1.93 Å (**fig. 2.9**).

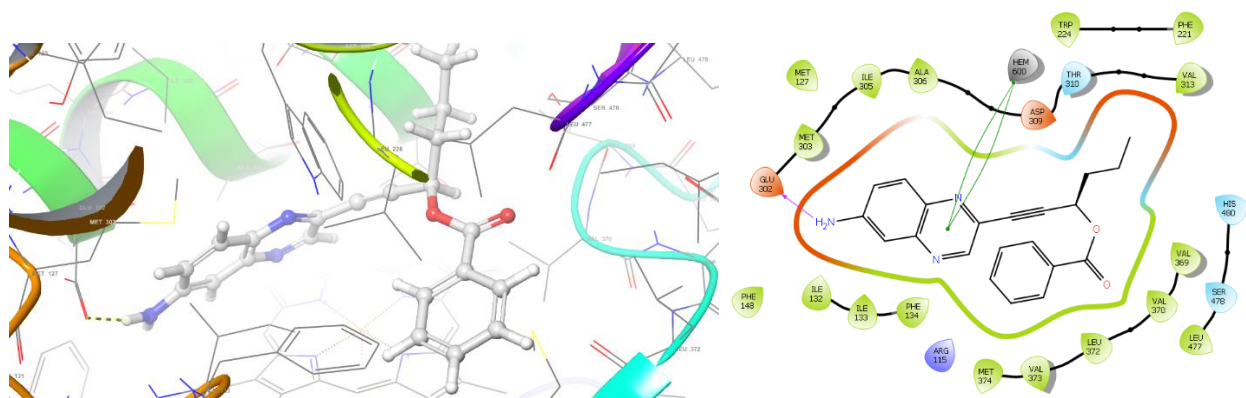


Figure 2.10: model representation of molecular interaction analysis of **40** in the active site aromatase (3EQM) and its 2D interaction profile respectively, pi-pi stacking is shown by green line and the hydrogen bond is shown by the purple line.

2.1.3.8. Binding mode of **40** in the active site of aromatase enzyme.

The highest docking score of compound **40** was found to be -6.455 kcal/mol, glide energy -55.232 kcal/mol, glide Emodel -74.460 kcal/mol, and IFD score -942.43 kcal/mol as depicted in **Table 2.3**. A total of three interactions were observed, two pi-pi stacking between pyrazine group of **40** and the ferric heme moiety. The other interaction was through hydrogen bond between the amino group of Glu 302 and the oxygen on the carbonyl group of **40** with a distance of 2.77 Å (**fig. 2.10**).

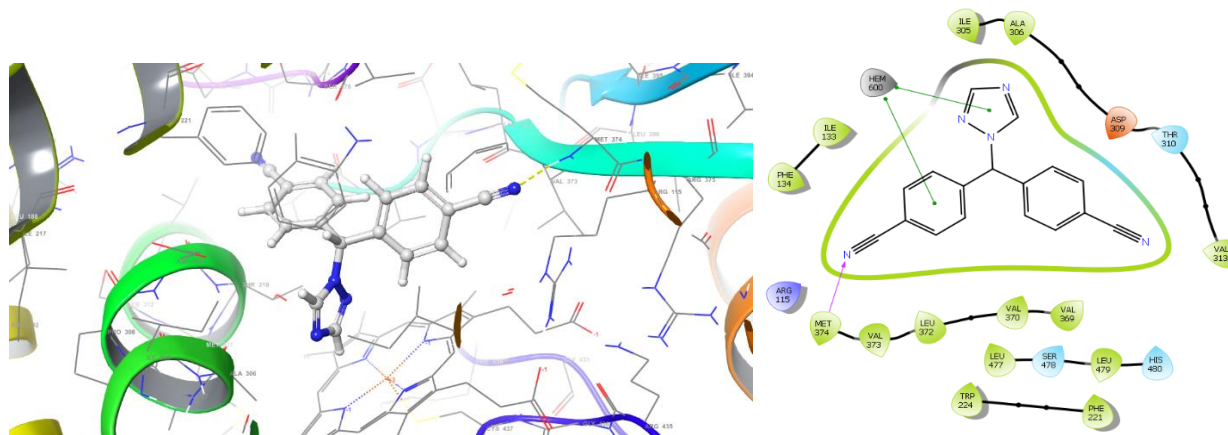


Figure 2.11: Model representation of molecular interaction analysis of **8 (std1)** in the active site of aromatase (3EQM) and its 2D interaction profile respectively, pi-pi stacking is shown by green line and the hydrogen bond is shown by the purple line.

2.1.3.9. Binding mode of **8** in the active site of aromatase enzyme.

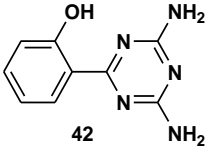
The highest docking score of compound **8** was found to be -8.630 kcal/mol, glide energy -52.351 kcal/mol, glide Emodel -78.366 kcal/mol, and IFD score -936.20 kcal/mol as depicted in **Table 2.3**. A total of three interactions were observed, two pi-pi stacking between triazole ring and one of the Benzonitrile rings of **8** with the ferric heme moiety. The other interaction was through hydrogen bond between the amino group of Met 374 and the nitrogen on one the cyanide group of **44** with a distance of 2.03 Å (**fig. 2.11**).

Compound **32** and **34** did not show any results from IFD. Therefore, that could suggest that they are considered to be false positive, however the enzyme-based assay results will confirm that.

2.1.4. Cross docking against CDK2 (PDB code: 3QQJ)

The following results show the docking studies of another target enzyme (CDK2). To verify the performance of the docking process, cross-docking of the co-crystallized ligand of the receptor is removed from the protein-ligand complex and then re-docked into the native receptor.

Table 2.4: Re-docking result of known co-crystallized structure, 2-(4,6-diamino-1,3,5-triazin-2-yl)phenol **42**.

Compound ID	Docking score (kcal/mol)	Glide E model (kcal/mol)	Glide energy (kcal/mol)	Total no. of Interactive bond	Interactive residues	IFD score (kcal/mol)
 42	-7.566	-54.584	-38.677	05	Gln 131 - 2.69 Asp 86- 2.00 Leu 83 - 2.08 Glu 81 - 2.17 H ₂ O - 1.92	-615.35

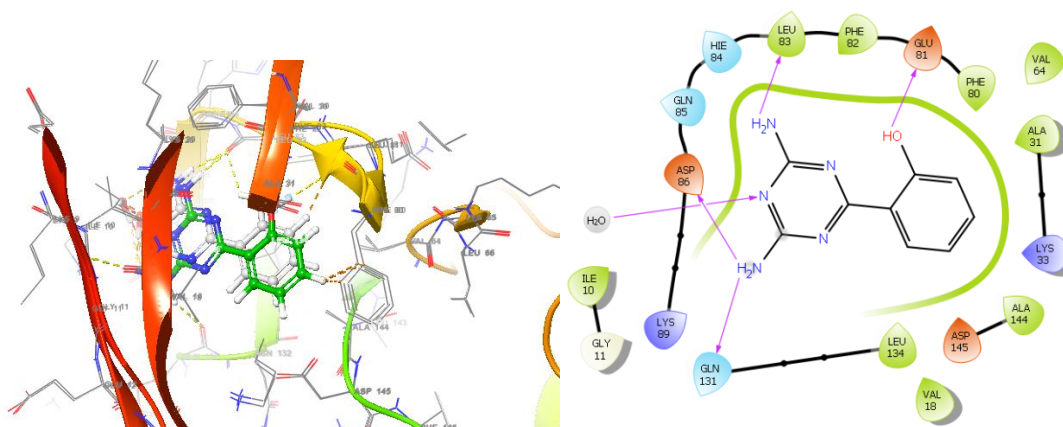


Figure 2.12: Model representation of molecular interaction analysis of both native (carbon in green colour) and docked (carbon in grey colour) structures of **42** (2-(4,6-diamino-1,3,5-triazin-2-yl)phenol) in the active site of cyclin dependent kinase 2 (3QQJ) and its 2D interaction profile, the hydrogen bond is shown by the purple line.

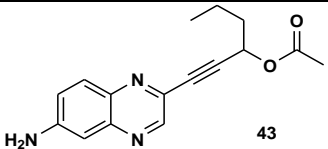
The highest docking score of compound **42** was found to be -7.566 kcal/mol, glide energy -38.677 kcal/mol, glide Emodel -54.584 kcal/mol, and IFD score -615.35 kcal/mol as depicted in **Table 2.4**. The total of five interactions were observed, two interactions were through hydrogen bonding between two hydrogens of one the amino group on **42** and the

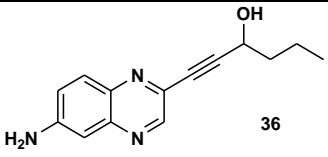
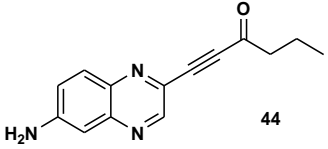
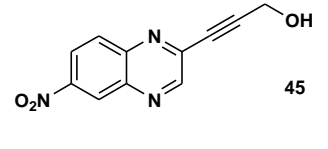
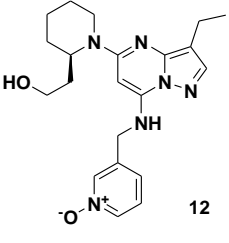
carboxyl group of Gln 131 as well as of Asp 86 with a distance of 2.11 and 1.91 Å respectively. One interaction was through hydrogen bond between hydrogen of another amino group on **42** and the carboxyl group of Leu 83 with a distance of 2.11 Å. Another one interaction was through hydrogen bond between hydroxyl group of **42** and the oxygen on carboxyl group of Glu 81 with a distance of 1.90 Å and another interaction was through hydrogen bond between H₂O and one of the nitrogen atoms in the ring on **42** with a distance of 2.18 Å. A degree of alignment was observed between native and docked structure with the RMSD value of 5.6011, indicating a successful docking procedure (**fig. 2.12**).

2.1.5. Structure based virtual screening against CDK2 (PDB code: 3QQJ)

Virtual screening workflow was applied on new chemical library of one hundred (100) different quinoxaline derivatives and four (4) were identified to be those structures which are most likely to bind to the therapeutic target, cyclin dependent kinase 2 (3QQJ). The docking score and glide energy of top 4 hit compounds are shown in **Table 2.5**. Docking results revealed the strong binding of top 4 hit compounds as well as the known molecule (dinaciclib **12**) with active site residues of binding pocket in the crystal structure of cyclin-dependent kinase 2.

Table 2.5: Docking results of the top 4 hit compounds identified from virtual screening as well as dinaciclib as a positive control inhibitor.

Compound ID	Docking score (kcal/mol)	Glide Evdw (kcal/mol)	Glide Ecoul (kcal/mol)	Glide energy (kcal/mol)	Total no. of Interactive bond	Interactive residues
 43	-8.147	-27.902	-6.842	-34.744	03	Leu 83 Lys 129 Thr 14

 36	-7.158	-31 103	-5 742	-36.845	02	Leu 83 Glu 12
 44	-6.330	-31 518	-3 294	-34.812	02	Leu 83 Glu 12
 45	-6.154	-31 868	-5 500	-37.367	02	Leu 83 Glu 12
 12	-6.937	-14.073	-5.552	-19.625	03	Glu 12 Leu 83 Asp 145

2.1.6. Induced fit docking and binding mode analysis

The identified four compounds were subsequently subjected to the flexible docking process through IFD in order to identify tight binding and also to establish whether protein flexibility improves the docking scores of the molecules that were prioritized for synthesis.

Table 2.6. Induced fit docking results of the top 4 hit compounds identified from virtual screening as well as dinaciclib as a positive control inhibitor.

Compound ID	Docking score (kcal /mol)	Glide E model (kcal /mol)	Glide energy (kcal /mol)	Total no. of Interactive bond	Interactive Residues-distance (Å)	IFD score (kcal /mol)
36	-7.931	-50.668	-41.495	03	Asp 145 - 1.78 Hie 84 - 2.18	-599.59

					H ₂ O - 2.00	
44	-7.882	-51.596	-36.292	02	Leu 83 - 2.17 Glu 12 - 2.00	-599.10
43	-7.752	-55.207	-37.312	01	Leu 83 - 2.60	-600.27
45	-6.351	-59.881	-43.175	02	Leu 83 - 2.14 Asp 145 - 1.79	-594.90
Dinaciclib 12	-11.301	-88.094	-51.693	02	Leu 83 - 2.28 Leu 83 - 2.60	-605.02

The binding mode of different compounds will be discussed in the following sections in order of the best to the poorest docking score.

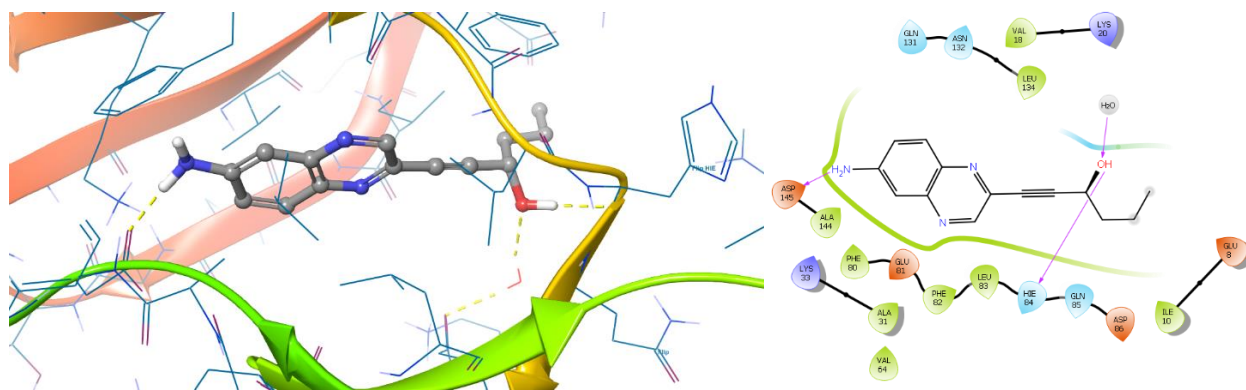


Figure 2.13: Model representation of molecular interaction analysis of **36** in the active site of cyclin dependent kinase 2 (3QQJ) and its 2D interaction profile, the hydrogen bond is shown by the purple line.

Binding mode of 36 in the active site of cyclin dependent kinase 2.

The highest docking score of compound **36** was found to be -7.931 kcal/mol, glide energy -41.495 kcal/mol, glide Emodel -50.668 kcal/mol, and IFD score -599.59 kcal/mol as depicted in **Table 2.6**. A total of three interactions were observed, two interactions were through hydrogen bonding between amino group from **36** and with the carboxyl group of Asp 145 and hydroxyl group with the carboxyl group of Hie 84 through a distance of 1.78 and 2.18 Å respectively. The other interaction was through hydrogen bond between Oxygen on the hydroxyl group of **36** with H₂O through a distance of 2.00 Å (**fig. 2.13**).

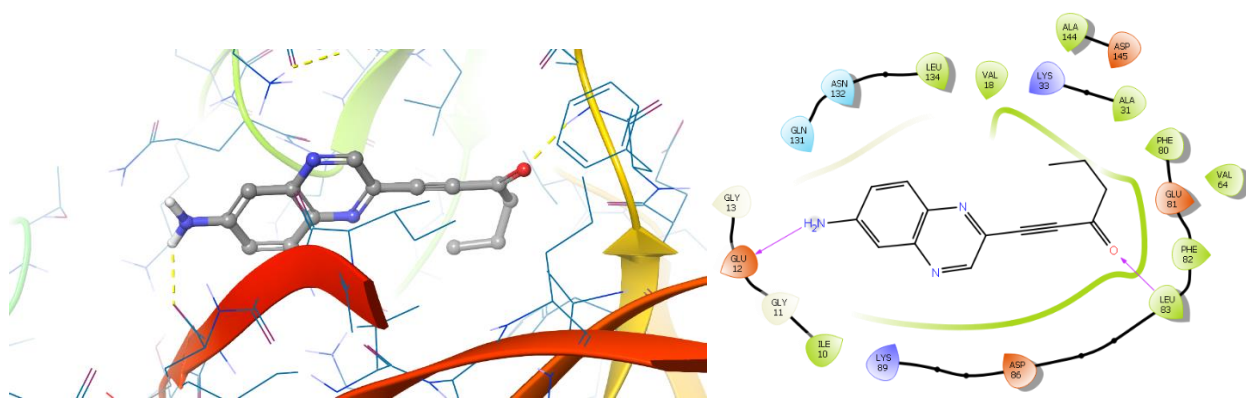


Figure 2.14: Model representation of molecular interaction analysis of **44** in the active site of cyclin dependent kinase 2 (3QQJ) and its 2D interaction profile respectively, the hydrogen bond is shown by the purple line.

Binding mode of 44 in the active site of cyclin dependent kinase 2.

The highest docking score of compound **44** was found to be -7.882 kcal/mol, glide energy -36.292 kcal/mol, glide Emodel -51.596 kcal/mol, and IFD score -599.10 kcal/mol as depicted in **Table 2.6**. A total of two interactions were observed, both interactions were through hydrogen bonding between amino group from **44** with Glu 12 through a distance of 2.00 Å and the amino group of Leu 83 with the oxygen on the carbonyl group of **44** with a distance of 2.17 Å (**fig. 2.14**).

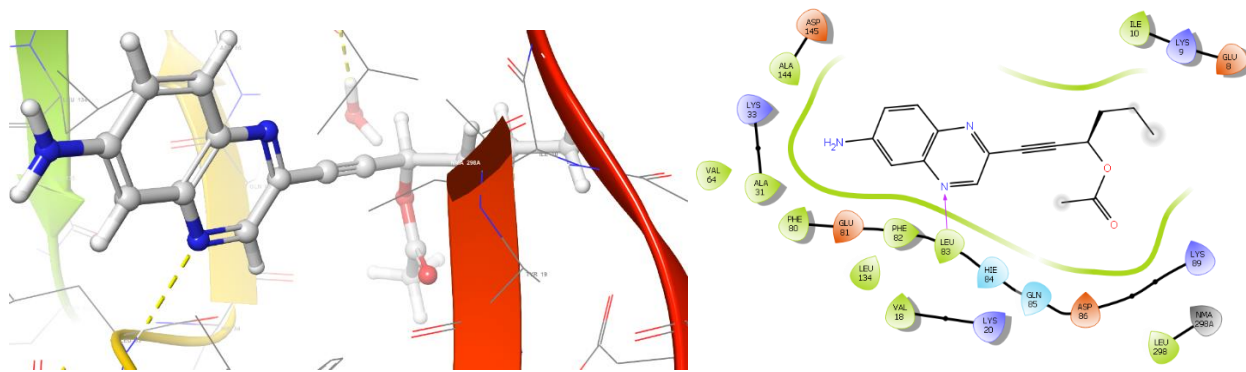


Figure 2.15: Model representation of molecular interaction analysis of **43** in the active site of cyclin dependent kinase 2 (3QQJ) and its 2D interaction profile respectively, the hydrogen bond is shown by the purple line.

Binding mode of **43** in the active site of cyclin dependent kinase 2.

The highest docking score of compound **43** was found to be -7.752 kcal/mol, glide energy -37.312 kcal/mol, glide Emodel -55.207 kcal/mol, and IFD score -600.27 kcal/mol as depicted in **Table 2.6**. Only one interaction was observed, amino group of Leu 83 interact with the nitrogen on the pyrazine ring of **43** through hydrogen bond with a distance of 2.60 Å (**fig. 2.15**).

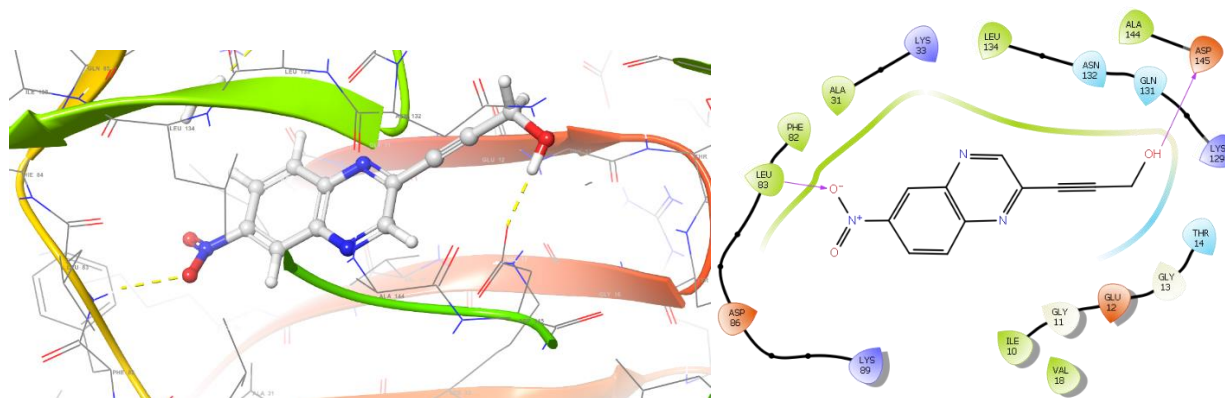


Figure 2.16: Model representation of molecular interaction analysis of **45** in the active site of cyclin dependent kinase (3QQJ) and its 2D interaction profile, the hydrogen bond is shown by the purple line.

Binding mode of 45 in the active site of cyclin dependent kinase 2.

The highest docking score of compound **45** was found to be -6.351 kcal/mol, glide energy -43.175 kcal/mol, glide Emodel -59.881 kcal/mol, and IFD score -594.90 kcal/mol as depicted in **Table 2.6**. A total of two interactions were observed, one interaction was through the amino group of Leu 83 with one of the oxygen on the nitro group of **45** through a distance of 2.14 Å, and another interaction was through hydrogen bond between hydrogen on the hydroxyl group of **45** with the carboxyl group of Asp 145 through a distance of 1.79 Å (**fig. 2.16**).

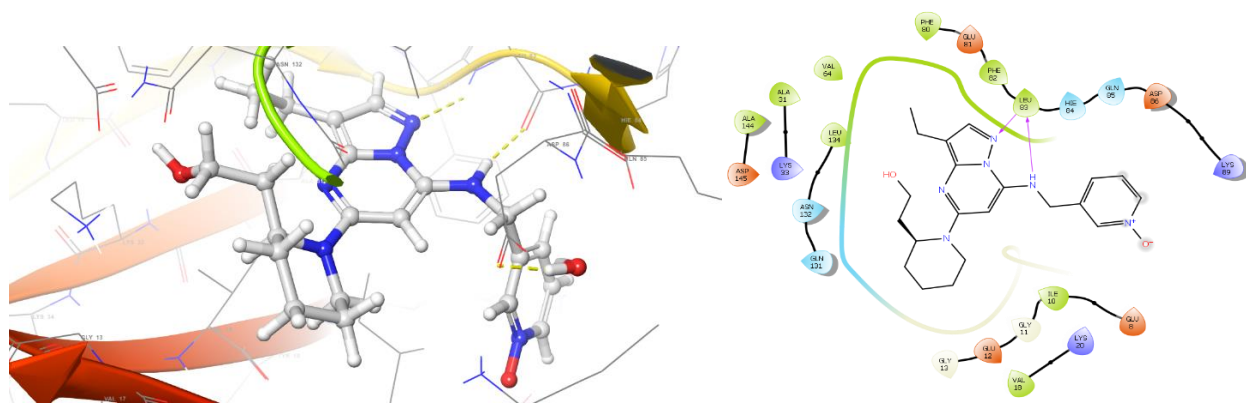


Figure 2.17: Model representation of molecular interaction analysis of **12** (dinaciclib) in the active site of cyclin dependent kinase (3QQJ) and its 2D interaction profile, the hydrogen bond is shown by the purple line.

Binding mode of 12 in the active site of cyclin dependent kinase 2.

The highest docking score of compound **12** was found to be -11.301 kcal/mol, glide energy -51.693 kcal/mol, glide Emodel -88.094 kcal/mol, and IFD score -605.02 kcal/mol as depicted in **Table 2.6**. A total of two interactions were observed, both interactions were through hydrogen bonding between the amino group and the carboxyl group of Leu 83 with nitrogen on the triazole group and the hydrogen on the secondary amine of **12** respectively with a distance of 2.60 and 2.28 Å (**fig. 2.17**).

There is no accurate correlation between docking score and the corresponding binding affinity, the docking scores can be employed just for classifying active ligands from inactives, but furthermore the in-vitro studies are required to check the potency of the compounds.

2.1.7. Physicochemical properties and ADME prediction

Physicochemical properties of hit compounds selected from both 3EQM and 3QQJ screening including known ligands from both enzymes were analysed to predict suitable ADME and drug like properties. The following results reveal the physicochemical properties of all identified compounds and all of them were found to have satisfactory ADME properties according to the criteria mentioned below and none of the compounds violated Lipinski's rule of five.

Table 2.7. ADME prediction of all selected compounds.

ID	MW	CNS	HBD	HBA	QPlogPo/w	QPlogS	QPlogBB	QPlogKp	%HOA	Rule Of Five
31	309.3 42	-2	1.500	5.000	2.824	-4.809	-1.342	-2.774	87.598	0
32	351.4 22	-2	1.500	5.000	3.991	-6.170	-1.428	-2.448	96.358	0
33	253.3 46	-1	1.500	3.000	3.491	-4.531	-0.936	-1.989	100.00	0
34	303.3 20	-2	1.500	5.000	2.833	-4.341	-1.381	-2.422	88.791	0
35	226.2 80	-1	3.500	4.000	0.996	-1.987	-0.743	-5.316	67.501	0
36	241.2 92	-2	2.500	4.700	1.832	-3.494	-1.277	-2.945	83.989	0
37	209.2 50	0	1.500	3.000	2.300	-3.488	-0.583	-2.380	94.530	0
38	225.2 93	-1	1.500	3.000	2.859	-4.041	-0.754	-2.181	100.00	0
39	199.2 12	-2	2.500	4.700	0.688	-2.230	-1.173	-3.384	74.728	0
40	345.4 00	-2	1.500	5.000	4.083	-6.123	-1.478	-2.140	100.00	0

41	241.2 49	-2	1.500	5.000	1.545	-3.638	-1.411	-3.523	78.465	0
43	283.3 29	-2	1.500	5.000	2.723	-4.835	-1.460	-3.102	88.023	0
44	239.2 76	-2	1.500	5.000	1.726	-3.486	-1.331	-3.292	81.097	0
45	229.1 95	-2	1.000	4.700	0.678	-2.897	-1.602	-4.188	67.691	0
8	285.3 07	-2	0.000	6.000	1.554	-3.947	-1.544	-3.202	75.737	0
12	396.4 91	-2	2.000	5.700	4.097	-5.722	-1.214	-2.662	100.00	0

Predicted properties concurred with standardized molecular descriptors criteria:

MW -Molecular weight of the molecule = (130.0 to 725.0).

CNS - Predicted central nervous system activity on a -2 (inactive) to +2 (active).

HBD - Estimated number of hydrogen bonds that would be donated by the solute to water molecules in an aqueous solution = (0.0 to 6.0).

HBA - Estimated number of hydrogen bonds that would be accepted by the solute from water molecules in an aqueous solution = (2.0 to 20.0).

QPlogPo/w - Predicted octanol/water partition coefficient = (-2.0 to 6.50).

QPlogS - Predicted aqueous solubility = (-6.5 to 0.5).

QPlogBB - Predicted brain/blood partition coefficient = (-3.0 to 1.2).

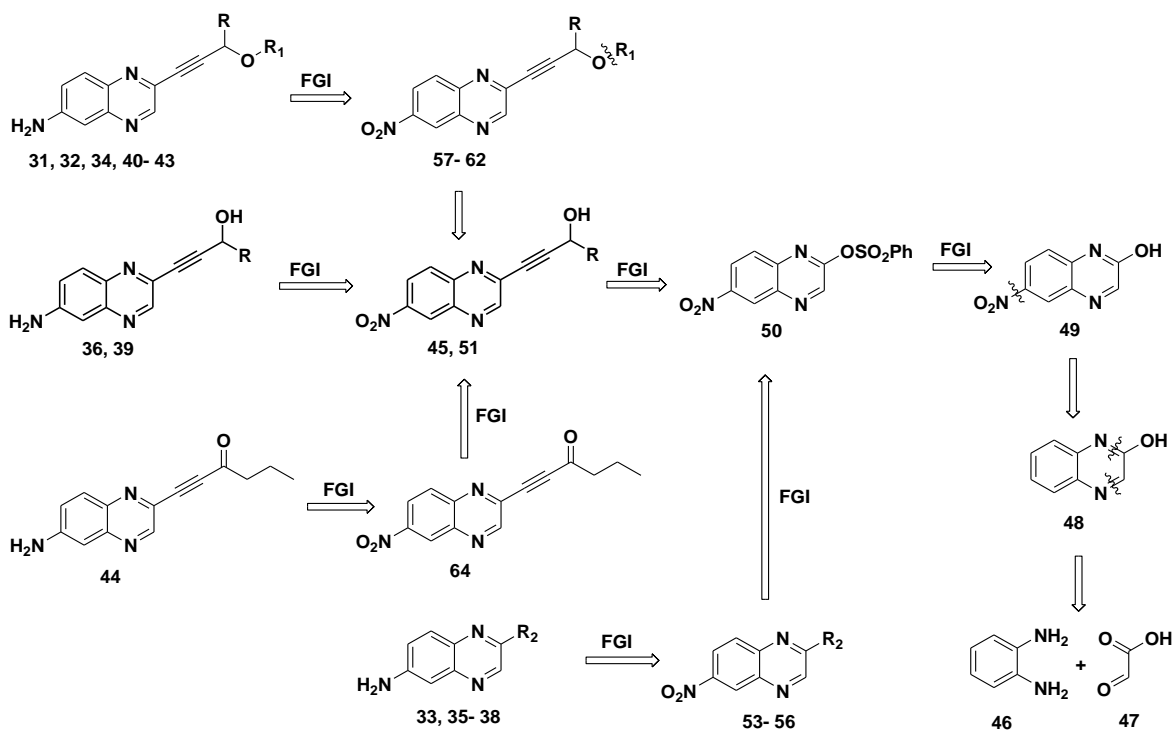
QPlogKp - Predicted skin permeability, log Kp = (-8.0 to -1.0).

%HOA - Predicted human oral absorption on 0 to 100% scale = >80% is high <25% is poor.

Rule of Five - The rules are: MW < 500, QPlogPo/w < 5, HBA ≤ 5, HBA ≤ 10. Compounds that satisfy these rules are considered drug-like. (The “five” refers to the limits, which are multiples of 5.) Number of violations of Lipinski’s rule of five = (maximum is 4).³

2.2. Chemistry

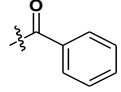
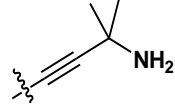
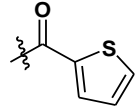

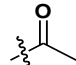
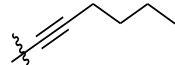
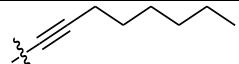
Based on the modelling results, it was decided that the compounds which were identified would be synthesised. **Scheme 2.0** shows a complete retrosynthetic route for the identified target molecules to the commercially available starting materials. Most of the step involves FGI because of the familiar reaction that can be used to introduce those groups. All amino quinoxalines derivatives **31- 43** can be obtained from nitro quinoxalines derivatives through amination reaction. The ketone derivative **44** and ester derivatives **57-62** can be obtained from derivatives with OH group through oxidation and esterification reactions respectively, whereas the alkyne can be introduced by Sonogashira cross-coupling reaction. The disconnection of **50** between O-S which can be connected by nucleophilic substitution reaction from hydroxyl group on **49**. The nitro group is cleaved, and it can be introduced by electrophilic aromatic substitution through nitration reaction. **48** is cleaved in two positions and it can easily be contracted by available reagents (*o*-phenylenediamine **46** and glyoxylic acid **47**) through cyclocondensation reaction.



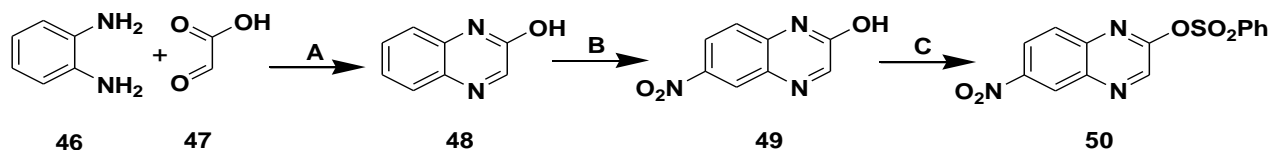
Scheme 2.0: Retrosynthesis of target molecules.

The table shows the possible representations of R, R₁ and R₂ on the **scheme 2.0**.

Table 2.8: Possible representation of R, R₁ and R₂.

R	R ₁	R ₂
-H		
-CH ₂ CH ₂ CH ₃		
		
		

The target quinoxaline derivatives were synthesized in a multi-step reaction sequence. The route to obtain the selected targets began with the synthesis of quinoxalin-2-ol **48** through cyclocondensation reaction between *o*-phenylenediamine **46** and glyoxylic acid **47** in a mixture of methanol and acetic acid. The resulting cream crude material was purified by recrystallization using dimethylformamide (DMF) to afford 75% yield of the desired product, quinoxaline-2-ol **48** as a tan solid following reaction A in **Scheme 2.1**. The nitration reaction was carried out following reaction B in **Scheme 2.1**. The nitronium ion, which was generated by mixture of potassium nitrate and sulfuric acid, underwent electrophilic aromatic substitution on the benzene ring of quinoxalin-2-ol **48** at six position to give 6-nitroquinoxalin-2-ol **49** in 97 % yield. The NMR analysis was found to be in good agreement with those reported in literature.⁴



Reagents and conditions: (A) Acetic acid, MeOH, 0 °C, 90 min, (B) KNO₃, H₂SO₄, rt, 120 min, (C) Benzenesulfonyl Chloride, DMAP, Et₃N, DCM, 0 °C, 90 min.

Scheme 2.1: Synthesis of quinoxalin-2-ol **48**, 6-nitroquinoxalin-2-ol **49** and 6-nitroquinoxalin-2-yl benzenesulfonate **50**.

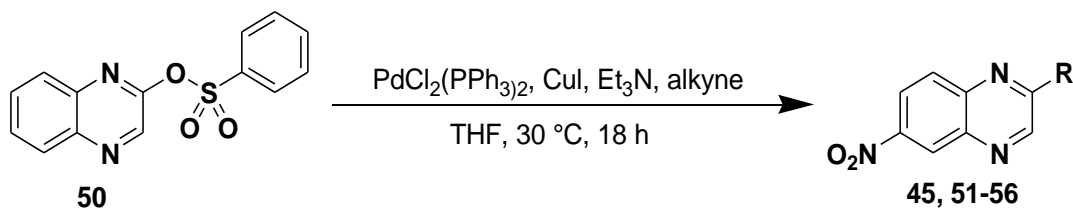
Hydroxyl group is not a good leaving group, so it was converted into benzene sulphonyl group which was reported to be a good leaving group during Sonogashira cross coupling reaction.⁴ 6-Nitroquinoxalin-2-ol **49** underwent base catalysed sulfonic esterification with benzene sulfonyl chloride in the presence of triethylamine and 4-dimethylaminopyridine (DMAP) using dichloromethane (DCM) as a solvent to afford 92% yield of 6-nitroquinoxalin-2-yl benzenesulfonate **50** as a yellow solid, which is a suitable starting material for the Sonogashira cross coupling reaction.

The disappearance of hydroxyl broad singlet signal around 12 ppm and the appearance of additional 3 signals which integrated for 5 hydrogens in the aromatic region on the proton NMR spectrum of compound **50** confirmed the successful incorporation of the benzene sulphonyl group. The sulphonyl intermediate **50** was subjected to Sonogashira cross-coupling reaction with propargyl alcohol in the presence of bis(triphenylphosphine) palladium(II) dichloride and copper iodide as catalysts and triethylamine as a base in tetrahydrofuran at 50 °C for 18 hour following a procedure from literature.⁵ The reaction was however unsuccessful, with starting material recovered. When the reaction was attempted at 25 °C, NMR spectrum revealed trace amounts of the product, 3-(6-nitroquinoxalin-2-yl) prop-2-yn-1-ol **45** together with a large amount of the starting material. When the reaction was attempted at 30 °C, a 66 % yield of **45** was obtained and it was confirmed by spectroscopic analysis as illustrated in **Table 2.9**. The -CH₂ protons signal was observed on the ¹H NMR spectrum at 4.44ppm integrating for two protons.

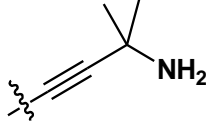
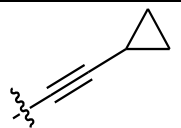
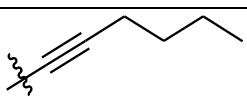
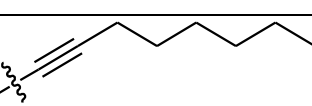
The new signals at 82.1 and 97.5 ppm on the ^{13}C NMR spectrum are consistent with carbons on the alkyne group, and the FTIR spectrum confirmed the presence of alkyne and hydroxyl functional groups with $\text{--C}\equiv\text{C--}$ stretching at 2340 cm^{-1} and OH stretching at 3282 cm^{-1} , respectively.

The Sonogashira cross coupling reaction was extended using numerous terminal alkynes under the same reaction conditions and the corresponding results are reported in **Table 2.9**.

Table 2.9. Sonogashira cross-coupling reaction on 6-nitroquinoxalin-2-yl benzenesulfonate using different terminal alkynes.



ID	R	% yield	ν_{max} $\text{C}\equiv\text{C}$ (cm^{-1})	Expected mass (g/mol)	Found mass (m/z)	mp. ($^\circ\text{C}$)
45		66	2340	230.9466 [M + H ⁺]	230.9597 [M + H ⁺]	117.3-118.5
51		89	2218	272.1037 [M + H ⁺]	272.1042 [M + H ⁺]	119.1-121.0
52		84	2226	258.0850 [M + H ⁺]	258.0886 [M + H ⁺]	195.0-195.9

53		98	2214	257.1040 [M + H ⁺]	257.1036 [M + H ⁺]	184.9-184.1
54		76	2210	240.9845 [M + H ⁺]	240.9881 [M + H ⁺]	197.4-199.1
55		63	2218	256.1088 [M + H ⁺]	256.1092 [M + H ⁺]	129.0-130.9
56		67	2214	284.1401 [M + H ⁺]	284.1404 [M + H ⁺]	200.5-202.5

All synthesized derivatives were purified using either column chromatography or trituration technique to obtain the products in a moderate to good yield (ranging from 63 to 98%). The ¹H NMR spectrum of compound **51** showed a triplet signal at 0.99 ppm, which integrated for three protons and that is consistent with a methyl group next to the methylene group. The two signals at 1.60 and 1.90 ppm, which both integrated for two protons are consistent with two methylene groups. The triplet signal at 4.74 ppm, which integrated for one proton is consistent with the methine group next to the electron withdrawing oxygen atom. A broad singlet signal at 2.8 ppm, which integrated for one proton is consistent with hydrogen of the hydroxyl group and that was also confirmed by the presence of OH stretching at 3249 cm⁻¹ in the FTIR spectrum. The signals at 81.8 and 98.0 ppm on the ¹³C NMR spectrum are consistent with carbons of the alkyne group and that was also confirmed by the presence of –C≡C– stretching at 2281 cm⁻¹ in the FTIR spectrum.

The ¹H NMR spectrum of compound **52** showed a singlet signal at 1.71 ppm, which integrated for six protons and that is consistent with two methyl groups on the tertiary alcohol. The signals at 79.6 and 99.9 ppm on the ¹³C NMR spectrum are consistent with

carbons of the alkyne group, and the FTIR spectrum confirmed the presence of alkyne and hydroxyl groups by showing $\text{--C}\equiv\text{C--}$ stretching at 2226 cm^{-1} and OH stretching at 3433 cm^{-1} .

The ^1H NMR spectrum of compound **53** showed a singlet signal at 1.51 ppm, which integrated for six protons and that is consistent with two methyl groups on the tertiary carbon next to NH_2 . The signals at 77.2 and 78.0 ppm on the ^{13}C NMR spectrum are consistent with carbons of the alkyne group, and the FTIR spectrum confirmed the presence of alkyne and primary amine groups by showing $\text{--C}\equiv\text{C--}$ stretching at 2214 cm^{-1} and NH_2 stretching at 3290 and 3319 cm^{-1} .

The ^1H NMR spectrum of compound **54** showed a doublet signal at 0.96 ppm, which integrated for four protons and that is consistent with two CH_2 groups that are chemically equivalent. The signals at 74.3 and 103.5 ppm on the ^{13}C NMR spectrum are consistent with carbons on the alkyne group, and the FTIR spectrum confirmed the presence of alkyne by showing $\text{--C}\equiv\text{C--}$ stretching at 2210 cm^{-1} .

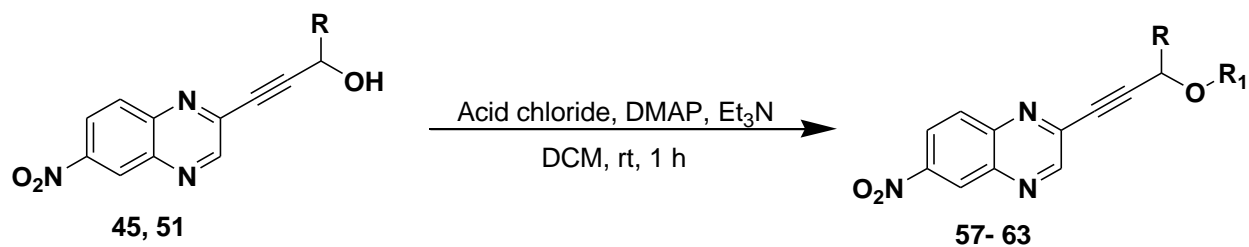
The ^1H NMR spectrum of compound **55** showed a triplet signal at 0.96 ppm, which integrated for three protons and that is consistent with a methyl group next to the methylene group. The two signals at 1.51 and 1.58 ppm, which each integrated for two protons are consistent with two methylene groups. The triple signal at 2.57 ppm, which integrated for two protons is consistent with the methylene group next to another methylene group and alkyne group. The ^{13}C NMR spectrum showed signals at 78.8 and 99.9 ppm that are consistent with carbons of the alkyne group and that was also confirmed by the presence of $\text{--C}\equiv\text{C--}$ stretching at 2218 cm^{-1} on the FTIR spectrum.

The ^1H NMR spectrum of compound **56** showed a triplet signal at 0.88 ppm, which integrated for three protons and that is consistent with a methyl group next to the

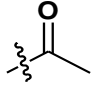
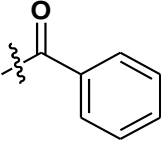
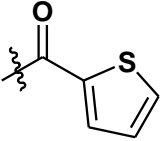

methylene group. The three signals at 1.31, 1.47 and 1.68 ppm, each integrating for two protons are consistent with three methylene groups. The triplet signal at 2.55 ppm, which is integrated for two protons, is consistent with a methylene group next to another methylene group and alkyne group. The ^{13}C NMR spectrum showed signals at 78.8 and 99.9 ppm which are consistent with carbons of the alkyne group and that was also confirmed by the presence of $-\text{C}\equiv\text{C}-$ stretching at 2214 cm^{-1} on the FTIR spectrum. The high-resolution mass spec of **45**, **51-56** gave the expected masses within 0.005 units as depicted in **Table 2.9**.

Taking advantage of hydroxyl group at the propargylic position of 3-(6-nitroquinoxalin-2-yl) prop-2-yn-1-ol **45** and 1-(6-nitroquinoxalin-2-yl)hex-1-yn-3-ol **51**, esterification reaction was performed using the method by Hussein M *et al.*⁶ To a solution of alcohol in DCM, triethylamine (3.5 eq.), 0.2 mol % of DMAP, was added 1.2 eq. of acyl chloride and the reaction mixture was stirred under nitrogen for 1 hour at room temperature.⁶

Table 2.10. Esterification reaction of alcohol at the propargylic position.



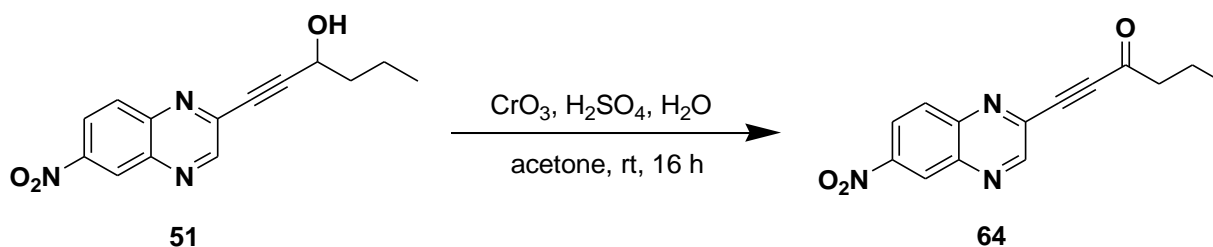
ID	R	R ₁	% yield	ν_{max} C=O (cm^{-1})	Expected Mass (g/mol)	Found mass (m/z)	mp. ($^{\circ}\text{C}$)
57	-H		42	1741	272.0693 [M + H ⁺]	272.0668 [M + H ⁺]	153.7- 155.3

58	- CH ₂ CH ₂ CH ₃		69	1741	314.1143 [M + H ⁺]	314.1146 [M + H ⁺]	109.2- 110.1
59	-H		46	1716	334.0830 [M + H ⁺]	334.0833 [M + H ⁺]	177.0- 179.3
60	- CH ₂ CH ₂ CH ₃		43	1724	376.1299 [M + H ⁺]	376.1309 [M + H ⁺]	78.5- 79.1
61	-H		40	1712	340.0394 [M + H ⁺]	340.399 [M + H ⁺]	168.0- 170.0
62	- CH ₂ CH ₂ CH ₃		54	1708	382.0863 [M + H ⁺]	382.0876 [M + H ⁺]	76.4- 77.2
63	-H		33	-	-	-	146.5- 148.9

A series of 6-nitroquinoxaline with functionally substituted alkyne ester derivatives **57- 62** were isolated after purification using column chromatography with yields ranging from 40 to 69 % and their structures were confirmed by FTIR, NMR and mass spectroscopy, the physical property (melting point) was also recorded. The FTIR spectra of the compounds **57- 62** revealed the presence of -C=O stretching at around 1741-1708 cm⁻¹ and asymmetrical -C-O-C and -C-O stretching at 1246-1171 cm⁻¹ in addition to the -C≡C- stretch which appeared as a weak stretch at 2340-2100 cm⁻¹. On the other hand, the ¹H NMR spectra of compounds **57- 62** showed additional proton signals corresponding to the hydrogens of the incoming acid chloride. The ¹³C NMR spectra of the compounds **57- 62** showed additional signals around 160 ppm which is consistent with the carbonyl carbon of the ester group. Mesylate ester derivative **63** was obtained in 33 % yield from **45**. The ¹H NMR spectrum of compound **63** showed the appearance of a singlet signal at 3.21 ppm, which integrated for three protons and that is consistent with CH₃ on the mesyl

group and that triggered CH₂ signal to shift from 4.44 to 5.19 ppm due the inductive effect caused by the introduced group. The high-resolution mass spec of **57-62** gave the expected masses within 0.005 units as depicted in **Table 2.10**.

Attempts to synthesise a ketone derivative from corresponding alcohol via oxidation reaction using Dess-Martin Periodinane for 16 hours following literature method,⁷ was unsuccessful. The NMR spectrum showed a trace amount of the product, together with a large amount of the starting material. The crude material was then further reacted with Jones reagent for same duration following the method previously reported by Mercier *et al.*, where full conversion was observed with 77 % yield obtained. The requirement for strong acidic conditions was demonstrated by the incapability of Dess-Martin Periodinane to promote oxidation reaction on **51** according Scheme 2.4.⁸



Scheme 2.4: Oxidation reaction.

The ¹H NMR spectrum (**Figure 2.19**) showed the disappearance of the OH singlet signal which was at 2.8 ppm on the structure of **51**. The disappearance of the hydrogen on the tertiary carbon signal which was at 4.7 ppm, triggered the signal for hydrogens at alpha carbon (C12) to change from multiplet to triplet. The ¹³C NMR spectrum of **64** showed a signal at 186.7 ppm as depicted in **Figure 2.20**, which is consistent with the carbonyl carbon at ketonic region and that was also confirmed by FTIR spectrum showing the disappearance of OH stretching and the appearance of -C=O stretching at 1671 cm⁻¹. The high-resolution mass spectrum is also in agreement with the molecular weight of structure (C₁₄H₁₂N₃O₃= 270.0880), where [M + H⁺] = m/z 270.0883 is observed in **Figure 2.21**, which is within 0.005 unit as expected.

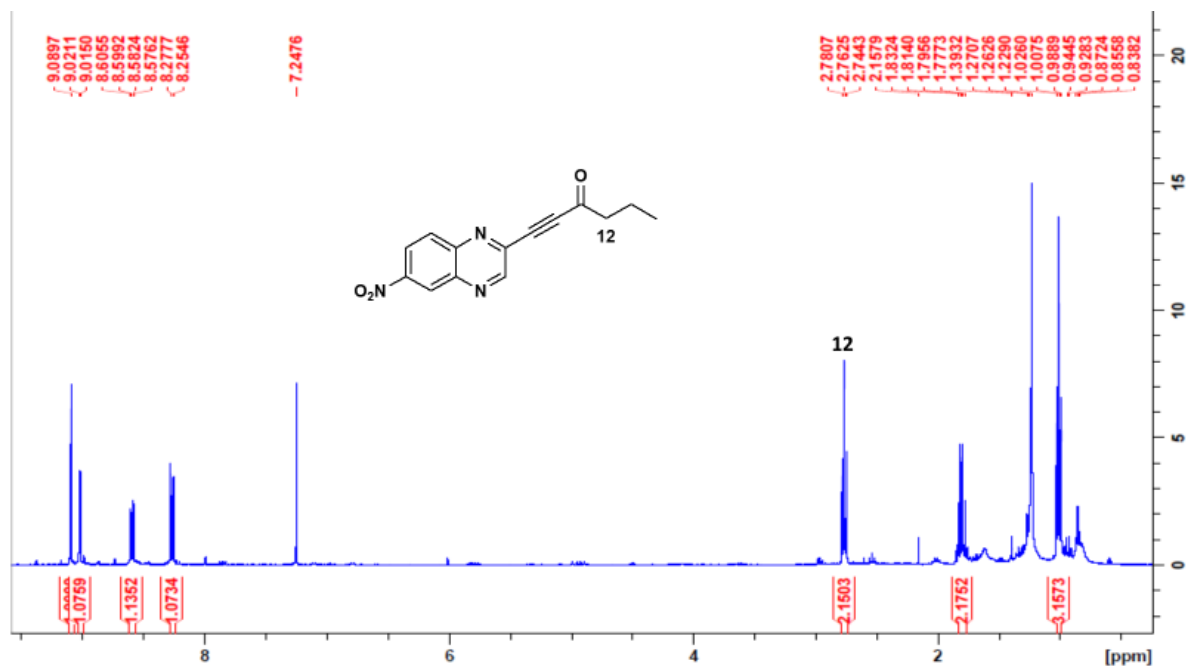


Figure 2.19: ¹H NMR spectrum of 1-(6-nitroquinoxalin-2-yl)hex-1-yn-3-one **64**

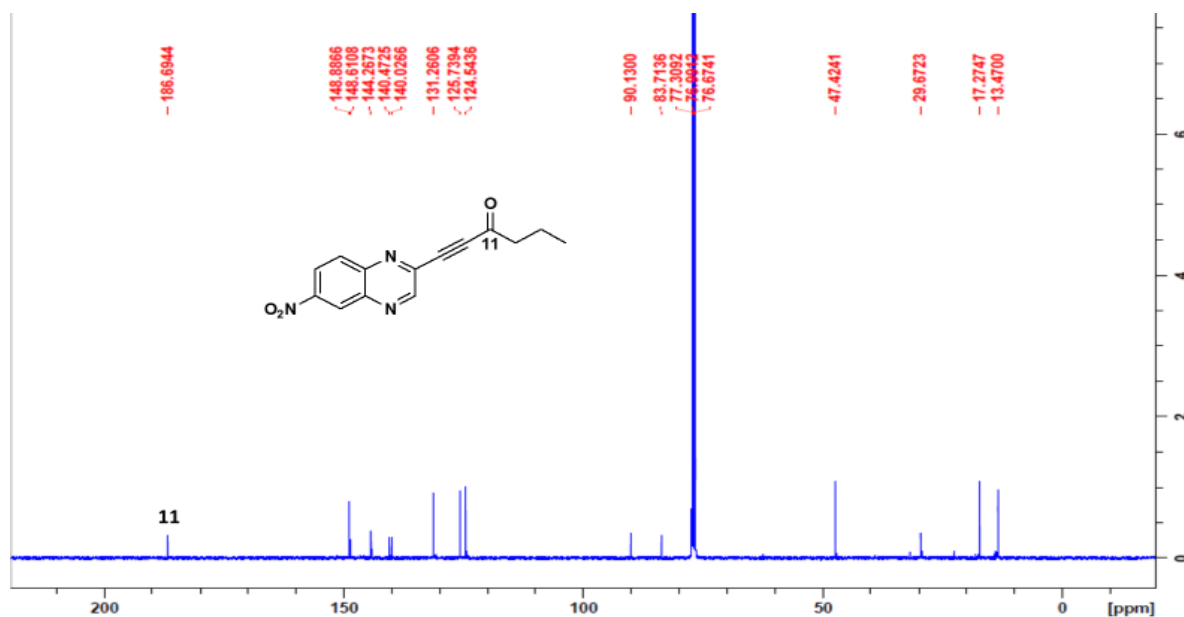


Figure 2.20: ¹³C NMR spectrum of 1-(6-nitroquinoxalin-2-yl)hex-1-yn-3-one **64**

When the reduction reactions were attempted on 3-(6-nitroquinoxalin-2-yl) prop-2-yn-1-ol **45** and 1-(6-nitroquinoxalin-2-yl)hex-1-yn-3-ol **51** following **Scheme 2.5** and its conditions, the reaction was unsuccessful.

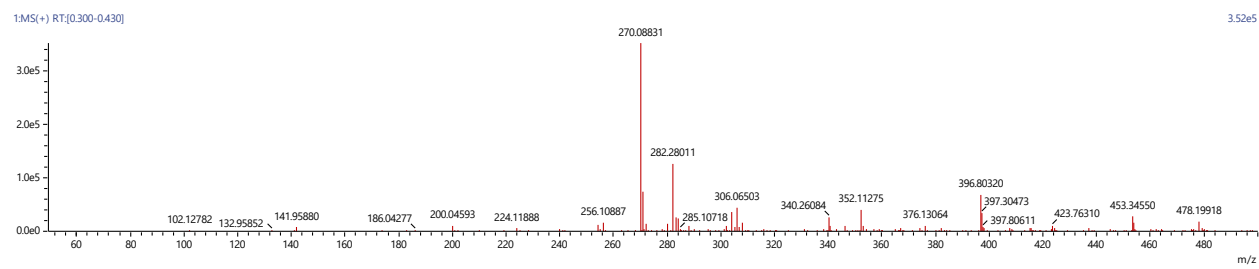
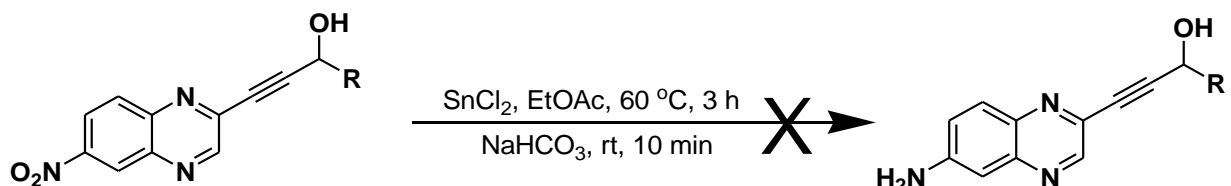


Figure 2.21: Mass spectrum of 1-(6-nitroquinoxalin-2-yl)hex-1-yn-3-ol **64**



Where R = -H, -CH₂CH₂CH₃

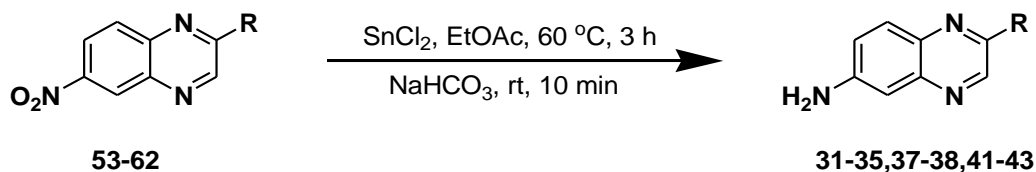
Scheme 2.5: Reduction reaction of 6-nitroquinoxaline with alkyne functionality.

Both attempts at reduction of the nitro group of 6-nitroquinoxaline with functionally substituted alkyne derivatives constituting hydroxyl group were not tolerated under the above reaction conditions (**Scheme 2.5**). The reason could be the molecule had both nucleophilic (NH₂) and electrophilic centre (C-OH) which could result in polymerisation as the starting materials were not recovered and the mixture could not be properly characterised.

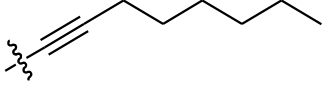
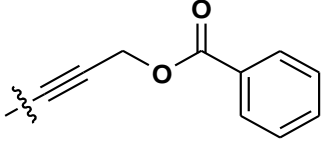
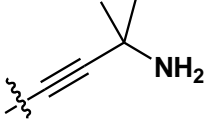

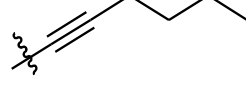
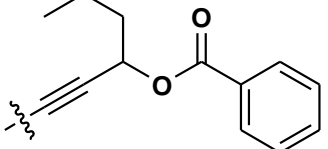
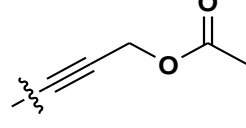
When the reduction reaction was attempted on 3-(6-nitroquinoxalin-2-yl)prop-2-ynylthiophene-2-carboxylate **61** under the same above-mentioned conditions, SnCl₂ as a mild reducing agent was able to reduce the nitro to amino group in the presence of another reducible group. Following a literature procedure, to a suspension of **61** in ethyl acetate was added SnCl₂ (5 eq.) and the reaction mixture was refluxed for 3 hours. After cooling to room temperature, saturated sodium hydrogen carbonate solution was added and stirred for a minimum of 10 minutes, insoluble SnClOH precipitated out of the solution to form a sticky residue which was filtered through gravitational filtration, followed by

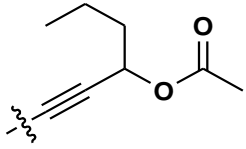
normal workup and a 43 % of **31** was obtained after purification with prep-TLC.⁹ The structure of **31** was confirmed through NMR, IR and mass spectroscopy. The NH₂ protons were observed in the ¹H NMR spectrum as a broad singlet signal at 4.38 ppm which integrated for two protons and was also confirmed by the presence of doublet vibrational signal of NH₂ stretching at 3225 and 3335 cm⁻¹. The reduction reaction was extended to other 6-nitroquinoxaline with functionally substituted alkyne under the same reaction conditions and the corresponding results are reported in **Table 2.11**.

Table 2.11. Reduction reaction of 6-nitroquinoxaline with alkynes functionality.



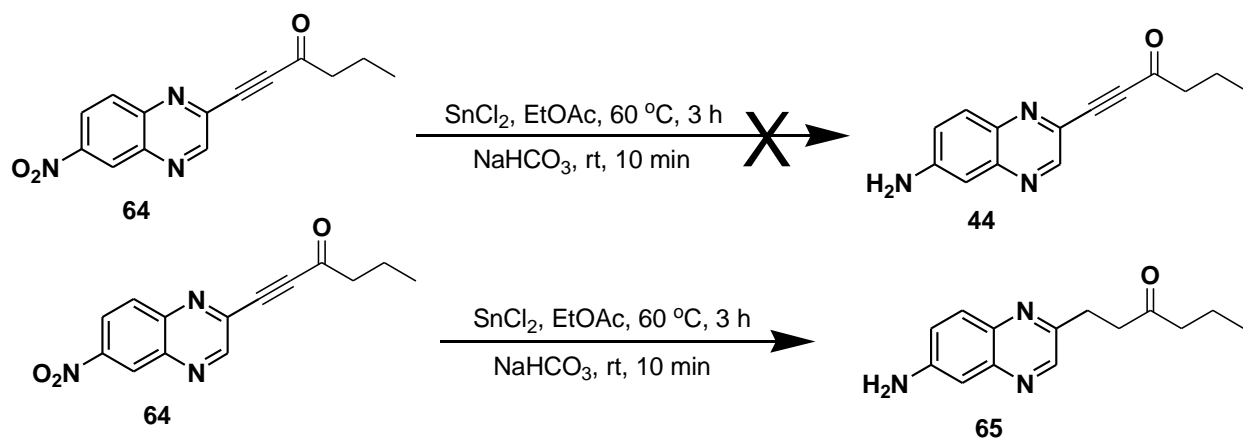
ID	R	% yield	V _{max} NH ₂ (cm ⁻¹)	Expected mass (g/mol)	Found mass (m/z)	Mp. (°C)
31		43	3335 & 3225	310.0652 [M + H ⁺]	310.0660 [M + H ⁺]	140.3- 141.9
32		66	3339 & 3217	352.1121 [M + H ⁺]	352.1134 [M + H ⁺]	220.5- 221.6

33		57	3347 & 3221	254.1659 [M + H ⁺]	254.1664 [M + H ⁺]	341.6- 343.1
34		75	3335 & 3221	304.1088 [M + H ⁺]	304.1094 [M + H ⁺]	199.3- 201.5
35		77	3323 & 3196	227.1298 [M + H ⁺]	227.1298 [M + H ⁺]	97.5-99.2
37		65	3307 & 3188	210.1033 [M + H ⁺]	210.1042 [M + H ⁺]	92.1-93.4
38		95	3335 & 3218	226,1346 [M + H ⁺]	226.1340 [M + H ⁺]	273.8- 274.7
40		89	3339 & 3217	346.1557 [M + H ⁺]	346.1572 [M + H ⁺]	250.5- 251.2
41		51	3307 & 3192	242.0931 [M + H ⁺]	242.0941 [M + H ⁺]	95.6- 96.9

43		96	3343 & 3217	284.1401 [M + H ⁺]	284.1410 [M + H ⁺]	114.9- 116.1
----	---	----	-------------------	-----------------------------------	-----------------------------------	-----------------

The target 6-aminoquinoxaline substituted alkynyl derivatives from **Table 2.11** were obtained in moderate to good yields by the reduction reaction of the nitro group. All synthesized derivatives from **Table 2.11** were confirmed by various spectroscopic techniques such as FTIR, NMR and mass spectrometry; the physical property (melting points) were also recorded as uncorrected. The ¹H NMR spectra of the compounds from **Table 2.11** showed the additional broad singlet signals at around 4 ppm which integrated for two protons and that is consistent with NH₂, and it was confirmed by the appearance of NH₂ stretching as two bands at around 3188-3343 cm⁻¹ in the FTIR spectra. In addition, the ¹H NMR spectra of compounds from **Table 2.11** also demonstrated that conversion of -NO₂ to NH₂ group triggered the doublet and doublet of doublet signals of protons at C5 and C7 to shift to lower chemical shift due to the lesser inductive effect of NH₂ as compared to the nitro group. The high-resolution mass spec of **31-35,37-38,40-43** gave the expected masses within 0.005 units as depicted in **Table 2.11**.

The reduction reaction of the nitro group on 1-(6-nitroquinoxalin-2-yl)hex-1-yn-3-one did not yield the expected product. Surprisingly, the mild reducing agent SnCl₂ was also able to reduce the triple bond to single bond in addition to reducing nitro group and compound **65** was isolated in low 22 % yield as shown in **Scheme 2.7**. It is likely that the conjugated pi system between carbonyl and alkyne groups weakened the triple bond. Oxygen is more electronegative than carbon, so it will withdraw pi electron towards itself causing carbon to be more electropositive leading to the weakening of the triple bond.



Scheme 2.7: Reduction reaction of 1-(6-nitroquinoxalin-2-yl)hex-1-yn-3-one

The ^1H NMR spectra of compound **65** (Figure 2.22) showed a broad singlet signal at 4.11 ppm which integrated for two protons, that is consistent with $-\text{NH}_2$. The appearance of two triplet signals, each integrating for 2 hydrogens at 2.97-3.22 ppm suggest additional two CH_2 's and is consistent with hydrogens at C9 and C10.

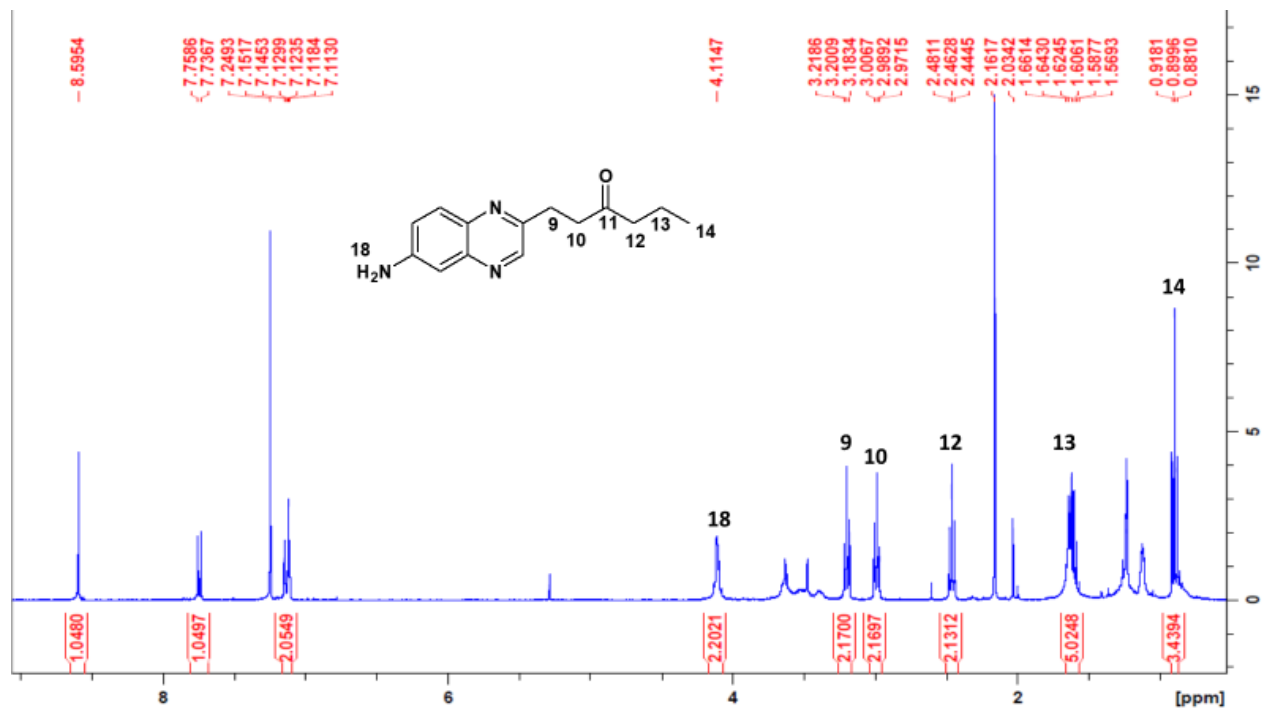


Figure 2.22: ^1H NMR spectrum of 1-(6-aminoquinoxalin-2-yl)hexan-3-one **65**

COSY spectrum (**Figure 2.23**) confirmed that hydrogen at C9 is only correlating with hydrogen at C10 and hydrogens at C13 is correlating with both hydrogens at C12 and C14. The high-resolution mass spectrum is also in agreement with the molecular weight of structure ($C_{14}H_{18}N_3O = 244.1452$), where $[M + H^+] = m/z 244.1466$ is observed in **Figure 2.24**. The DEPT spectrum (**Figure 2.25**) also confirmed the suggestion by showing the 4 negative signals at up field region which is consistent with four CH_2 's on **65**.

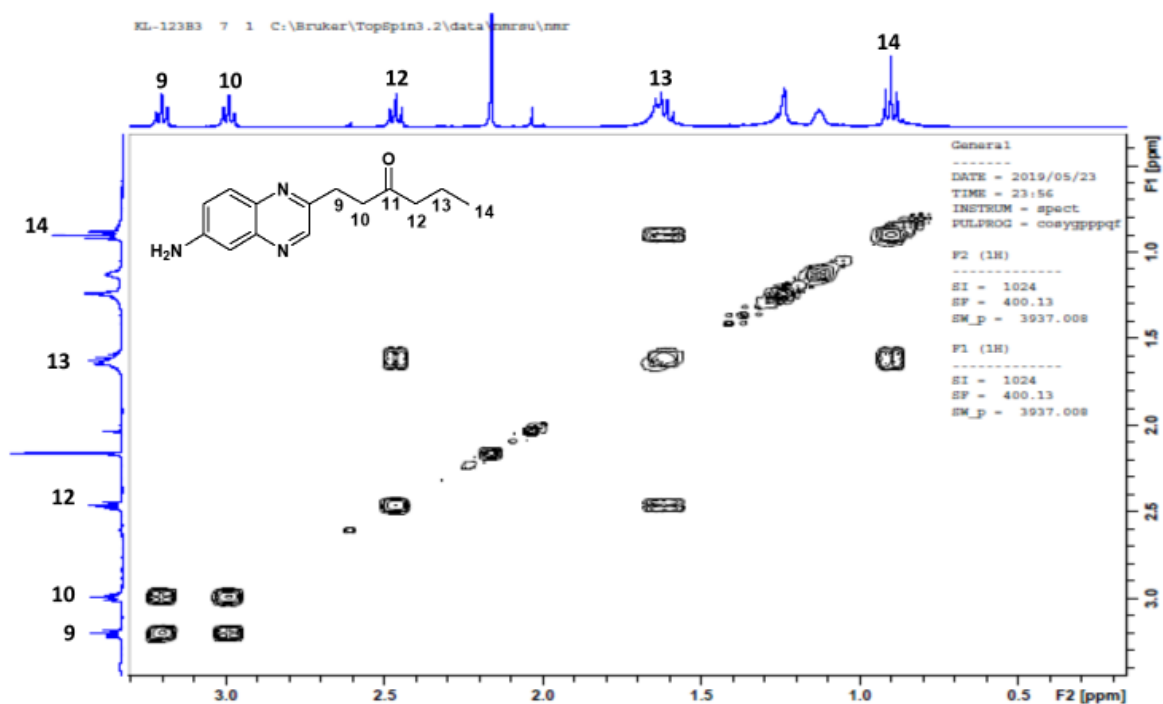


Figure 2.23: COSY NMR spectrum of 1-(6-aminoquinoxalin-2-yl)hexan-3-one **65**

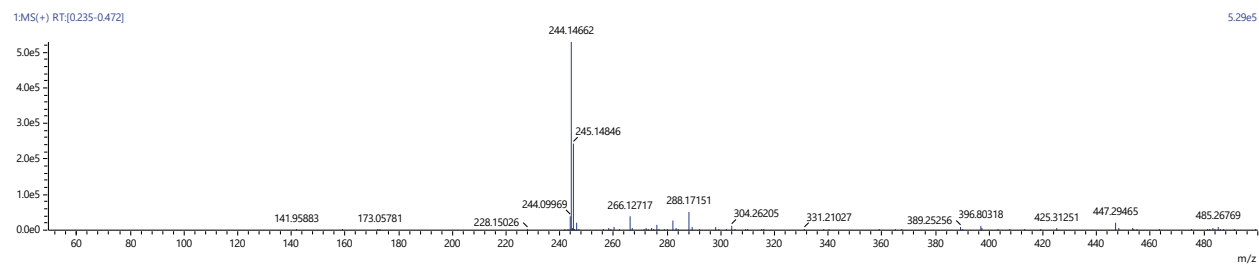


Figure 2.24: Mass spectrum of 1-(6-aminoquinoxalin-2-yl)hexan-3-one **65**

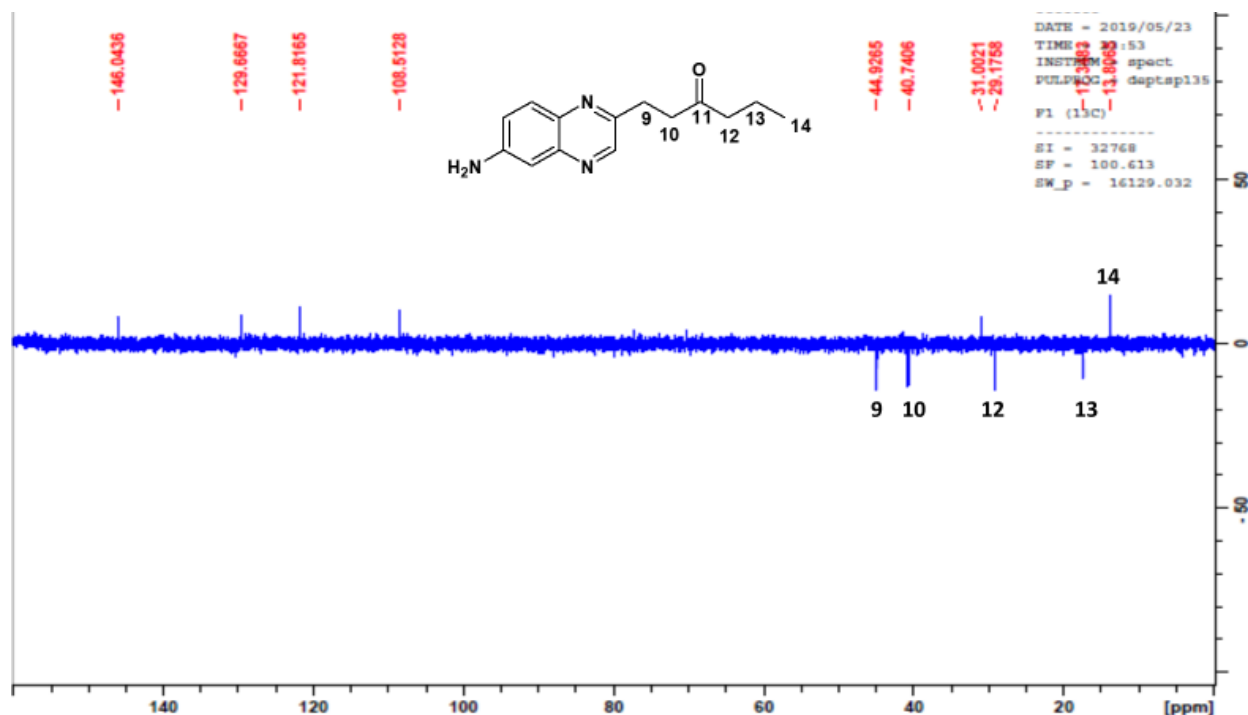
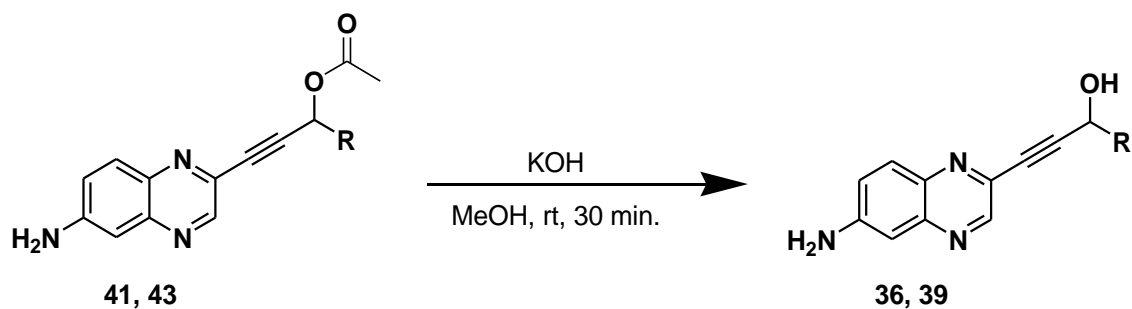


Figure 2.25: DEPT NMR spectrum of 1-(6-aminoquinoxalin-2-yl)hexan-3-one **65**



Where, R = CH₂CH₂CH₃, H

Scheme 2.8: Hydrolysis reaction of 6-aminoquinoxaline with acetate group.

The two esters, **41** and **43** underwent hydrolysis reactions (**scheme 2.8**) after being dissolved in a solution of methanol (10 ml) and KOH (1 eq.), and stirred for 30 min at room temperature to yield both 1-(6-aminoquinoxalin-2-yl)hex-1-yn-3-ol **36** in 13 % yield

and 3-(6-aminoquinoxalin-2-yl)prop-2-yn-1-ol **39** in 25 % yield separately according to Scheme 2.8 following literature method reported elsewhere.¹⁰

The yields of both 1-(6-aminoquinoxalin-2-yl)hex-1-yn-3-ol **36** and 3-(6-aminoquinoxalin-2-yl)prop-2-yn-1-ol **39** were increased to 83 % and 87 %, respectively, by allowing the methanol to evaporate without concentrating it on a rotary evaporator because it was realised that both crude materials changed colour from yellow to black when heated. This suggested that both crude materials were heat sensitive and could be undergoing polymerisation, as observed previously. The products were obtained as yellow solids and FTIR, NMR and mass spectral data were consistent with both proposed structures.

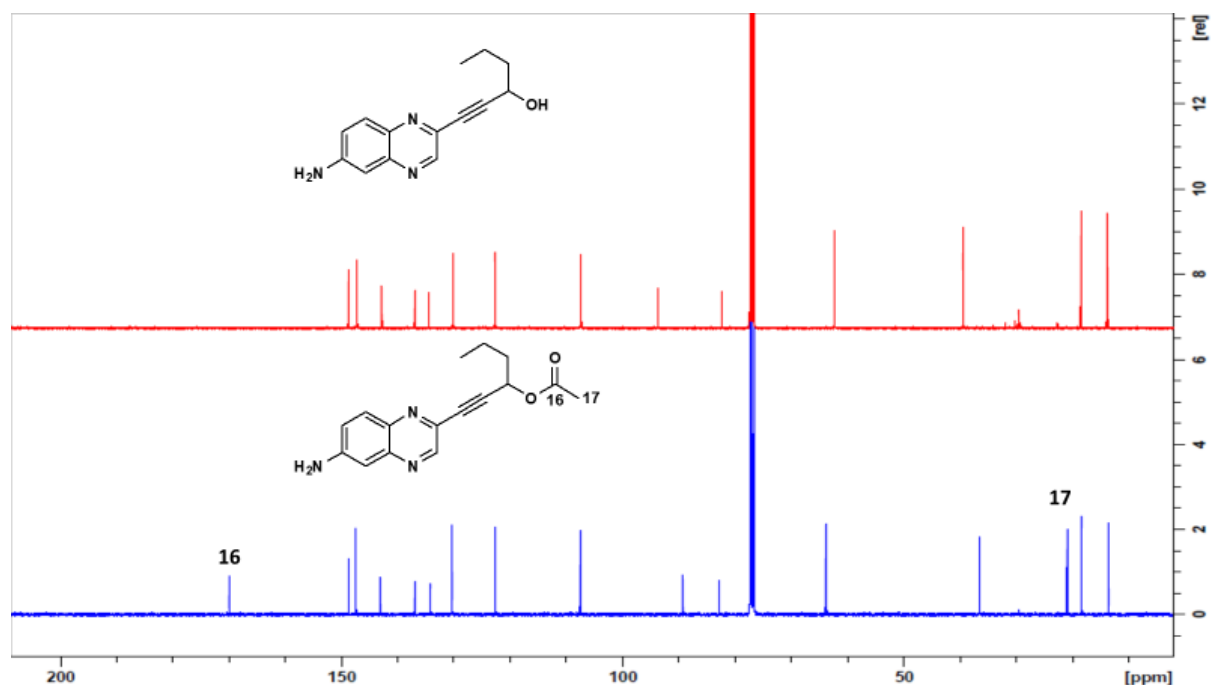


Figure 2.26: The stacked ¹³C NMR spectrum of 1-(6-aminoquinoxalin-2-yl)hex-1-yn-3-yl acetate **43** (in blue) and 1-(6-aminoquinoxalin-2-yl)hex-1-yn-3-ol **36** (in red)

The FTIR spectra of both **36** and **39** showed the disappearance of C=O stretching at 1741-1708 cm⁻¹ and that was also confirmed by ¹³C NMR spectra of both compounds **36**

and **39** showing the disappearance of $-\text{CH}_3$ of the acetyl group C17 signal at aliphatic region and the carbonyl carbon of the ester group C16 signal at around 170 ppm. The ^{13}C NMR spectrum (in red) showed a total number of 14 carbons, which correspond to the total number of carbons in the 1-(6-aminoquinoxalin-2-yl)hex-1-yn-3-ol **36** (**Figure 2.26**). The high-resolution mass spectrum is also in agreement with the molecular weight of structure ($\text{C}_{14}\text{H}_{15}\text{N}_3\text{OH} = 242.1295$), where $[\text{M} + \text{H}^+] = m/z$ 242.1264 is observed in **Figure 2.27**, which is within 0.005 unit as expected.

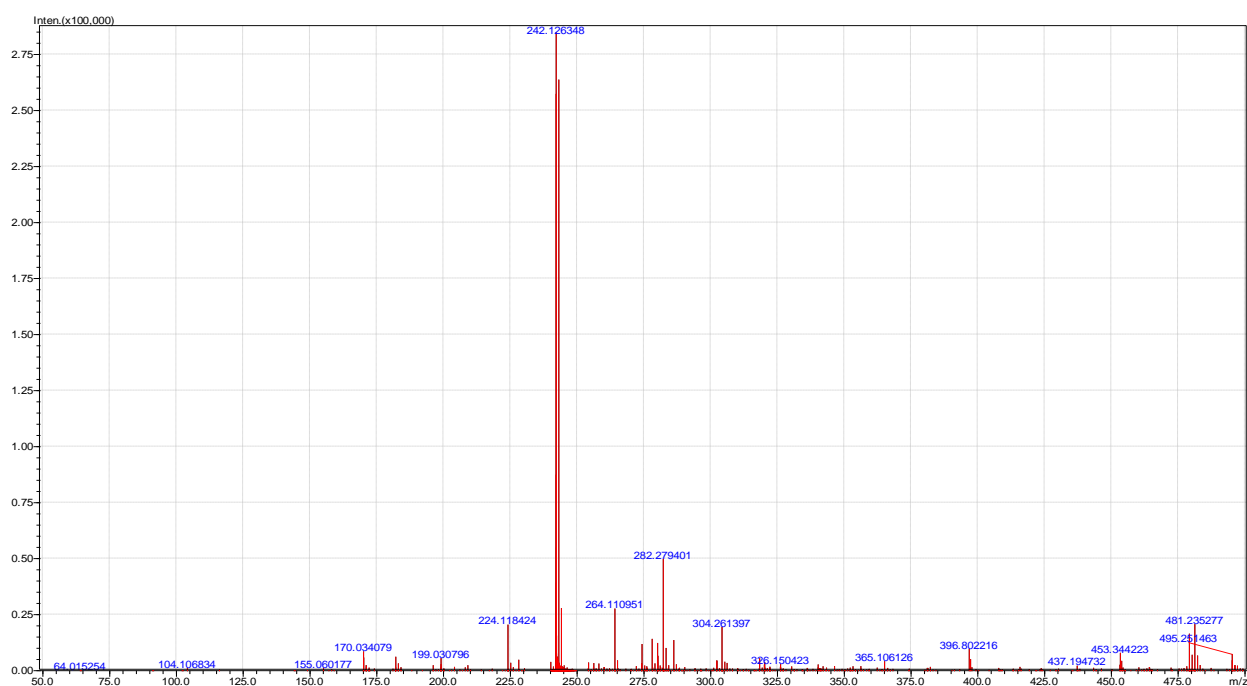


Figure 2.27: Mass spectrum of 1-(6-aminoquinoxalin-2-yl)hex-1-yn-3-ol **36**

2.3. Biological evaluation

2.3.1. Evaluation of synthesised compounds against breast cancer (MCF-7)

The biological activity of the newly synthesised series of amino and quinoxaline derivatives were evaluated against breast cancer (MCF-7) at the University of Limpopo, biochemistry department. The cell viability was assessed by MTT (3-(4,5-Dimethylthiazol2-yl)-2,5-Diphenyltetrazolium Bromide) assay on human breast cancer cell line (MCF-7) in the concentration range of 0 - 100 μM . The preliminary data obtained is shown in **Table 2.12**.

Table 2.12: The preliminary results of the *in vitro* evaluation of synthesised compounds against breast cancer (MCF-7).

Entry	Compound ID	MCF-7 IC_{50} (μM)	Raw 264.7 IC_{50} (μM)
1	31	69.660	>100
2	32	>100	
3	33	>100	>100
4	34	35.597	>100
5	35	>100	79.983
6	36	>100	>100
7	37	>100	>100
8	38	>100	>100
9	39	>100	
10	40	>100	
11	41	69.807	>100

12	43	>100	>100
13	45	>100	
14	51	>100	
15	54	29.116	20.214
16	55	>100	
17	56	16.328	81.703
18	59	9.102	0.205
19	61	32.115	41.559
20	65	>100	

Quinoxaline nucleuses exhibit potential anticancer activity, some quinoxaline derivatives have been previously reported to show very promising activity against breast cancer (MCF-7).¹¹ The newly synthesised novel amino and nitro-quinoxaline derivatives were evaluated for anti-proliferative activity against breast cancer (MCF-7). Based on the results on **Table 2.12**, the synthesized quinoxaline derivatives showed dose dependent inhibitory activities, with most of them showing activity at high concentrations. Compound **59** was shown to possess more potent inhibition against MCF-7 with IC₅₀ of 9.102 μ M, whereas compounds **34**, **54**, **56** and **61** showed promising activity against MCF-7 with an IC₅₀ value of < 50 μ M. Compounds **31** and **41** had low activity against MCF-7 with an IC₅₀ value of > 50 μ M, while the other compounds had no activity against MCF-7. In addition, the results of MTT assay illustrated that **59** had an IC₅₀ value of 0.205 μ M against Raw 264.7 cell line, which confirmed that **59** could not selectively kill tumour cells. Compound **34** was the only compound with IC₅₀ value of < 50 μ M activity against MCF-7 which had IC₅₀ value of > 100 μ M against Raw 264.7 cell line and that confirmed its selectivity to inhibit only tumour cells.

The in vitro anti-aromatase activity of the compounds **31** and **34** was valued using a commercial Aromatase (CYP19A) assay kit (fluorimetric). The results are shown in **Figure 2.28**.

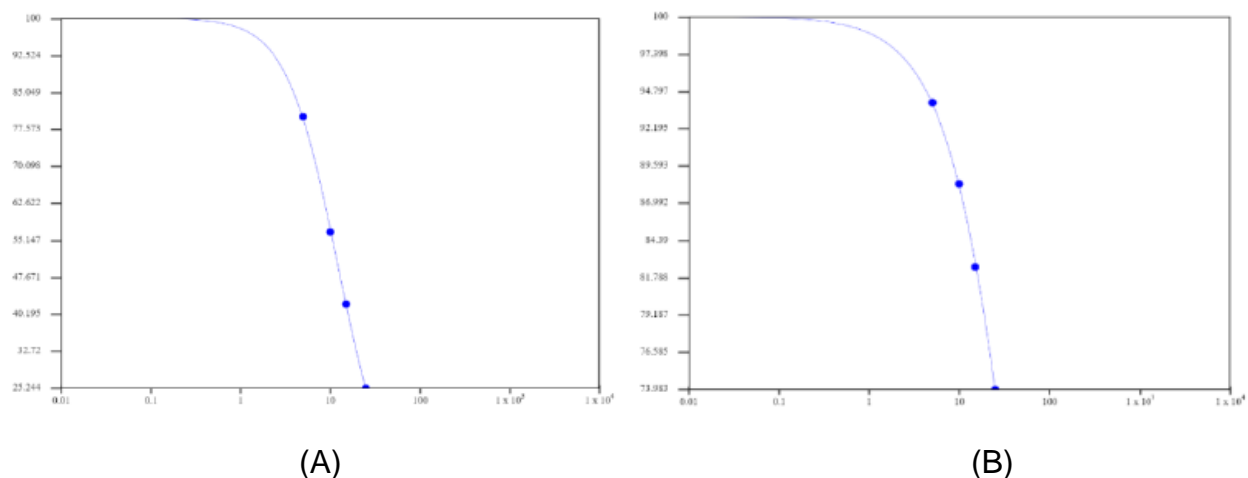


Figure 2.28: The dose-response plots of (A) compound **31** with IC₅₀ of 12.166 μM and compound **34** with IC₅₀ of 66.744 μM.

Compounds **31** and **34** were evaluated for anti-proliferative activity against CYP19A enzyme. Compound **31** was shown to possess good inhibition against CYP19A with an IC₅₀ of 12.166 μM, whereas compound **34** had low activity against CYP19A enzyme with an IC₅₀ value of > 50 μM. Compounds **31** and **34** served as a starting point toward studying the correlation between molecular modelling (*in-silico*) and CYP19A inhibition activities, and a good correlation between them (**Fig. 2.28**) was observed as compounds **31** and **34** were identified to be those molecules which are most likely to bind to the drug targets (CYP19A) with the docking score of -8.372 and 7.630 kcal/mol in **Table 2.2**.

2.3.2. Evaluation of synthesised compounds against *M tuberculosis*

Small molecules with quinoxaline moiety were recently reported as potent inhibitors of *Mycobacterium tuberculosis* H₃₇Rv strain. Some of the compounds have shown promising inhibition activity against *Mycobacterium tuberculosis*. Because of the structural similarities, a series of novel amino and nitro-quinoxaline derivatives were

evaluated for antimycobacterial activity as part of the secondary study against *Mycobacterium tuberculosis* since their antimycobacterial properties on the H₃₇Rv strains were not evaluated before.^{12,13}

The in-vitro antimycobacterial activity of the synthesised compounds was performed at the drug discovery and development centre (H₃D), university of Cape Town. The preliminary results are presented in **Table 2.13** for in-vitro antimycobacterial activity was obtained following broth dilution method in 7H9 CAS GLU TX media. The compounds were assayed within a 14-day period using Mtb H₃₇RV strain with rifampicin as a reference drug. A compound was considered inactive when it showed activity at a concentration >100 μM.

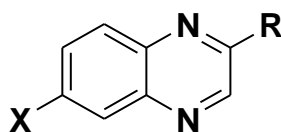
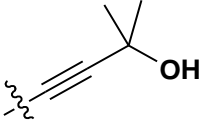
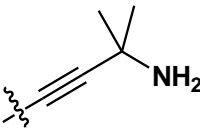
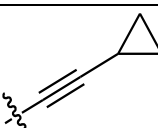
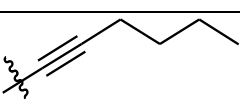
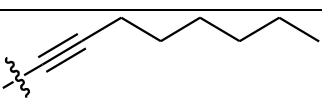


Table 2.13: The preliminary results of amino and nitro-quinoxaline with functionally substituted alkyne derivatives against Mtb H₃₇Rv strain.

Entry	Compound ID	X	R	MIC ₉₀ (μM)
1	45	-NO ₂		4,26
2	39	-NH ₂		>100
3	51	-NO ₂		9,51
4	36	-NH ₂		29,77
5	64	-NO ₂		14,36

6	52	-NO ₂		4,97
7	53	-NO ₂		>100
8	35	-NH ₂		>100
9	54	-NO ₂		60,52
10	37	-NH ₂		86,62
11	55	-NO ₂		63,92
12	38	-NH ₂		>100
13	56	-NO ₂		>100
14	33	-NH ₂		>100

In previous studies 3-(quinoxalin-3-yl)prop-2-yn-1-ol **30** and 3-(6-chloroquinoxalin-3-yl)prop-2-yn-1-ol found to possess potential antimycobacterial properties with MIC₉₀ of 52.77 and 1.63 μM respectively.¹³ As a part of our ongoing program, 3-(6-nitroquinoxalin-2-yl) prop-2-yn-1-ol **45** was assessed against Mtb H₃₇Rv strain and it was found to possess antimycobacterial activity at MIC₉₀ of 4.26 μM. However, its corresponding amino derivative **39** was found to exhibit poor antimycobacterial at MIC₉₀ > 100 μM. Compound **51** with a secondary alcohol was shown to be one of the most active compounds with MIC₉₀ value of 9.51 μM. When the nitro group of **51** was replaced with the amino group at C-6 of quinoxaline moiety, there was a significant decrease in antitubercular activity (compound **36**, MIC₉₀ = 29.77 μM). However, when the secondary alcohol of **51** was replaced with the ketonic group, there was a minor decrease in activity for compound **64** (MIC₉₀ = 14.36 μM). Compound **52** with a terminal tertiary alcohol was found to possess antimycobacterial activity at MIC₉₀ of 4.97 μM. However, compound **53** with a terminal tertiary amine and its corresponding amino derivative **35** were found to exhibit poor antimycobacterial at MIC₉₀ > 100 μM. Compounds **54**, **37**, **55**, **38**, **56** and **33** with aliphatic

groups were found to be ranging from slightly poor activity to completely inactive with MIC₉₀ values of 60.52 to >100 μM.

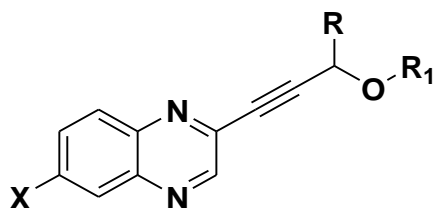


Table 2.14: The preliminary results of amino and nitro-quinoxaline ester derivatives against Mtb H₃₇Rv strain.

Entry	Compound ID	X	R	R ₁	MIC ₉₀ (μM)
1	57	-NO ₂	-H		1.80
2	41	-NH ₂	-H		>100
3	58	-NO ₂	-CH ₂ CH ₂ CH ₃		1,56
4	43	-NH ₂	-CH ₂ CH ₂ CH ₃		>100
5	59	-NO ₂	-H		93.76
6	34	-NH ₂	-H		25,83
7	60	-NO ₂	-CH ₂ CH ₂ CH ₃		<0.65
8	40	-NH ₂	-CH ₂ CH ₂ CH ₃		>100
9	61	-NO ₂	-H		2.74
10	31	-NH ₂	-H		50,52
11	62	-NO ₂	-CH ₂ CH ₂ CH ₃		<0.64
12	32	-NH ₂	-CH ₂ CH ₂ CH ₃		>100
13	63	-NO ₂	-H		1.59

Quinoxaline alkynyl ester derivatives **57** - **63** bearing a nitro group at C-6 were found to exhibit improved antimycobacterial activity at $MIC_{90} < 2.74 \mu M$ except a compound **59** with a phenyl ester which exhibited poor activity at MIC_{90} value of $93.76 \mu M$. Compounds **60** and **62** were found to be most active against Mtb H37Rv with the high activity at MIC_{90} of <0.65 and $<0.64 \mu M$ respectively. As shown in Table 2.14, compounds **57** - **62** with nitro-quinoxaline derivatives exhibited potent activities on the Mtb H₃₇Rv strain as compared to their corresponding amino derivatives with the exception of compound **59** and its corresponding amino derivative.

2.4. References

1. Gumede, N. J., Nxumalo, W., Bisetty, K., Gilabert, L. E. and Medina-hernandez, M. J. Prospective computational design and in vitro bio-analytical tests of new chemical entities as potential selective CYP17A1 lyase inhibitors. *Bioorg. Chem.*, 1-20 (2019).
2. Kitchen, D. B., Decornez, H., Furr, J. R. and Bajorath, J. Docking and scoring in virtual screening for drug discovery: Methods and applications. *Nat. Rev. Drug Discov.*, **3**, 935–949 (2004).
3. Panwar, U. and Singh, S. K. Structure-based virtual screening toward the discovery of novel inhibitors for impeding the protein-protein interaction between HIV-1 integrase and human lens epithelium-derived growth factor (LEDGF /p75). *J. Biomol. Struct. Dyn.*, **1102**, 1–19 (2017).
4. Nxumalo, W. and Dinsmore, A. Preparation of 6-Ethynylpteridine Derivatives by Sonogashira Coupling. *ChemInform*, **44**, 79-89 (2013).
5. Sibiya, M. A., Raphoko, L., Mangokoana, D., Makola, R., Nxumalo, W. and Matsebatlela, T. M. Induction of Cell Death in Human A549 Cells Using 3-(Quinoxaline-3-yl) Prop-2-ynyl Methanosulphonate and 3-(Quinoxaline-3-yl) Prop-2-yn-1-ol. *Molecules*, **24**, 1-16 (2019)
6. Hussein, M., Dine, A. N., Farès, F., Dorcet, V., Hachem, A. and Grée, R. A new direct synthesis of α -methylene- and α -alkylidene- β -lactams. *Tet. Lett.*, **57**, 1990–1993 (2016).
7. Karim, R., Hebray, M., Collison, D., David, C. and Joule, J. A. A bis (h 5 - cyclopentadienyl) cobalt complex of a bis-dithiolene : a chemical analogue of the metal centres of the DMSO reductase family of molybdenum and tungsten enzymes, in particular ferredoxin aldehyde oxidoreductase. *Tetrahedron*, **614**, 11010–11019 (2005).
8. Mercier, L. G., Remorova, A. A., Fillion, E., Tre, V. E. and Carson, R. J. Oxidative

coupling of 2-substituted 1,2-dihydro-1-naphthols using Jones reagent: a simple entry into 3,3,0-disubstituted. *Tet. Lett.*, **46**, 1091–1094 (2005).

9. Laurent, D., Ferrié, L., Sepulveda-Diaz, J. E., Majid Amar, M., Harfouche, A., Séon-Méniel, B., Raisman-Vozari, R., Michel, P. P. and Figade, B. New 6-Aminoquinoxaline Derivatives with Neuroprotective Effect on Dopaminergic Neurons in Cellular and Animal Parkinson Disease Models. *J. Med. Chem.*, **59**, 6169–6186 (2016).
10. Riss, P. J., Hummerich, R. and Schloss, P. Synthesis and monoamine uptake inhibition of conformationally constrained 2 β -carbomethoxy-3 β -phenyl tropanes. *Org. Biomol. Chem.*, **7**, 2688–2698 (2009).
11. Pereira, J. A., Pessoa, A. M., Cordeiro, M. N. D., Fernandes, R., Prudêncio, C., Noronha, J. P. and Vieira, M. Quinoxaline, its derivatives and applications: A State of the Art review. *Eur. J. Med. Chem.* **97**, 664–672 (2015).
12. Yang, J., Pi, W., Xiong, L., Ang, W., Yang, T., He, J., Liu, Y., Chang, Y., Ye, W., Wang, Z., Luo, Y. and Wei, Y. three protons -1, 2, 4-Dithiazol-3-one compounds as novel potential affordable antitubercular agents. *Bioorg. Med. Chem. Lett.* **23**, 1424–1427 (2013).
13. Raphoko, L. A. Synthesis of quinoxaline-ferrocene compounds and their medicinal properties against mycobacterium tuberculosis. (MSc dissertation). University of Limpopo, South Africa, 1–108 (2019).

Chapter 3

Conclusions

3.1. Conclusion

A Library of novel one hundred (100) quinoxaline derivatives were successfully designed based on the chemical we have in our laboratory catalogue and screened against target proteins (CYP19A1 and CDK2) using virtual screening technique and thirteen (13) molecules were identified to be hit compounds against both targets with the docking score ranging from -6.143 to -8.372 kcal/mol representing the binding affinity. The hit compounds were subjected to IFD in order to identify tight binding through the intermolecular interactions with active site residues of the binding pocket of the target proteins. Docking results exposed the solid interactions of hit compounds with active residues of binding pocket in the crystal structure of human placental aromatase (3EQM) and the active site residues of binding pocket in the crystal structure of cyclin-dependent kinase 2 (3QQJ). All identified nitro and amino quinoxaline alkyne derivatives were successfully synthesised in moderate to good yields and their spectroscopic analysis (NMR, FTIR and MS) were in good agreement with the proposed structure.

The newly synthesised novel amino and nitro-quinoxaline derivatives were evaluated for anti-proliferative activity against breast cancer (MCF-7). In conclusion, compound **59** was shown to possess good inhibition against MCF-7, whereas compounds **34**, **54**, **56** and **61** showed promising activity against MCF-7. Compounds **31** and **41** had low activity against MCF-7, while the other compounds (**32**, **33**, **35-40**, **43**, **45**, **51**, **55**, **65**) had no activity against MCF-7. Based on the MTT results, it was concluded that **59** was shown to be toxic with an IC₅₀ value of 0.205 µM against Raw 264.7 cell line. The results have indicated that **31** and **34** had the promising anti-cancer activity against CYP19A and the correlation between molecular modelling (*in-silico*) and CYP19A inhibition activities (*in-vitro*), was established as compounds **31** and **34** were identified to bind to the drug target (CYP19A).

All the synthesized compounds were evaluated for the antitubercular activity against Mtb H₃₇Rv strain. As the results shown in **Tables 2.13 and 2.14**, these derivatives showed different inhibitory effects against Mtb and most of the compounds **36**, **37**, **45**, **51**, **52**, **54**,

55, 57- 64 showed quite moderate to excellent antitubercular activities. In specific, compounds **57 - 62** with nitro-quinoxaline derivatives exhibited potent activities on the Mtb H₃₇Rv strain as compared to their corresponding amino derivatives with the exception of compound **59** and its corresponding amino derivative. This indicates that the most electron withdraw group (NO₂) at C-6 position on quinoxaline moiety may play a part on the potency in this structural class of compounds.

3.2. Future work

In future, the evaluation for *in-vitro* antiproliferative activity against breast cancer cell lines (MCF-7) for the rest of the synthesised compounds will be performed. The enzyme-based assay for the rest of the predicted compounds will be performed in order to establish the correlation between the biological results and the molecular modeling studies. Furthermore, all compounds showing promising antimycobacterial and antiproliferative activity will be evaluated for cytotoxicity to determine the safety of the compounds. Due to the current COVID-19 situation, we couldn't finish all the outstanding work and we can never be certain on when results will be ready, and this may delay us even more. Furthermore, new derivatives containing electron withdrawing groups (MeO) at C-6 can be explored for anticancer and antimycobacterial activity and perform docking by incorporating metal coordination constraints, to design drugs that follow type II interaction.

Chapter 4

Methodology

4.1. Molecular modelling

All computational studies were performed on Schrödinger Suite 2018. Maestro was used to access Schrödinger modules: LigPrep, Protein Preparation Wizard Prime, Visual Screening workflow, Induced Fit Docking and QikProp. The crystal structure of human placental aromatase (PDB code: 3EQM with the resolution of 2.90 Å) and cyclin dependent kinase (PDB code: 3QQJ with the resolution of 1.70 Å) were retrieved from the protein data bank (www.rcsb.org). Cross-docking was employed to verify the performance of the docking process. Virtual Screening process was executed in the VSW using *in silico* protocol such as high-throughput virtual screening (HTVS), standard precision, and extra precision with default parameters to screen a library of one hundred (100) compounds and filter best possible compounds with higher score of docking. The identified hit compounds (according to docking score) were subjected to the flexible docking process through Induced Fit Docking (IFD) using default parameters with a maximum number of 10 poses. Physicochemical properties of all identified compounds were analysed by QikProp module to predict suitable ADME and drug like properties following the method ascribed in the literature.^{1,2}

4.2. Chemistry

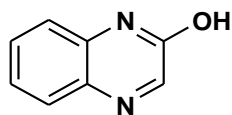
General information

Commercially available reagents and solvents were purchased from Sigma Aldrich and Merck (South Africa). All materials were used as received from commercial sources without further purification, unless stated otherwise. All reactions involving moisture-sensitive reagents were performed under nitrogen (N₂) atmosphere using oven-dried glassware. Tetrahydrofuran (THF) was freshly distilled over sodium/benzophenone under N₂ atmosphere before use. Teflon-coated magnetic stir bars were soaked in concentrated nitric acid for at least 5 minutes, washed repeatedly with deionized water then acetone prior to use. All measurements were performed at room temperature. Thin layer chromatography was conducted on self-cut Merck silica gel F254 0.255 mm plates, and spots were visualised where appropriate, by ultraviolet fluorescence at 254 or 297 nm. Flash column chromatography was performed using Merck Kiesel gel 60 (230–400

mesh). Analytical preparative thin layer chromatography (TLC) on silica gel plates was employed during some of the purification.

The structural properties of the compounds were recorded and confirmed by: High-resolution mass spectra were recorded using Waters Synapt G2, ESI probe, ESI Pos, Cone Voltage 15 V (Waters Corp., Milford, MA, USA); Melting points were obtained using Lasec/SA-melting point apparatus from Lasec company, SA (Johannesburg, South Africa) and were recorded as uncorrected; IR spectra were recorded using Bruker Alpha platinum-ATR, FTIR spectrometer; and Nuclear Magnetic Resonance (NMR) (Bruker Ascend 400 MHz Topspin 3.2). All chemical shifts are reported in parts per million downfield from tetramethylsilane. Peak multiplicities are denoted by brs (broad singlet), s (singlet), d (doublet), t (triplet), q (quartet), quin (quintet), sex (sextet) and m (multiplet) or by a combination of these e.g. dd (double of doublet), with coupling constants (J) given in Hz. ^1H NMR and ^{13}C NMR spectra were referenced internally using solvent signals, ^1H NMR: 7.25 ppm for CDCl_3 , 2.50 ppm for DMSO-d_6 , 3.31 ppm for MeOD; ^{13}C NMR: 77.0 ppm for CDCl_3 , 39.9 ppm for DMSO-d_6 , 49.1 ppm for MeOD respectively at room temperature.

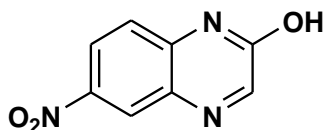
4.2.1. Preparation of quinoxalin-2-ol (**48**)³



O-phenylenediamine **46** (10.0 g, 92 mmol) was dissolved in a mixture of acetic acid (20 mL) and methanol (20 mL). The solution was cooled to 0 °C with stirring. A solution of 50 % glyoxylic acid **47** in water (8.50 g, 92 mmol, 1 eq.) was added dropwise over 30 minutes and the solution was further stirred for 90 minutes at 0°C. The solvent was removed by filtration, then the residue was washed with water (15 mL), followed by methanol (15 mL) and air dried to give a cream white solid. The resulting solid was purified by recrystallization in dimethylformamide (DMF) to give quinoxaline-2-ol **48** as a tan solid (10.069 g, 75%); M.p 265-267 °C (Lit. 266-267 °C);³ ^1H NMR (400 MHz, DMSO-d_6 , ppm)

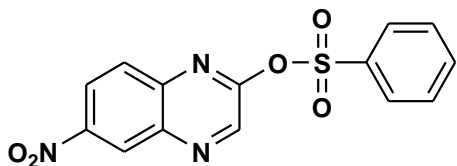
7.29-7.32 (m, 2H), 7.53-7.57 (m, 1H), 7.78 (d, 1H, $J = 8.0$ Hz), 8.17 (s, 1H), 12.46 (brs, 1H); ^{13}C NMR (100 MHz, DMSO- d_6 , ppm) 116.2, 123.8, 129.2, 131.2, 132.2, 132.5, 152.0, 155.4.

4.2.2. Preparation of 6-nitroquinoxalin-2-ol (**49**)⁴



Potassium nitrate (3.459 g, 34 mmol, 1eq.) was added to the solution of quinoxalin-2-ol **48** (5.0 g, 34 mmol) in concentrated sulfuric acid (30 mL). The resulting solution was stirred for 30 minutes at 0 °C and further stirred for 120 minutes at room temperature, then poured into ice water (50 mL). The resulting powder was collected after filtration and washed with water and dried to give 6-nitroquinoxalin-2-ol **49** as a light brown solid (6.353 g, 97%); M.p 222–225 °C (Lit 224–226 °C);³ ^1H NMR (400 MHz, DMSO- d_6 , ppm) 7.44 (d, 1H, $J = 9.0$ Hz), 8.32 (s, 1H), 8.38 (dd, 1H, $J = 9.2$ and 2.8 Hz), 8.55 (d, 1H, $J = 2.5$ Hz), 12.95 (brs, 1H); ^{13}C NMR (100 MHz, DMSO- d_6 , ppm), 117.3, 124.9, 125.9, 131.7, 137.8, 143.0, 154.8, 155.4.

4.2.3. Preparation of 6-nitroquinoxalin-2-yl benzenesulfonate (**50**)³



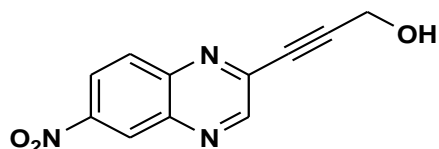
In a round bottom flask, 6-nitroquinoxaline-2-ol **49** (1.250 g, 6.5 mmol), DMAP (79 mg, 0.65 mmol, 10 mol %), and benzene sulfonyl chloride (1.66 mL, 13 mmol, 2 eq.) were dissolved in dry DCM (40 mL), cooled to 0°C and stirred for 5 minutes. Et₃N (1.81 mL, 19.5 mmol, 3 eq.) was added dropwise over 5 minutes. The solution was stirred at room temperature for 1 hour and then quenched with 20 mL of saturated NaHCO₃ solution, two layers were separated, and the aqueous layer washed with DCM (2 x 15 mL). The

combined organic layers were dried with anhydrous Na_2SO_4 , concentrated and then purified by silica gel column chromatography eluting with 0.5:9.5 MeOH: DCM to give 6-nitroquinoxalin-2-yl benzenesulfonate **50** as a yellowish solid (1.995 g, 92 %); M.p 158.1–160.4 °C; ^1H NMR (400 MHz, CDCl_3 , ppm) 7.61-7.66 (m, 2H), 7.72-7.77 (m, 1H), 8.03 (d, 1H, $J = 9.2$ Hz), 8.18-8.21 (m, 2H), 8.54 (dd, 1H, $J = 9.2$ and 2.5 Hz), 8.77 (s, 1H), 8.99 (d, 1H, $J = 2.4$ Hz); ^{13}C NMR (100 MHz, CDCl_3 , ppm), 124.6, 125.4, 129.2, 129.3, 129.9, 135.1, 136.0, 139.8, 141.4, 142.6, 147.6, 152.7.

4.2.4. General procedure for the Sonogashira coupling reaction on 6-nitroquinoxalin-2-yl benzenesulfonate

To an oven-dried 100 mL round bottom flask equipped with a teflon-coated magnetic stirrer bar, was added 6-nitroquinoxalin-2-yl benzenesulfonate, $\text{PdCl}_2(\text{PPh}_3)_2$ (5 mol %), CuI (10 mol %), Et_3N (2 eq.) and the corresponding terminal alkyne (1.2 eq.) in dry THF (10 mL). The reaction was allowed to stir at 30 °C for 18 hours. Upon completion, the reaction mixture was quenched with saturated ammonium chloride solution (10 mL) and extracted with EtOAc (2 x 15 mL). The organic layers were combined and dried over anhydrous Na_2SO_4 , concentrated and purified by either flash silica or trituration techniques.⁵

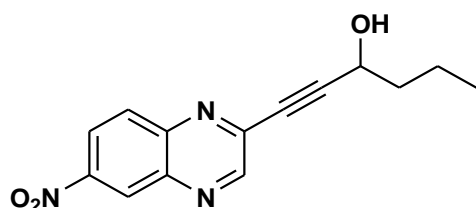
4.2.4.1. Synthesis of 3-(6-nitroquinoxalin-2-yl) prop-2-yn-1-ol (**45**)



Following procedure for Sonogashira coupling, compound **50** (200 mg, 0.6 mmol) was treated with propargyl alcohol (0.04 mL, 0.72 mmol, 1.2 eq.). Purification by trituration technique (Suspend & Filter) with diethyl ether and washed with n-hexane afforded 3-(6-nitroquinoxalin-2-yl) prop-2-yn-1-ol **45** as a brown solid (91 mg, 66 %). M.p 117.3-118.5 °C; ^1H NMR (400 MHz, DMSO-d_6 , ppm) 4.44 (s, 2H), 8.23 (d, 1H, $J = 9.2$ Hz), 8.55 (dd, 1H, $J = 9.2$ and 2.4 Hz), 8.87 (d, 1H, $J = 2.4$ Hz), 9.08 (s, 1H); ^{13}C NMR (100 MHz, DMSO-d_6 , ppm) 44.4, 82.3, 85.5, 88.7, 90.8.

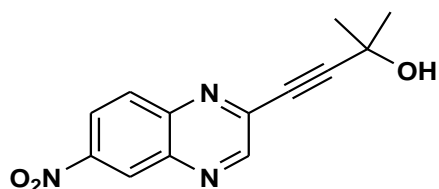
d₆, ppm) 49.9, 82.1, 97.5, 124.8, 125.5, 131.3, 139.7, 142.1, 144.4, 148.3, 149.9; V_{max} (FTIR) 538,742,791, 1031,1182, 1341, 1521, 2340,2923, 3282 cm⁻¹; HRMS (ESI) [M + H⁺]: m/z 230.9597; Calculated mass for C₁₁H₈N₃O₃ is 230.9466.

4.2.4.2. Synthesis of 1-(6-nitroquinoxalin-2-yl)hex-1-yn-3-ol (51)



Following procedure for Sonogashira coupling, compound **50** (80 mg, 0.24 mmol) was treated with hex-1-yn-3-ol (0.03 mL, 0.29 mmol, 1.2 eq.). Purification on flash silica, eluting with 1:1 EtOAc: n-hexane afforded 1-(6-nitroquinoxalin-2-yl)hex-1-yn-3-ol **51** as a brown solid (58 mg, 89%). M.p 119.1-121.0 °C; ¹H NMR (400 MHz, CDCl₃, ppm) 0.99 (t, 3H, J = 7.4 Hz), 1.56-1.62 (m, 2H), 1.85-1.90 (m, 2H), 2.79 (brs, 1H), 4.74 (t, 2H, J = 6.7 Hz), 8.17 (d, 1H, J = 9.2 Hz), 8.52 (dd, 1H, J = 9.2 and = 2.4 Hz), 8.95 (d, 1H, J = 2.4 Hz), 8.96 (s, 1H); ¹³C NMR (100 MHz, CDCl₃, ppm) 13.7, 18.4, 39.2, 62.5, 81.8, 98.0, 124.1, 125.5, 130.7, 139.7, 141.8, 144.2, 147.9, 149.0; V_{max} (FTIR) 530, 742, 791, 1015, 1341, 1521, 2218, 2960, 3046, 3249 cm⁻¹; HRMS (ESI) [M + H⁺]: m/z 272.1042; Calculated mass for C₁₄H₁₄N₃O₃ is 272.1037.

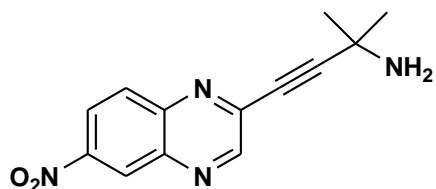
4.2.4.3. Synthesis of 2-methyl-4-(6-nitroquinoxalin-2-yl)but-3-yn-2-ol (52)



Following procedure for Sonogashira coupling, compound **50** (100 mg, 0.3 mmol) was treated with 2-methyl-3-butyn-2-ol (0.04 mL, 0.36 mmol, 1.2 eq.). Purification by trituration technique (Solvent then Anti-Solvent) with 2 mL of acetone then 8 mL of n-hexane

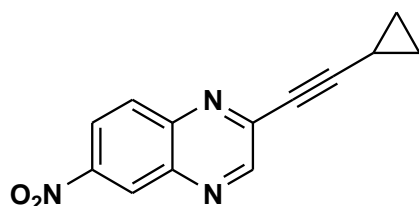
afforded 2-methyl-4-(6-nitroquinoxalin-2-yl) but-3-yn-2-ol **52** as a brown solid (60 mg, 84%). M.p 195.0–195.9 °C. ¹H NMR (400 MHz, CDCl₃, ppm) 1.71 (s, 6H), 8.21 (d, 1H, *J* = 9.2 Hz), 8.54 (dd, 1H, *J* = 9.2 and 2.4 Hz), 8.98 (s, 1H), 8.99 (d, 1H, *J* = 2.4 Hz); ¹³C NMR (100 MHz, CDCl₃, ppm) 30.9, 65.7, 79.6, 99.9, 124.2, 125.6, 130.8, 139.8, 141.9, 144.3, 147.9, 149.1; *V*_{max} (FTIR) 534, 742, 941, 1158, 1345, 1516, 2226, 2915, 3050, 3433 cm⁻¹; HRMS (ESI) [*M* + *H*⁺]: *m/z* 258.0886; Calculated mass for C₁₂H₁₂N₃O₃ is 258.0850.

4.2.4.4. Synthesis of 2-methyl-4-(6-nitroquinoxalin-2-yl)but-3-yn-2-amine (**53**)



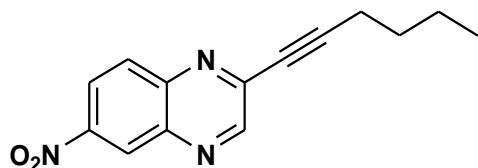
Following procedure for Sonogashira coupling, compound **50** (200 mg, 0.6 mmol) was treated with 2-methylbut-3-yn-2-amine (0.07 mL, 0.72 mmol, 1.2 eq.). Purification on flash silica, eluting with 1:9 MeOH: DCM afforded 2-methyl-4-(6-nitroquinoxalin-2-yl)but-3-yn-2-amine **53** as a black solid (151 mg, 98 %). M.p 184.9-184.1 °C; ¹H NMR (400 MHz, CDCl₃, ppm) 1.57 (s, 6H), 8.18 (d, 1H, *J* = 9.2 Hz), 8.52 (dd, 1H, *J* = 9.2 and 2.4 Hz), 8.94 (s, 1H), 8.96 (d, 1H *J* = 2.4 Hz); ¹³C NMR (100 MHz, CDCl₃, ppm) 31.1, 45.9, 77.2, 78.0, 124.1, 125.6, 130.7, 139.6, 142.4, 144.4, 147.4, 149.2; *V*_{max} (FTIR) 550, 742, 941, 1072, 1337, 1516, 2214, 2972, 3290, 3319 cm⁻¹; HRMS (ESI) [*M* + *H*⁺]: *m/z* 257.1036; Calculated mass for C₁₂H₁₃N₄O₂ is 257.1040.

4.2.4.5. Synthesis of 2-(2-cyclopropylethynyl)-6-nitroquinoxaline (**54**)



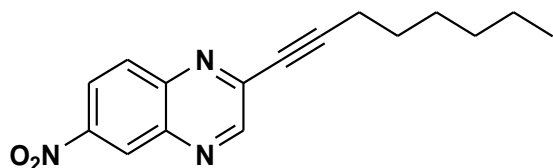
Following procedure for Sonogashira coupling, compound **50** (200 mg, 0.6 mmol) was treated with cyclopropyl acetylene (0.06 mL, 0.72 mmol, 1.2 eq.). Purification by trituration technique (Suspend & Filter) with acetone and washing with n-hexane afforded 2-(2-cyclopropylethynyl)-6-nitroquinoxaline **54** as a brown solid (108 mg, 76 %). M.p 197.4-199.1 °C; ¹H NMR (400 MHz, CDCl₃, ppm) 0.96 (d, 4H, *J* = 6.6 Hz), 1.60 (quin, 1H, *J* = 5.2 Hz), 8.14 (d, 1H, *J* = 9.2 Hz), 8.51 (dd, 1H, *J* = 9.2 and 2.4 Hz), 8.90 (s, 1H), 8.95 (d, 1H, *J* = 2.4 Hz); ¹³C NMR (100 MHz, CDCl₃, ppm) 9.7, 30.9, 74.3, 103.5, 124.0, 125.5, 130.48, 139.3, 142.9, 144.5, 147.5, 149.3; *V*_{max} (FTIR) 521, 742, 852, 941, 1064, 1178, 1333, 1516, 2210, 2046 cm⁻¹; HRMS (ESI) [*M* + *H*⁺]: *m/z* 240.9881; Calculated mass for C₁₃H₁₀N₃O₂ is 240.9845.

4.2.4.6. Synthesis of 2-(hex-1-ynyl)-6-nitroquinoxaline (**55**)



Following procedure for Sonogashira coupling, compound **50** (200 mg, 0.6 mmol) was treated with 1-hexyne (0.04 mL, 0.72 mmol, 1.2 eq.). Purification on flash silica, eluting with 3:7 EtOAc: n-hexane afforded 2-(hex-1-ynyl)-6-nitroquinoxaline **55** as a brown solid (97 mg, 33 %). M.p 129.0-130.9 °C; ¹H NMR (400 MHz, CDCl₃, ppm) 0.96 (t, 3H, *J* = 7.4 Hz), 1.51 (sex, 2H, *J* = 7.6 Hz), 1.68 (quin, 2H, *J* = 7.2 Hz), 2.57 (t, 2H, *J* = 7.2 Hz), 8.16 (d, 1H, *J* = 9.2 Hz), 8.51 (dd, 1H, *J* = 9.2 and 2.4 Hz), 8.92 (s, 1H), 8.95 (d, 1H, *J* = 2.4 Hz); ¹³C NMR (100 MHz, CDCl₃, ppm) 13.6, 19.4, 22.1, 30.0, 78.8, 99.9, 124.0, 125.6, 130.6, 139.5, 142.9, 144.5, 147.6, 149.4; *V*_{max} (FTIR) 538, 742, 946, 1072, 1182, 1341, 1516, 2318, 2923, 3042 cm⁻¹; HRMS (ESI) [*M* + *H*⁺]: *m/z* 256.1092; Calculated mass for C₁₄H₁₄N₃O₂ is 256.1088.

4.2.4.7. Synthesis of 6-nitro-2-(oct-1-ynyl) quinoxaline (56)

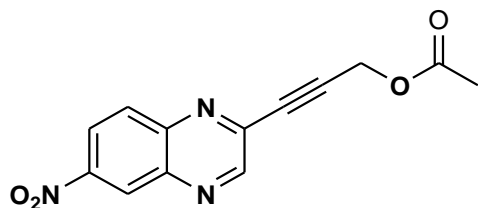


Following procedure for Sonogashira coupling, compound **50** (300 mg, 0.9 mmol) was treated with 1-octyne (0.15 mL, 1 mmol, 1.2 eq.). Purification on flash silica, eluting with 1:9 EtOAc: n-hexane afforded 6-nitro-2-(oct-1-ynyl) quinoxaline **56** as a brown solid (172 mg, 67 %). M.p 200.5-202.5 °C; ¹H NMR (400 MHz, CDCl₃, ppm) 0.88 (t, 3H, *J* = 6.8 Hz), 1.31 (m, 4H), 1.47 (quin, 2H, *J* = 7.2 Hz), 1.68 (quin, 2H, *J* = 7.2 Hz), 2.55 (t, 2H, *J* = 7.2 Hz), 8.15 (d, 1H, *J* = 9.2 Hz), 8.50 (dd, 1H, *J* = 9.2 Hz and 2.4 Hz), 8.91 (s, 1H), 8.93 (d, 1H, *J* = 2.4 Hz); ¹³C NMR (100 MHz, CDCl₃, ppm) 14.0, 19.7, 22.5, 28.0, 28.6, 31.2, 78.8, 99.9, 123.9, 125.5, 130.6, 139.4, 142.9, 144.5, 147.6, 149.4; *V*_{max} (FTIR) 538, 742, 741, 1072, 1182, 1337, 1516, 2214, 2923, 3037 cm⁻¹; HRMS (ESI) [*M* + H⁺]: *m/z* 284.1404 ; Calculated mass for C₁₆H₁₈N₃O₂ is 284.1401.

4.2.5. General esterification reaction at alcohol group

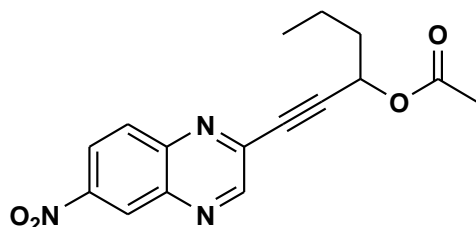
To a solution of alcohol in DCM, triethylamine (3.5 eq.), 0.2 mol % of DMAP, 1.2 eq. of acyl chloride (protecting group) were added and the reaction mixture was stirred under nitrogen for 1 hour at room temperature. The reaction was quenched with a saturated ammonium chloride solution, extracted with EtOAc (10 mL x 3). The combined organic layers were washed with water, dried over anhydrous MgSO₄ and concentrated under vacuum.⁶

4.2.5.1. Synthesis of 3-(6-nitroquinoxalin-2-yl)prop-2-ynyl acetate (57)



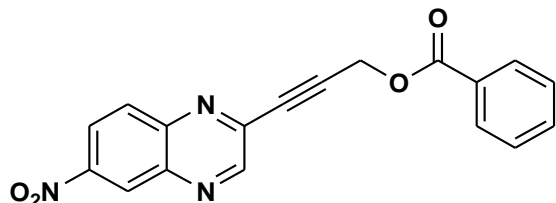
Following the procedure for esterification reaction, compound **45** (200 mg, 0.87 mmol) was treated with acetyl chloride (0.07 mL, 1 mmol, 1.2 eq.). After purification by column chromatography on silica gel, using DCM as eluent, 3-(6-nitroquinoxalin-2-yl)prop-2-ynyl acetate **57** was obtained as orange solid (98 mg, 42 %). M.p 153.7–155.3 °C ; ¹H NMR (400 MHz, CDCl₃, ppm) 2.17 (s, 3H), 5.01 (s, 2H), 8.21 (d, 1H, *J* = 9.2 Hz), 8.55 (dd, 1H, *J* = 9.2 and 2.4 Hz), 8.99 (d, 1H, *J* = 2.4 Hz), 9.00 (s, 1H); ¹³C NMR (100 MHz, CDCl₃, ppm) 20.6, 51.9, 83.2, 90.3, 124.2, 125.6, 130.9, 139.9, 141.3, 144.3, 148.1, 148.9, 170.0; *V*_{max} (FTIR) 588, 787, 1015, 1031, 1341, 1516, 1741, 2238, 2850, 2919 cm⁻¹; HRMS (ESI) [M + H]⁺ :m/z 272.0668; Calculated mass for C₁₃H₁₀N₃O₄ is 272.0693.

4.2.5.2. Synthesis of 1-(6-nitroquinoxalin-2-yl)hex-1-yn-3-yl acetate (**58**)



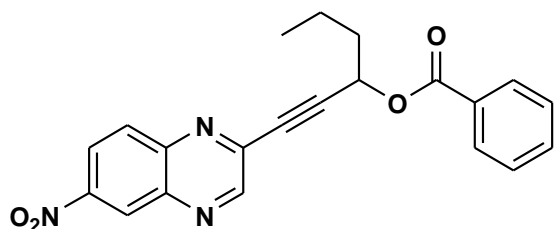
Following the procedure for esterification reaction, compound **51** (200 mg, 0.74mmol) was treated with acetyl chloride (0.06 mL, 0.89 mmol, 1.2 eq.). After purification by column chromatography on silica gel using 2:8 EtOAc: n-hexane as eluent, 1-(6-nitroquinoxalin-2-yl)hex-1-yn-3-yl acetate **58** was obtained as yellow solid (159 mg, 69 %). M.p 109.2-110.1 °C. ¹H NMR (400MHz, CDCl₃, ppm) 0.99 (t, 3H, *J* = 7.4 Hz), 1.52-1.61 (m, 2H), 1.90-1.95 (m, 2H), 2.14 (s, 3H), 5.66 (t, 2H, *J* = 6.7 Hz), 8.16 (d, 1H, *J* = 9.2 Hz), 8.54 (dd, 1H, *J* = 9.2 and 2.4 Hz), 8.97 (m, 2H); ¹³C NMR (100 MHz, CDCl₃, ppm) 13.57, 18.38, 20.89, 36.25, 63.61, 82.12, 94.02, 124.13, 125.60, 130.84, 139.84, 141.53, 144.29, 147.97, 149.06, 169.9; *V*_{max} (FTIR) 530, 742, 852, 1015, 1211, 1345, 1521, 1741, 2226, 2923 cm⁻¹; HRMS (ESI) [M + H]⁺ :m/z 314.1146; Calculated mass for C₁₆H₁₆N₃O₄ is 314.1143.

4.2.5.3. Synthesis of 3-(6-nitroquinoxalin-2-yl)prop-2-ynyl benzoate (59)



Following the procedure for esterification reaction, compound **45** (200 mg, 0.87 mmol) was treated with benzoyl chloride (0.12 mL, 1 mmol, 1.2 eq.). After purification by column chromatography on silica gel, using DCM as eluent, 3-(6-nitroquinoxalin-2-yl)prop-2-ynyl benzoate **59** was obtained as orange solid (132 mg, 46 %). M.p 177.0–179.3 °C; ¹H NMR (400 MHz, CDCl₃, ppm) 5.27 (s, 2H), 7.46-7.50 (m, 2H), 7.59-7.63 (m, 1H), 8.10-8.12 (m, 2H), 8.21 (d, 1H, *J* = 9.2 Hz), 8.55 (dd, 1H, *J* = 9.2 and = 2.4 Hz), 8.99 (d, 1H, *J* = 2.4 Hz), 9.03 (s, 1H); ¹³C NMR (100 MHz, CDCl₃, ppm) 52.50, 83.4, 90.4, 124.2, 125.7, 128.6, 128.9, 129.9, 130.9, 133.6, 140.0, 141.3, 144.3, 148.1, 148.9, 165.7; *V*_{max} (FTIR) 538, 701, 795, 1019, 1260, 1525, 1716, 2234, 2864, 2960 cm⁻¹; HRMS (ESI) [M + H]⁺ :*m/z* 334.0833; Calculated mass for C₁₈H₁₂N₃O₄ is 334.0830.

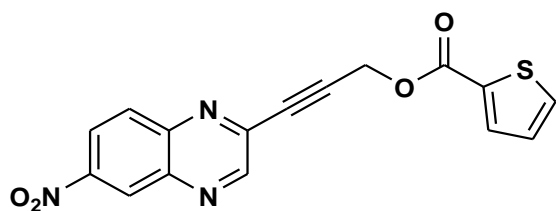
4.2.5.4. Synthesis of 1-(6-nitroquinoxalin-2-yl)hex-1-yn-3-yl benzoate (60)



Following the procedure for esterification reaction, compound **51** (0.1 g, 0.37mmol) was treated with benzoyl chloride (0.05 mL, 0.44 mmol, 1.2 eq.). After purification by column chromatography on silica gel using 2:8 EtOAc: n-hexane as eluent, 1-(6-nitroquinoxalin-2-yl)hex-1-yn-3-yl benzoate **60** was obtained as yellow solid (60 mg, 43 %). M.p 78.5-79.1 °C; ¹H NMR (400 MHz, CDCl₃, ppm) 1.04 (t, 3H, *J* = 7.4 Hz), 1.64-1.70 (m, 2H), 2.07-2.16 (m, 2H), 5.92 (t, 2H, *J* = 6.7 Hz), 7.46-7.50 (m, 2H), 7.45-7.48 (m, 1H), 8.08-

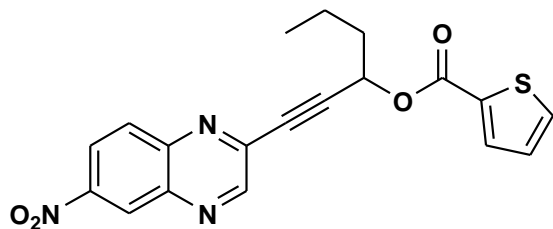
8.10 (m, 2H), 8.20 (d, 1H, $J = 9.2$ Hz), 8.53 (dd, 1H, $J = 9.2$ and 2.4 Hz), 8.97 (d, 1H, $J = 2.4$ Hz), 8.99 (s, 1H); ^{13}C NMR (100 MHz, CDCl_3 , ppm) 13.7, 18.5, 36.4, 64.1, 82.3, 94.1, 124.1, 125.6, 128.5, 129.4, 129.8, 130.8, 133.5, 139.8, 141.5, 144.3, 148.0, 149.1, 165.4; V_{max} (FTIR) 664, 705, 848, 1064, 1260, 1341, 1521, 1724, 2234, 2931 cm^{-1} ; HRMS (ESI) $[\text{M} + \text{H}]^+$:m/z 376.1309; Calculated mass for $\text{C}_{21}\text{H}_{18}\text{N}_3\text{O}_4$ is 376.1299.

4.2.5.5. Synthesis of 3-(6-nitroquinoxalin-2-yl)prop-2-ynyl thiophene-2-carboxylate (**61**)



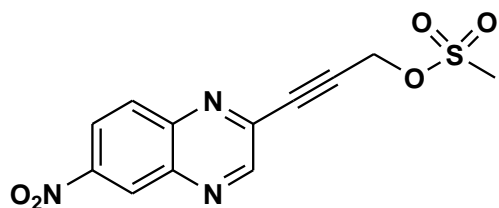
Following the procedure for esterification reaction, compound **45** (200 mg, 0.87 mmol) was treated with thiophene-2-carbonyl chloride (0.11 mL, 1 mmol, 1.2 eq.). After purification by column chromatography on silica gel, using DCM as eluent, 3-(6-nitroquinoxalin-2-yl)prop-2-ynylthiophene-2-carboxylate **61** was obtained as orange solid (118 mg, 40 %). M.p 168.0-170.0 $^{\circ}\text{C}$; ^1H NMR (400 MHz, CDCl_3 , ppm) 5.24 (s, 2H), 7.14 (dd, 1H, $J = 4.8$ and 1.0 Hz), 7.63 (dd, 1H, $J = 4.8$ and 1.2 Hz), 7.90 (dd, 1H, $J = 3.6$ and 1.2 Hz), 8.21 (d, 1H, $J = 9.2$ Hz), 8.55 (dd, 1H, $J = 9.2$ and 2.4 Hz), 8.99 (d, 1H, $J = 2.4$ Hz), 9.02 (s, 1H); ^{13}C NMR (100 MHz, CDCl_3 , ppm) 52.5, 83.5, 90.1, 124.2, 125.7, 127.9, 130.9, 132.2, 133.5, 134.5, 139.9, 141.3, 144.3, 148.1, 148.9, 161.2; V_{max} (FTIR) 542, 721, 787, 1064, 1243, 1516, 1712, 2340, 2846, 3042 cm^{-1} ; HRMS (ESI) $[\text{M} + \text{H}]^+$:m/z 340.0399; Calculated mass for $\text{C}_{16}\text{H}_{10}\text{N}_3\text{O}_4\text{S}$ is 340.0394.

4.2.5.6. Synthesis of 1-(6-nitroquinoxalin-2-yl)hex-1-yn-3-yl thiophene-2-carboxylate (62)



Following the procedure for esterification reaction, compound **51** (100 mg, 0.37 mmol) was treated with thiophene-2-carbonyl chloride (0.05 mL, 0.44 mmol, 1.2 eq.). After purification by column chromatography on silica gel using 2:8 EtOAc: n-hexane as eluent, 1-(6-nitroquinoxalin-2-yl)hex-1-yn-3-yl thiophene-2-carboxylate **62** was obtained as yellow solid (76 mg, 54 %). M.p 76.4-77.2 °C. ¹H NMR (400 MHz, CDCl₃, ppm) 1.03 (t, 3H, *J* = 7.4 Hz), 1.60-1.70 (m, 2H), 2.03-2.10 (m, 2H), 5.88 (t, 2H, *J* = 6.7 Hz), 7.13 (dd, 1H, *J* = 4.8 and 1.0 Hz), 7.61 (dd, 1H, *J* = 4.8 and 1.2 Hz), 7.88 (dd, 1H, *J* = 3.6 and 1.2 Hz), 8.21 (d, 1H, *J* = 9.2 Hz), 8.54 (dd, 1H, *J* = 9.2 and 2.4 Hz), 8.99 (d, 1H, *J* = 2.4 Hz), 8.99 (s, 1H); ¹³C NMR (100 MHz, CDCl₃, ppm) 13.6, 18.5, 36.4, 64.3, 82.5, 93.8, 124.2, 125.6, 127.9, 130.9, 132.7, 133.2, 134.2, 139.9, 141.5, 144.3, 148.0, 149.1, 161.1; *V*_{max} (FTIR) 415, 742, 933, 1068, 1251, 1341, 1525, 1708, 2234, 2960 cm⁻¹; HRMS (ESI) [M + H]⁺ : *m/z* 382.0876; Calculated mass for (C₁₉H₁₆N₃O₄S) 382.0863.

4.2.5.7. Synthesis of 3-(6-nitroquinoxalin-2-yl)prop-2-ynyl methane sulfonate (63)

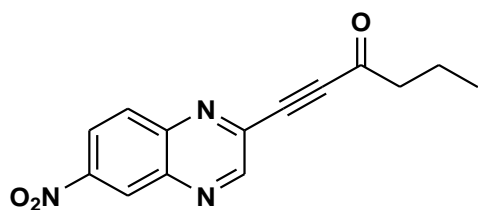


Following the procedure for esterification reaction, compound **45** (200 mg, 0.87 mmol) was treated with methane sulfonyl chloride (0.08 mL, 1 mmol, 1.2 eq.). After purification by column chromatography on silica gel, using 1:1 EtOAc: n-hexane as eluent, 3-(6-nitroquinoxalin-2-yl)prop-2-ynyl methane sulfonate **63** was obtained as black solid (89mg,

33 %). M.p 146.5-148.9 °C; ¹H NMR (400MHz, CDCl₃, ppm) 3.21 (s, 3H), 5.19 (s, 2H), 8.23 (d, 1H, *J* = 9.2 Hz), 8.58 (dd, 1H, *J* = 9.2 and 2.4 Hz), 9.01 (d, 1H, *J* = 2.4 Hz), 9.03 (s, 1H); ¹³C NMR (100 MHz, CDCl₃, ppm) 38.9, 56.6, 85.5, 87.2, 124.4, 125.7, 131.0, 140.2, 140.5, 144.2, 148.3, 148.6; V_{max} (FTIR) 460, 521, 791, 1166, 1260, 1345, 1451, 1525, 2854, 2923 cm⁻¹.

4.2.6. Oxidation reaction

4.2.6.1. Synthesis of 1-(6-nitroquinoxalin-2-yl)hex-1-yn-3-one (**64**)⁷

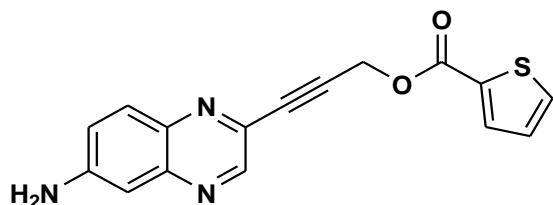


To a solution of compound **51** (180 mg, 0.66 mmol) in acetone (10 mL) was added mixture of chromium trioxide (99 mg, 0.99 mmol, 1.5 eq.), concentrated sulphuric acid (0.065 mL) and water (1 mL) dropwise over a period of 15 minutes at 0 °C. After a further 16 hours stirring at room temperature, the reaction was diluted further with water (4 mL) and the product was isolated by extraction into ether (3 x 30 mL), drying over anhydrous Na₂SO₄ and concentration. After purification by column chromatography on silica gel using 2:8 EtOAc: n-hexane as eluent, 1-(6-nitroquinoxalin-2-yl)hex-1-yn-3-one **64** was obtained as brown solid (137 mg, 77 %). M.p 135.4-138.0 °C; ¹H NMR (400 MHz, CDCl₃, ppm) 1.01 (t, 3H, *J* = 7.4 Hz), 1.80 (sex, 2H, *J* = 7.4 Hz), 2.76 (t, 2H, *J* = 7.3 Hz), 8.26 (d, 1H, *J* = 9.2 Hz), 8.59 (dd, 1H, *J* = 9.2 and 2.4 Hz), 9.02 (d, 1H, *J* = 2.4 Hz), 9.09 (s, 1H); ¹³C NMR (100 MHz, CDCl₃, ppm) 13.5, 17.3, 47.4, 83.7, 90.1, 124.5, 125.74, 131.3, 140.0, 140.5, 144.3, 148.6, 148.9, 186.7; V_{max} (FTIR) 546, 742, 787, 982, 1068, 1341, 1521, 1671, 2214, 2923 cm⁻¹; HRMS (ESI) [M + H]⁺ :m/z 270.0883; Calculated mass for C₁₄H₁₂N₃O₃ is 270.0880.

4.2.7. General reduction reaction at nitro group

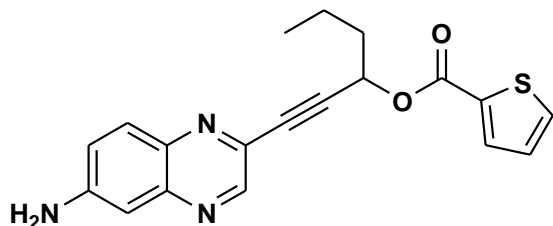
To a suspension of nitro quinoxaline with alkyne derivatives in EtOAc (10 mL) was added SnCl₂ (5 eq.) and the reaction mixture refluxed for 3H. After cooling to room temperature, NaHCO₃ solution (10 mL) was added and stirred for 10 minutes. The suspension was partitioned, and aqueous layer was washed with EtOAc, the combined organic layers were washed with brine and concentrated after drying with anhydrous Na₂SO₄.⁸

4.2.7.1. Synthesis of 3-(6-aminoquinoxalin-2-yl)prop-2-ynyl thiophene-2-carboxylate (**31**)



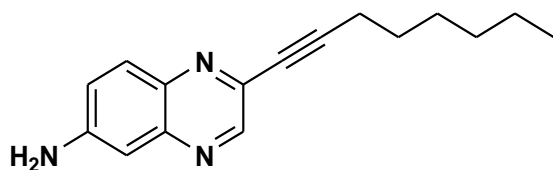
To a suspension of compound **61** (90 mg, 0.27 mmol) in EtOAc (10 mL) was added SnCl₂ (256 mg, 1.35 mmol, 5 eq.) according to procedure of reduction reaction. Purification on prep TLC with EtOAc: n-hexane (8.5:1.5) afforded 3-(6-aminoquinoxalin-2-yl)prop-2-ynyl thiophene-2-carboxylate **31** as yellow solid (35 mg, 43 %). M.p 140.3-141.9; ¹H NMR (400 MHz, CDCl₃, ppm) ¹H NMR (400 MHz, CDCl₃, ppm) 4.38 (brs, 2H), 5.19 (s, 2H), 7.08 (d, 1H, *J* = 2.5 Hz), 7.11 (dd, 1H, *J* = 4.8 and 1.0 Hz), 7.18 (dd, 1H, *J* = 9.0 and 2.6 Hz), 7.59 (dd, 1H, *J* = 4.8 and 1.2 Hz), 7.82 (d, 1H), 7.87 (dd, 1H, *J* = 3.6 and 1.2 Hz), 8.72 (s, 1H); ¹³C NMR (100 MHz, CDCl₃, ppm) 52.9, 84.4, 85.5, 107.5, 122.8, 127.9, 130.4, 132.6, 133.2, 133.9, 134.3, 137.1, 143.2, 147.3, 148.9, 161.4; *V*_{max} (FTIR) 546, 742, 1076, 1227, 1353, 1614, 1704, 2091, 2919, 3225, 3335 cm⁻¹; HRMS (ESI) [M + H]⁺ :*m/z* 310.0660; Calculated mass for C₁₆H₁₂N₃O₂S is 310.0652.

4.2.7.2. Synthesis of 1-(6-aminoquinoxalin-2-yl)hex-1-yn-3-yl thiophene-2-carboxylate (**32**)



To a suspension of compound **62** (50 mg, 0.13 mmol) in EtOAc (10 mL) was added SnCl₂ (123 mg, 0.65 mmol, 5 eq.) according to procedure of reduction reaction. Purification on prep TLC with EtOAc: n-hexane (2:8) afforded 1-(6-aminoquinoxalin-2-yl)hex-1-yn-3-yl thiophene-2-carboxylate **32** as yellow solid (30 mg, 66 %). M.p 220.5-221.6 °C. ¹H NMR (400 MHz, CDCl₃, ppm) 1.01 (t, 3H, *J* = 7.4 Hz), 1.60-1.65 (m, 2H), 2.01-2.04 (m, 2H), 4.26 (brs, 2H), 5.88 (t, 2H, *J* = 6.7 Hz), 7.08 (d, 1H, *J* = 2.5 Hz), 7.11 (dd, 1H, *J* = 4.8 and 1.0 Hz), 7.17 (dd, 1H, *J* = 9.0 and 2.6 Hz), 7.69 (dd, 1H, *J* = 4.8 and 1.2 Hz), 7.82 (d, 1H, *J* = 9.0 Hz), 7.86 (dd, 1H, *J* = 3.6 and 1.2 Hz), 8.71 (s, 1H); ¹³C NMR (100 MHz, CDCl₃, ppm) 13.7, 18.5, 36.7, 64.7, 83.2, 89.1, 107.7, 122.6, 127.8, 130.4, 132.9, 133.2, 134.0, 134.2, 137.1, 143.1, 147.6, 148.7, 161.2; V_{max} (FTIR) 448, 827, 1068, 1227, 1353, 1414, 1614, 1704, 2923, 3217, 3339 cm⁻¹; HRMS (ESI) [M + H]⁺ :m/z 352.1134; Calculated mass for C₁₉H₁₈N₃O₂S is 352.1121.

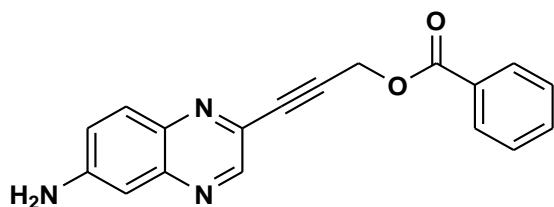
4.2.7.3. Synthesis of 2-(oct-1-ynyl)quinoxalin-6-amine (**33**)



To a suspension of compound **56** (50 mg, 0.18 mmol) in EtOAc (10 mL) was added SnCl₂ (171 mg, 0.9 mmol, 5 eq.) according to procedure of reduction reaction. Purification on prep TLC with EtOAc: n-hexane (1:1) afforded 2-(oct-1-ynyl)quinoxalin-6-amine **33** as orange solid (26 mg, 57 %). M.p 341.6-343.1 °C; ¹H NMR (400 MHz, CDCl₃, ppm) 0.89 (t, 3H, *J* = 7.0 Hz), 1.27-1.32 (m, 4H), 1.42-1.50 (m, 2H), 1.65 (quin, 2H, *J* = 7.2 Hz), 2.49

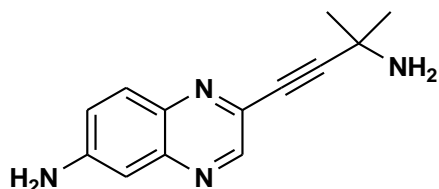
(t, 2H, $J = 7.2$ Hz), 4.25 (brs, 2H), 7.08 (d, 1H, $J = 2.5$ Hz), 7.15 (dd, 1H, $J = 9.0$ and 2.6 Hz), 7.81 (d, 1H, $J = 9.0$ Hz), 8.65 (s, 1H); ^{13}C NMR (100 MHz, CDCl_3 , ppm) 14.1, 19.5, 22.48, 28.3, 28.7, 31.3, 78.8, 94.4, 107.9, 122.3, 130.2, 135.9, 137.1, 142.6, 147.7, 149.1; V_{max} (FTIR) 574, 685, 799, 1019, 1260, 1467, 618, 2222, 2919, 3221, 3347 cm^{-1} ; HRMS (ESI) $[\text{M} + \text{H}]^+$:m/z 254.1664; Calculated mass for $(\text{C}_{16}\text{H}_{20}\text{N}_3)$ 254.1659.

4.2.7.4. Synthesis of 3-(6-aminoquinoxalin-2-yl)prop-2-ynyl benzoate (34)



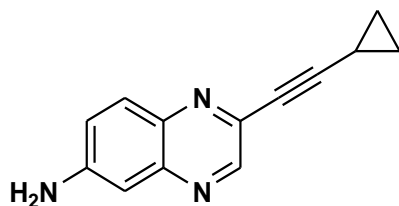
To a suspension of compound **59** (60 mg, 0.18 mmol) in EtOAc (10 mL) was added SnCl_2 (171 mg, 0.9 mmol, 5 eq.) according to procedure of reduction reaction. Purification on prep TLC with EtOAc: n-hexane (1:1) afforded 3-(6-aminoquinoxalin-2-yl)prop-2-ynyl benzoate **34** as yellow solid (41 mg, 75 %). M.p 199.3-201.5 $^\circ\text{C}$. ^1H NMR (400 MHz, CDCl_3 , ppm) 4.35 (brs, 2H), 5.22 (s, 2H), 7.08 (d, 1H, $J = 2.5$ Hz), 7.18 (dd, 1H, $J = 9.0$ and 2.6 Hz), 7.43-7.47 (m, 2H), 7.55-7.60 (m, 1H), 7.82 (d, 1H, $J = 9.0$ Hz), 8.08-8.10 (m, 2H), 8.73 (s, 1H); ^{13}C NMR (100 MHz, CDCl_3 , ppm) 52.9, 84.3, 85.7, 107.6, 122.7, 128.4, 129.3, 129.9, 130.4, 133.4, 133.9, 137.1, 143.3, 147.3, 148.9, 165.8; V_{max} (FTIR) 546, 705, 1096, 1260, 1476, 1614, 1708, 2087, 2919, 3221, 3335 cm^{-1} ; HRMS (ESI) $[\text{M} + \text{H}]^+$:m/z 304.1094; Calculated mass for $\text{C}_{18}\text{H}_{14}\text{N}_3\text{O}_2$ is 304.1088.

4.2.7.5. Synthesis of 2-(3-amino-3-methylbut-1-ynyl)quinoxalin-6-amine (35)



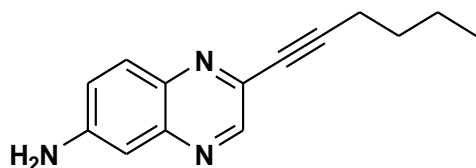
To a suspension of compound **53** (100 mg, 0.39 mmol) in EtOAc (10 mL) was added SnCl₂ (379 mg, 2 mmol, 5 eq.) according to procedure of reduction reaction. Purification on prep TLC with MeOH: DCM (3:7) to 2-(3-amino-3-methylbut-1-ynyl)quinoxalin-6-amine **35** as yellow solid (68 mg, 77 %). M.p 97.5-99.2 °C; ¹H NMR (400 MHz, CDCl₃, ppm) 1.52(s, 6H), 4.32 (brs, 2H), 7.07 (d, 1H, *J* = 2.5 Hz), 7.15 (dd, 1H, *J* = 9.0 and 2.6 Hz), 7.81 (d, 1H, *J* = 9.0 Hz), 8.65 (s, 1H); ¹³C NMR (100 MHz, CDCl₃, ppm) 31.5, 19.5, 45.9, 78.5, 100.2, 107.9, 122.37 130.4, 135.4, 137.2, 143.0, 147.7, 148.6; *V*_{max} (FTIR) 546, 823, 1080, 1349, 1480, 1614, 2087, 2919, 3196, 3323 cm⁻¹; HRMS (ESI) [M + H]⁺ :m/z 227.1298; Calculated mass for C₁₃H₁₅N₄ is 227.1298.

4.2.7.6. Synthesis of 2-(2-cyclopropylethynyl)quinoxalin-6-amine (**37**)



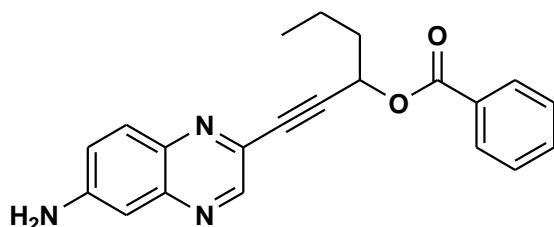
To a suspension of compound **54** (50 mg, 0.2 mmol) in EtOAc (10 mL) was added SnCl₂ (198 mg, 1 mmol, 5 eq.) according to procedure of reduction reaction. Purification on prep TLC with EtOAc afforded 2-(2-cyclopropylethynyl)quinoxalin-6-amine **37** as maroon solid (27 mg, 65 %). M.p 92.1-93.4 °C; ¹H NMR (400 MHz, CDCl₃, ppm) 0.92 (d, 4H, *J* = 6.6 Hz), 1.52 (quin, 1H, *J* = 6.7 Hz), 4.26 (brs, 2H), 7.06 (d, 1H, *J* = 2.5 Hz), 7.13 (dd, 1H, *J* = 9.0 and 2.6 Hz), 7.78 (d, 1H, *J* = 9.0 Hz), 8.62 (s, 1H); ¹³C NMR (100 MHz, CDCl₃, ppm) 8.94, 29.7, 74.1, 97.3, 107.9, 122.3, 130.1, 135.8, 137.0, 142.6, 147.6, 148.1; *V*_{max} (FTIR) 550, 799, 994, 1227, 1366, 1476, 1614, 2214, 2919, 3188, 3307 cm⁻¹; HRMS (ESI) [M + H]⁺ :m/z 210.1042; Calculated mass for C₁₃H₁₂N₃ is 210.1033.

4.2.7.7. Synthesis of 2-(hex-1-ynyl)quinoxalin-6-amine (38)



To a suspension of compound **55** (40 mg, 0.15 mmol) in EtOAc (10 mL) was added SnCl₂ (142 mg, 0.75 mmol, 5 eq.) according to procedure of reduction reaction. Purification on prep TLC with EtOAc: n-hexane (8:2) afforded 2-(hex-1-ynyl)quinoxalin-6-amine **38** as green solid (32 mg, 95 %). M.p 273.8-274.7 °C. ¹H NMR (400 MHz, CDCl₃, ppm) 0.94 (t, 3H, *J* = 7.3 Hz), 1.49 (sex, 2H, *J* = 7.3 Hz), 1.60-1.67 (m, 2H), 2.49 (t, 2H, *J* = 7.2 Hz), 4.26 (brs, 2H), 7.08 (d, 1H, *J* = 2.5 Hz), 7.15 (dd, 1H, *J* = 9.0 and 2.6 Hz), 7.80 (d, 1H, *J* = 9.0 Hz), 8.65 (s, 1H); ¹³C NMR (100 MHz, CDCl₃, ppm) 13.6, 19.2, 22.1, 30.3, 78.8, 94.2, 107.9, 122.3, 130.1, 135.8, 137.0, 142.6, 147.6, 148.1; V_{max} (FTIR) 570, 795, 1088, 1230, 1353, 1467, 1565, 2222, 2923, 3218, 3335 cm⁻¹; LRMS (ESI) [M + H]⁺ :m/z 226.1340; Calculated mass for C₁₄H₁₆N₃ is 226.1346.

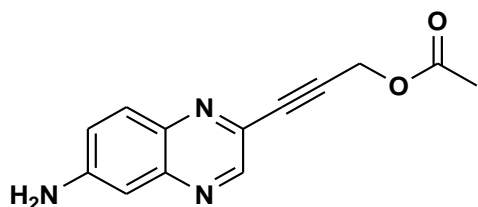
4.2.7.8. Synthesis of 1-(6-aminoquinoxalin-2-yl)hex-1-yn-3-yl benzoate (40)



To a suspension of compound **60** (50 mg, 0.13 mmol) in EtOAc (10 mL) was added SnCl₂ (123 mg, 0.65 mmol, 5 eq.) according to procedure of reduction reaction. Purification on prep TLC with EtOAc: n-hexane (2:8) afforded 1-(6-aminoquinoxalin-2-yl)hex-1-yn-3-yl benzoate **40** as yellow solid (40 mg, 89 %). M.p 250.5-251.2°C; ¹H NMR (400 MHz, CDCl₃, ppm) 1.04 (t, 3H, *J* = 7.4 Hz), 1.64-1.70 (m, 2H), 2.06-2.09 (m, 2H), 4.34 (brs, 2H), 5.96 (t, 2H, *J* = 6.7 Hz), 7.11 (d, 1H, *J* = 2.5 Hz), 7.20 (dd, 1H, *J* = 9.0 and 2.6 Hz), 7.46-7.50 (m, 2H), 7.58-7.62 (m, 1H), 7.85 (d, 1H, *J* = 9.0 Hz), 8.11-8.13 (m, 2H), 8.74

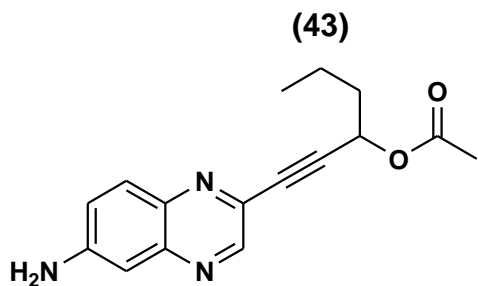
(s, 1H); ^{13}C NMR (100 MHz, CDCl_3 , ppm) 13.7, 18.6, 36.8, 64.5, 82.3, 89.4, 107.7, 122.7, 128.4, 129.8, 129.9, 130.4, 133.3, 134.3, 137.1, 143.2, 147.6, 148.7, 165.6; V_{max} (FTIR) 448, 827, 1060, 1231, 1353, 1447, 1557, 1716, 2923, 3217, 3339 cm^{-1} ; HRMS (ESI) $[\text{M} + \text{H}]^+$:m/z 346.1572; Calculated mass for $\text{C}_{21}\text{H}_{20}\text{N}_3\text{O}_2$ is 346.1557.

4.2.7.9. Synthesis of 3-(6-aminoquinoxalin-2-yl)prop-2-ynyl acetate (41)



To a suspension of compound **57** (40 mg, 0.18 mmol) in EtOAc (10 mL) was added SnCl_2 (142 mg, 0.75 mmol, 5 eq.) according to procedure of reduction reaction. Purification on prep TLC with EtOAc afforded 3-(6-aminoquinoxalin-2-yl)prop-2-ynyl acetate **41** as orange solid (18 mg, 51 %). M.p 95.6- 96.9 $^{\circ}\text{C}$. ^1H NMR (400 MHz, CDCl_3 , ppm) 2.14 (s, 3H), 4.34 (brs, 2H), 4.97 (s, 2H), 7.09 (d, 1H, $J = 2.5$ Hz), 7.18 (dd, 1H, $J = 9.0$ and 2.6 Hz), 7.82 (d, 1H, $J = 9.0$ Hz), 8.71 (s, 1H); ^{13}C NMR (100 MHz, CDCl_3 , ppm) 20.7, 52.4, 84.1, 85.6, 107.6, 122.7, 130.4, 133.9, 137.1, 143.2, 147.3, 148.7, 170.2; V_{max} (FTIR) 591, 827, 1023, 1223, 1357, 1618, 1741, 2083, 2919, 3192, 3307 cm^{-1} ; HRMS (ESI) $[\text{M} + \text{H}]^+$:m/z 242.0941; Calculated mass for $\text{C}_{13}\text{H}_{12}\text{N}_3\text{O}_2$ is 242.0931.

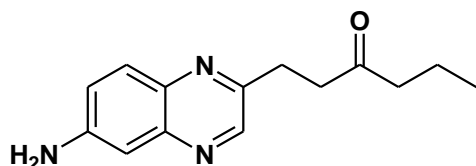
4.2.7.10. Synthesis of 1-(6-aminoquinoxalin-2-yl)hex-1-yn-3-yl acetate (43)



To a suspension of compound **58** (150 mg, 0.48 mmol) in EtOAc (10 mL) was added SnCl_2 (455 mg, 5 eq, 2.4 mmol) according to procedure of reduction reaction. Purification

on prep TLC with EtOAc: n-hexane (2:8) afforded 1-(6-aminoquinoxalin-2-yl)hex-1-yn-3-yl acetate **43** as yellow solid (93 mg, 69 %). M.p 114.9-116.1°C; ¹H NMR (400MHz, CDCl₃, ppm) 0.97 (t, 3H, *J* = 7.4 Hz), 1.54 (sex, 2H, *J* = 7.4 Hz), 1.85-1.91 (m, 2H), 2.11 (s, 3H), 4.36 (brs, 2H), 5.65 (t, 2H, *J* = 6.7 Hz), 7.07 (d, 1H, *J* = 2.5 Hz), 7.16 (dd, 1H, *J* = 9.0 and 2.6 Hz), 7.81 (d, 1H, *J* = 90 Hz), 8.68 (s, 1H); ¹³C NMR (100 MHz, CDCl₃, ppm) 13.6, 18.4, 20.9, 36.5, 63.9, 82.8, 89.3, 107.6, 122.6, 130.3, 134.2, 136.9, 143.1, 147.4, 148.7, 170.0; V_{max} (FTIR) 550, 827, 1015, 1223, 1347, 1435, 1614, 1733, 2923, 3217, 3343 cm⁻¹; HRMS (ESI) [M + H]⁺ :m/z 284.1410; Calculated mass for C₁₆H₁₈N₃O₂ is 284.1401.

4.2.7.11. Synthesis of 1-(6-aminoquinoxalin-2-yl)hexan-3-one (**65**)

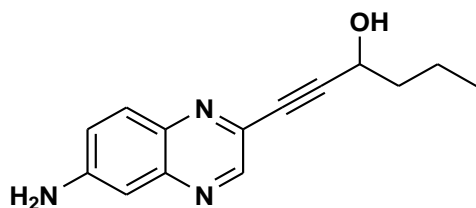


To a suspension of 1-(6-nitroquinoxalin-2-yl)hex-1-yn-3-one **64** (50 mg, 0.19 mmol) in EtOAc (10 mL) was added SnCl₂ (176 mg, 0.65 mmol, 5 eq.) according to procedure of reduction reaction. Purification on prep TLC with EtOAc: n-hexane (8:2) afforded 1-(6-aminoquinoxalin-2-yl)hexan-3-one **65** as yellow solid (10 mg, 22 %); M.p 97.0-97.6 °C; ¹H NMR (400MHz, CDCl₃, ppm) 0.90 (t, 3H, *J* = 7.4 Hz), 1.57-1.66 (m, 2H), 2.46 (t, 2H, *J* = 7.3 Hz), 2.99 (t, 2H, *J* = 7.1 Hz), 3.20 (t, 2H, *J* = 7.1 Hz), 4.11 (brs, 2H), 7.11-7.13 (m, 1H), 7.15 (d, 1H, *J* = 2.6 Hz), 7.75 (d, 1H, *J* = 8.9 Hz), 8.60 (s, 1H); ¹³C NMR (100 MHz, CDCl₃, ppm) 13.8, 17.3, 29.2, 40.7, 44.9, 108.5, 121.8, 129.6, 136.9, 142.9, 146.0, 147.1, 151.8; HRMS (ESI) [M + H]⁺ :m/z 244.1466; Calculated mass for C₁₄H₁₈N₃O 244.1452.

4.2.8. General hydrolysis reaction of ester

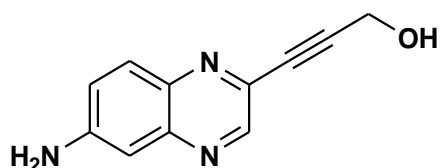
Ester was dissolved in methanol (10 mL) containing KOH (1 eq.) and stirred at rt for 30 minutes after which all acetate had been consumed. The solvent from reaction mixture was left to evaporate in the fume hood to leave a waxy, solid residue that was taken up in Et₂O (20 mL). The solids were filtered off and the ethereal solution was washed with water (10 mL), followed by brine (5 mL).⁹

4.2.8.1. Synthesis of 1-(6-aminoquinoxalin-2-yl)hex-1-yn-3-ol (36)



Compound **43** (50 mg, 0.18 mmol) was dissolved in methanol (10 mL) containing KOH (10 mg, 0.35 mmol, 1 eq.) according to procedure of hydrolysis reaction. The organic layer was dried over anhydrous Na₂SO₄ and concentrated to afford 1-(6-aminoquinoxalin-2-yl)hex-1-yn-3-ol **36** as yellow solid (37 mg, 87 %). M.p 107.1-108.3 °C; ¹H NMR (400 MHz, CDCl₃, ppm) 0.96 (t, 3H, *J* = 7.4 Hz), 1.54-1.59 (m, 2H), 1.81-1.86 (m, 2H), 4.68 (t, 2H, *J* = 6.7 Hz), 7.09 (d, 1H, *J* = 2.5 Hz), 7.16 (dd, 1H, *J* = 9.0 and 2.6 Hz), 7.79 (d, 1H, *J* = 9.0 Hz), 8.69 (s, 1H); ¹³C NMR (100 MHz, CDCl₃, ppm) 13.7, 18.5, 39.5, 62.4, 82.4, 93.7, 107.4, 122.7, 130.2, 134.4, 137.0, 142.8, 147.2, 148.8; V_{max} (FTIR) 550, 827, 1015, 1223, 1353, 1614, 1704, 2083, 2923, 3217, 3343 cm⁻¹; HRMS (ESI) [M + H]⁺ :m/z 242.1264; Calculated mass for C₁₄H₁₅N₃OH is 242.1295.

3.2.8.1. Synthesis of 3-(6-aminoquinoxalin-2-yl)prop-2-yn-1-ol (39)



Compound **41** (50 mg, 0.20 mmol) was dissolved in methanol (10 mL) containing KOH (12 mg, 0.20 mmol, 1 eq.) according to procedure of hydrolysis reaction. The organic layer was dried over anhydrous Na₂SO₄ and concentrated to afford 3-(6-aminoquinoxalin-2-yl)prop-2-yn-1-ol **39** as orange solid (33 mg, 83 %). M.p 163.3-166.0 °C; ¹H NMR (400 MHz, MeOD, ppm) 4.49 (s, 2H), 6.98 (d, 1H, *J* = 2.5 Hz), 7.31 (dd, 1H, *J* = 9.1 and 2.6 Hz), 7.68 (d, 1H, *J* = 9.1 Hz), 8.62 (s, 1H); ¹³C NMR (100 MHz, MeOD, ppm) 51.2, 83.0, 92.2, 106.0, 124.9, 130.3, 134.2, 137.6, 144.7, 148.1, 153.4 ppm; V_{max} (FTIR) 587, 819, 1003, 1231, 1353, 1614, 2104, 2919, 3209, 3335 cm⁻¹; HRMS (ESI) [M + H]⁺ :m/z 200.0824; Calculated mass for C₁₁H₉N₃OH is 200.0826.

4.3. Biological evaluation

4.3.1. MTT Assay

The synthesised compounds were evaluated for cytotoxicity assay against raw (264.7) and breast cancer (MCF-7) cell lines. Cell viability was determined using MTT [3-(4,5-Dimethylthiazol-2-yl)-2,5-diphenyltetrazolium Bromide] assay. Briefly MCF-7 and raw 264.7 cells were seeded at a density of 6×10^5 pre-well in a 96 well-plate and incubated at 37 °C in a CO₂ incubator, overnight. Cells were then treated with active compounds at various concentrations (25 µM, 50 µM and 100 µM), 0.5% DMSO in culture medium and 50 µg/mL Curcumin (positive control) for 24 hours. Subsequently, 10 µl of MTT reagent (5 mg/mL, Sigma Aldrich, Saint Louis, MI, USA) was added into each well-plate and incubated for 3 hours at 37 °C in a CO₂ incubator, followed by replacement of the aqueous medium with 100 µL DMSO. The blue formazan crystals were allowed to dissolve in DMSO by incubating in the dark for 30 min. Absorbance was then measured at 560 nm using GloMax-Multi microplate reader (Promega, USA). The relative cell viability was expressed as [(Abs sample/Abs control) × 100%].⁵

4.3.2. Broth micro-dilution method

The synthesised compounds were evaluated for in-vitro anti-mycobacterial activity against Mtb H₃₇Rv strain. The inhibitory activity against Mtb was conducted at the University of Cape Town, drug discovery and development centre (H3-D), following broth micro-dilution method. The broth micro-dilution method allows a range of antibiotic concentrations to be tested on a single 96-well microtitre plate in order to determine the minimum inhibitory concentration (MIC). Briefly, a 10 mL culture of a mutant Mtb (H₃₇Rv) strain constitutively expressing recombinant alamar blue assay of a plasmid integrated at the attB locus is grown to an OD₆₀₀ of 0.6–0.7. The H₃₇Rv strain culture is then diluted 1:100 in 7H9 GLU CAS TX. In a 96-well microtitre plate, 50 µL of 7H9 GLU CAS TX medium is added to all wells from Rows 2-12. The compounds to be tested are added to Row 2-12 in duplicate, at a final concentration of 640 µM (stocks are made up to a concentration of 12.8 mM in DMSO and diluted to 640 µM in 7H9 GLU CAS TX medium).

A two-fold serial dilution is prepared, by transferring 50 μ L of the liquid in Row 1 and 2 to mix. 50 μ L of the liquid in Row 2 is then transferred to Row 3 and aspirated. The procedure is repeated until Row 12 is reached, from which 50 μ L of the liquid is discarded to bring the final volume in all wells to 50 μ L. Finally, 50 μ L of the 1:100 diluted Mtb cultures are added to all wells in Rows 2-12. Row 1 serves as a contamination control which includes media, 5 % DMSO and rifampicin. The microtitre plate is stored in a secondary container and incubated at 37 °C with humidifier to prevent evaporation of the liquid. The lowest concentration of compounds which inhibit growth of more than 90% of the bacterial population is considered to be the MIC₉₀. The pellet data is reported as visual score and calculated MIC during 14-day post inoculation.¹⁰

4.4. References

1. Gumede, N. J., Nxumalo, W., Bisetty, K., Gilabert, L. E. and Medina-hernandez, M. J. Prospective computational design and in vitro bio-analytical tests of new chemical entities as potential selective CYP17A1 lyase inhibitors. *Bioorg. Chem.*, 1-20 (2019).
2. Panwar, U. and Singh, S. K. Structure-based virtual screening toward the discovery of novel inhibitors for impeding the protein-protein interaction between HIV-1 integrase and human lens epithelium-derived growth factor (LEDGF/p75). *J. Biomol. Struct. Dyn.*, **1102**, 1–19 (2017).
3. Nxumalo, W. and Dinsmore, A. Preparation of 6-Ethynylpteridine Derivatives by Sonogashira Coupling. *ChemInform*, **44**, 79-89 (2013).
4. Qian, X., Tang, E., Fan, J., Zhu, K., Zhu, J., Shabaker, J., Lo, E., Malley M. and Deshpande, R. A stereoselective synthesis of (S)-2-(((3-fluoro-4-methylphenoxy)carbonyl)(1-(4-((5-methyl-2-phenyloxazol-4-yl)methoxy)phenyl)ethyl)amino) acetic acid, a highly potent PPAR α/γ dual agonist. *Tetrahedron*, **71**, 9408-9414 (2015).
5. Sibiya, M. A., Raphoko, L., Mangokoana, D., Makola, R., Nxumalo, W. and Matsebatlela, T. M. Induction of Cell Death in Human A549 Cells Using 3-(Quinoxaline-3-yl) Prop-2-ynyl Methanosulphonate and 3-(Quinoxaline-3-yl) Prop-2-yn-1-ol. *Molecules*, **24**, 1-16 (2019).
6. Hussein, M., Dine, A. N., Farès, F., Dorcet, V., Hachem, A. and Grée, R. A new direct synthesis of α -methylene- and α -alkylidene- β -lactams. *Tet. Lett.*, **57**, 1990–1993 (2016).
7. Mercier, L. G., Remorova, A. A., Fillion, E., Tre, V. E. and Carson, R. J. Oxidative coupling of 2-substituted 1, 2-dihydro-1-naphthols using Jones reagent: a simple entry into 3, 3 0 -disubstituted. *Tet. Lett.*, **46**, 1091–1094 (2005)
8. Laurent, D., Ferrié, L., Sepulveda-Diaz, J. E., Majid Amar, M., Harfouche, A., Séon-Méniel, B., Raisman-Vozari, R., Michel, P. P. and Figade, B. New

- 6-aminoquinoxaline derivatives with neuroprotective effect on dopaminergic neurons in cellular and animal Parkinson disease models. *J. Med. Chem.*, **59**, 6169–6186 (2016).
9. Riss, P. J., Hummerich, R. and Schloss, P. Synthesis and monoamine uptake inhibition of conformationally constrained 2-b-carbomethoxy-3-b-phenyl tropanes. *Org. Biomol. Chem.*, **7**, 2688–2698 (2009).
 10. Yang, J., Pi, W., Xiong, L., Ang, W., Yang, T., He, J., Liu, Y., Chang, Y., Ye, W., Wang, Z., Luo, Y. and Wei, Y. three protons -1, 2, 4-Dithiazol-3-one compounds as novel potential affordable antitubercular agents. *Bioorg. Med. Chem. Lett.* **23**, 1424–1427 (2013).

Chapter 5

APPENDIX

The spectral analysis of all compounds identified from molecular docking.

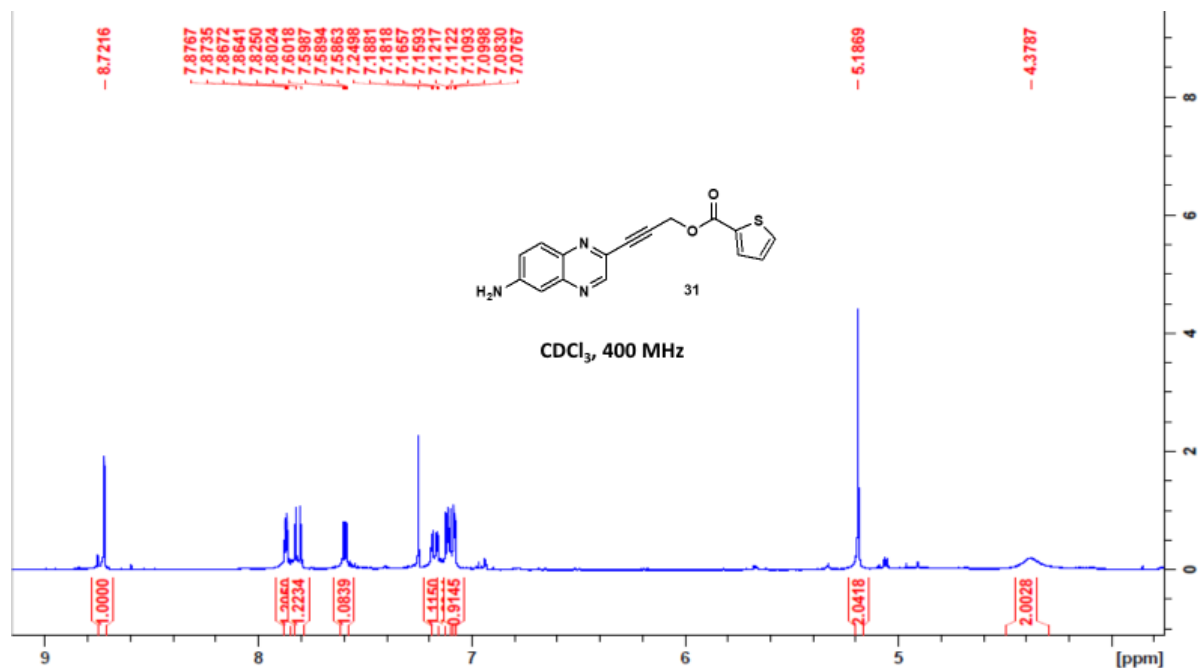


Figure 5.1: ^1H NMR spectrum of 3-(6-aminoquinoxalin-2-yl)prop-2-ynyl thiophene-2-carboxylate **31**

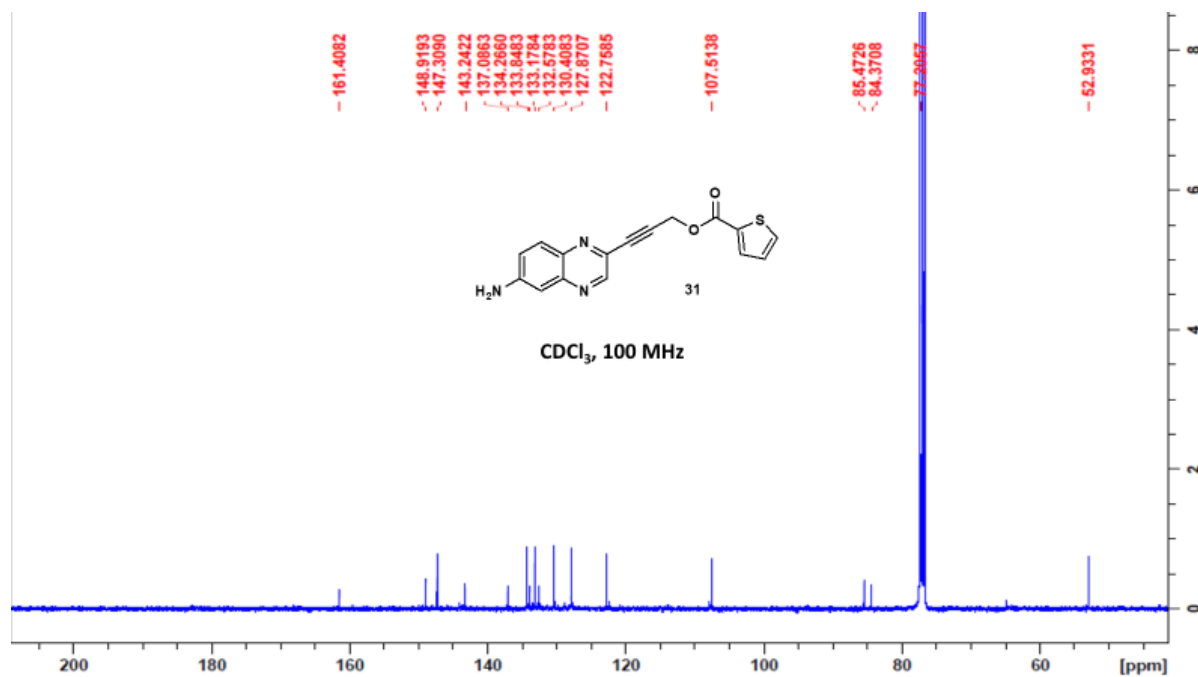


Figure 5.2: ^{13}C NMR spectrum of 3-(6-aminoquinoxalin-2-yl)prop-2-ynyl thiophene-2-carboxylate **31**

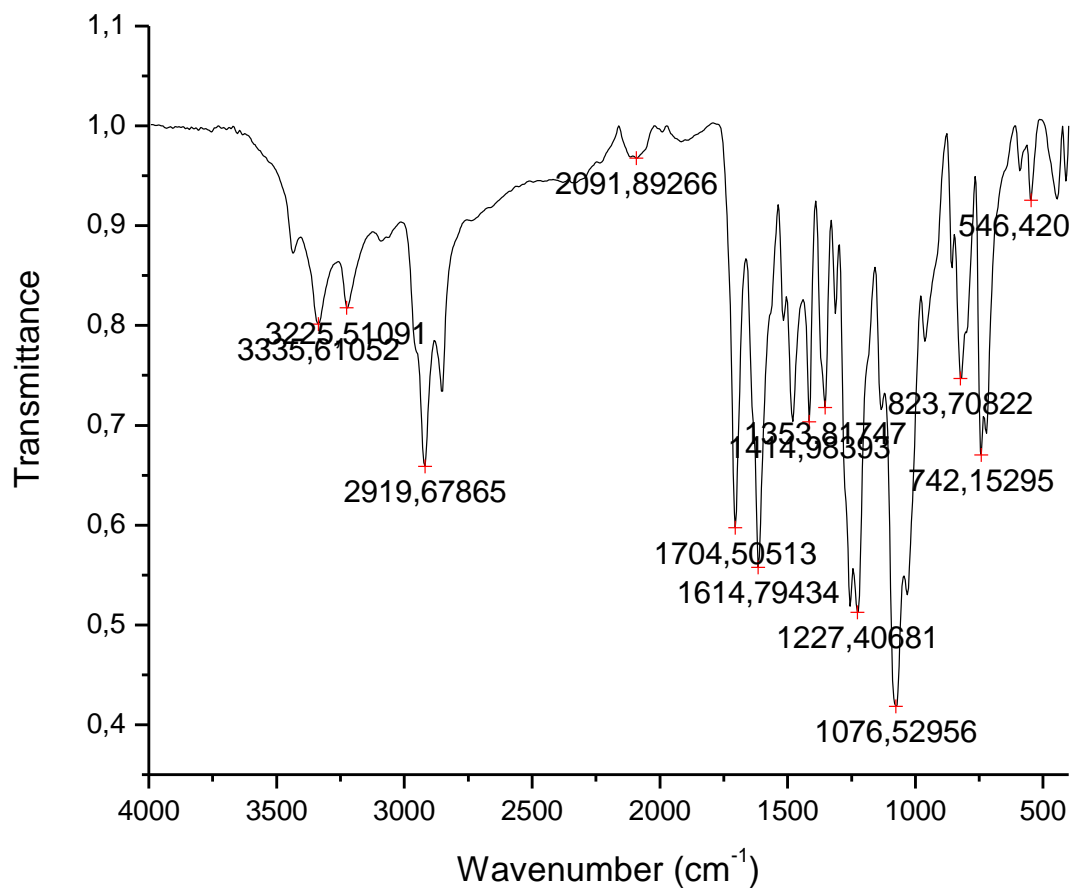


Figure 5.3: The FTIR spectrum of 3-(6-aminoquinoxalin-2-yl)prop-2-ynyl thiophene-2-carboxylate **31**

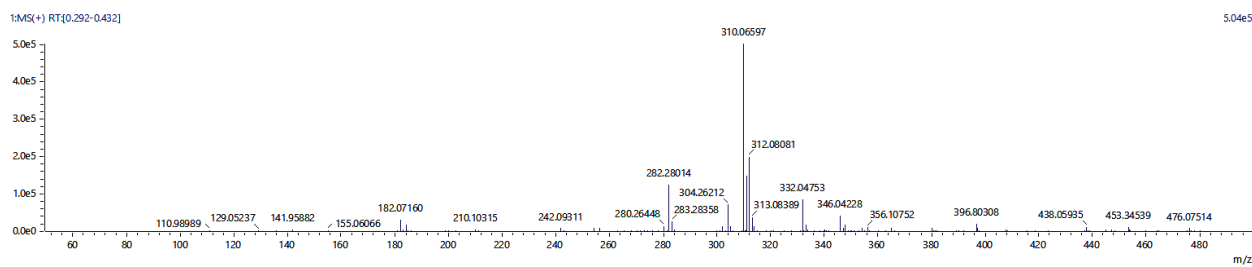


Figure 5.4: Mass spectrum of 3-(6-aminoquinoxalin-2-yl)prop-2-ynyl thiophene-2-carboxylate **31**

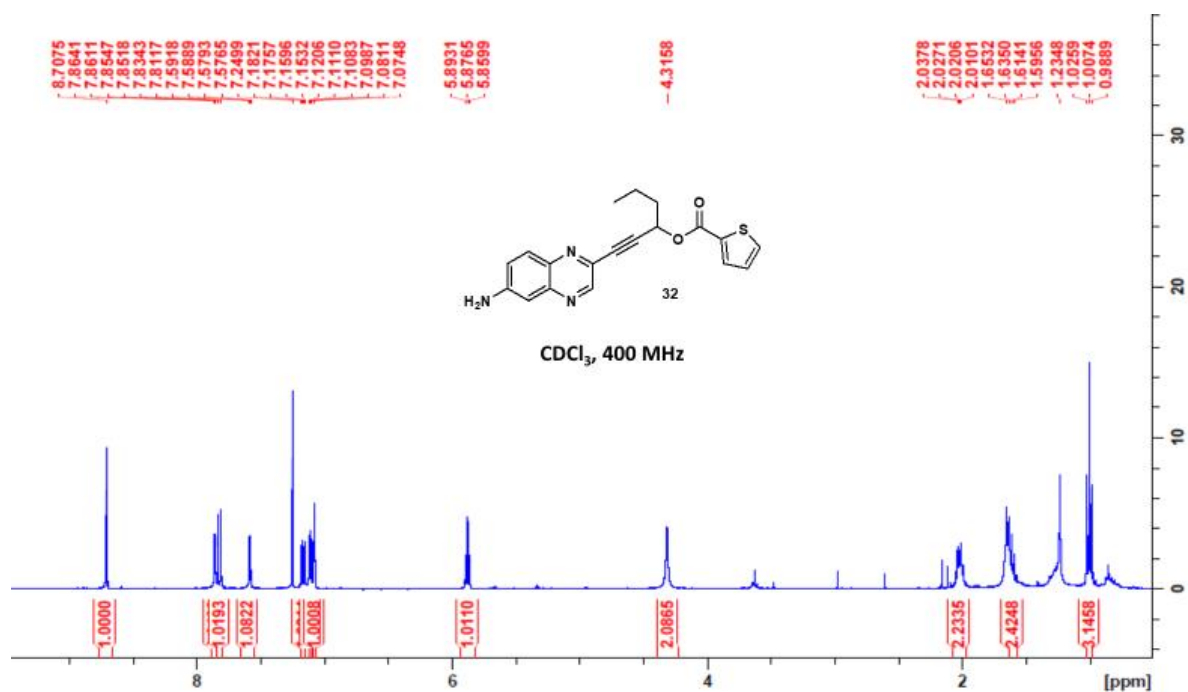


Figure 5.5: ¹H NMR spectrum of 1-(6-aminoquinoxalin-2-yl)hex-1-yn-3-yl thiophene-2-carboxylate **32**

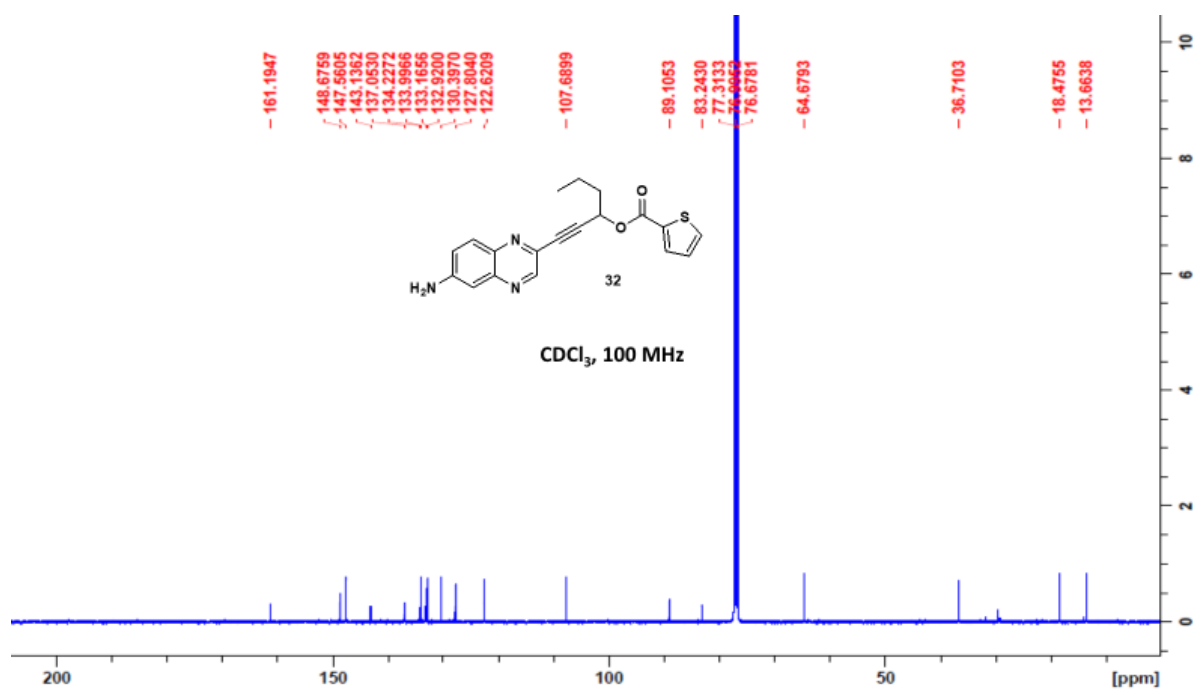


Figure 5.6: ¹³C NMR spectrum of 1-(6-aminoquinoxalin-2-yl)hex-1-yn-3-yl thiophene-2-carboxylate **32**

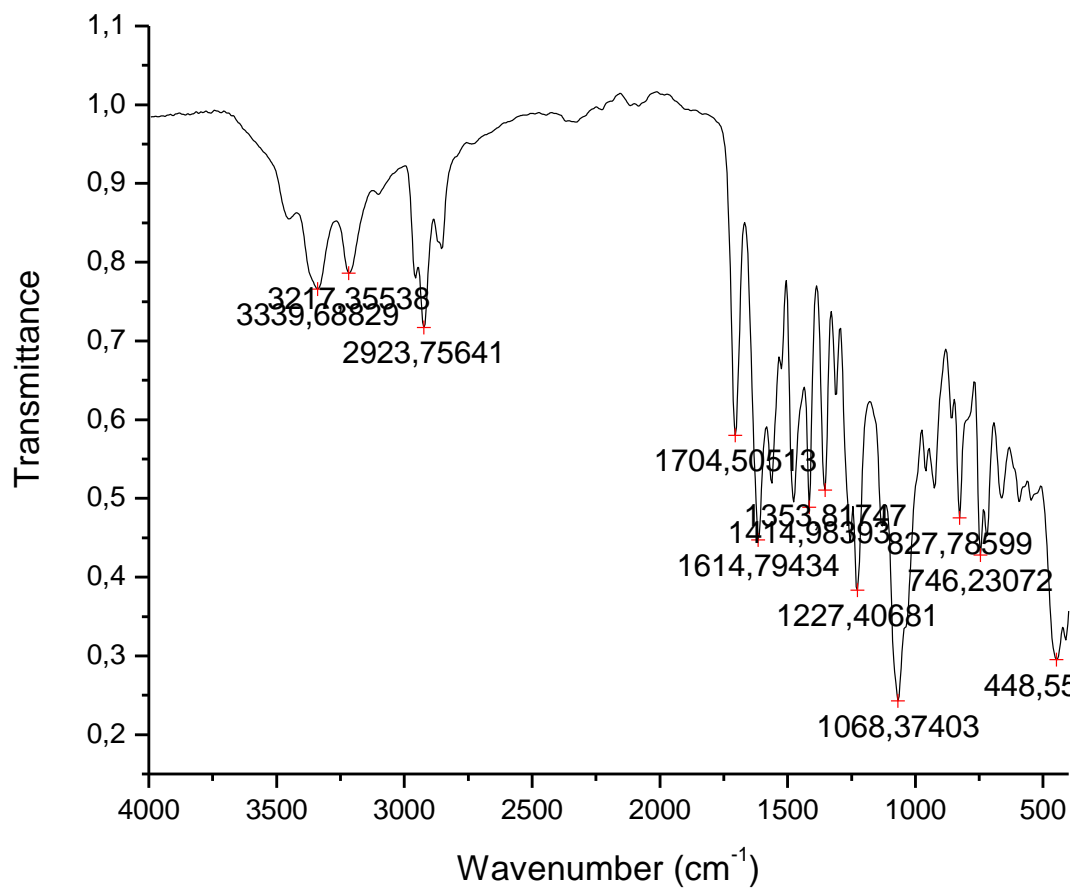


Figure 5.7: The FTIR spectrum of 1-(6-aminoquinoxalin-2-yl)hex-1-yn-3-yl thiophene-2-carboxylate **32**

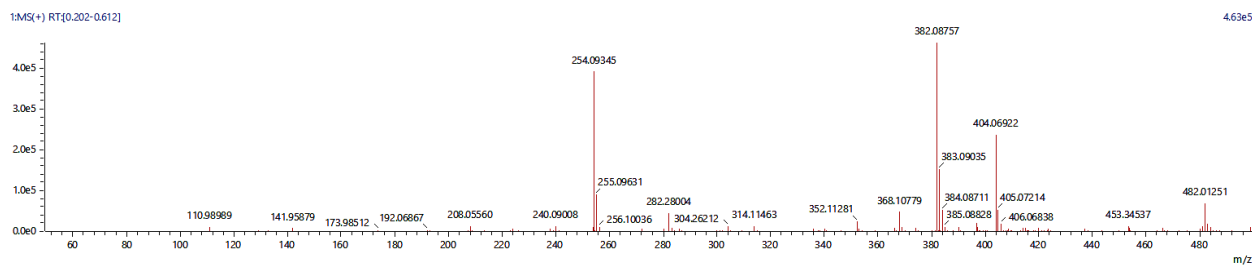


Figure 5.8: Mass spectrum of 1-(6-aminoquinoxalin-2-yl)hex-1-yn-3-yl thiophene-2-carboxylate **32**

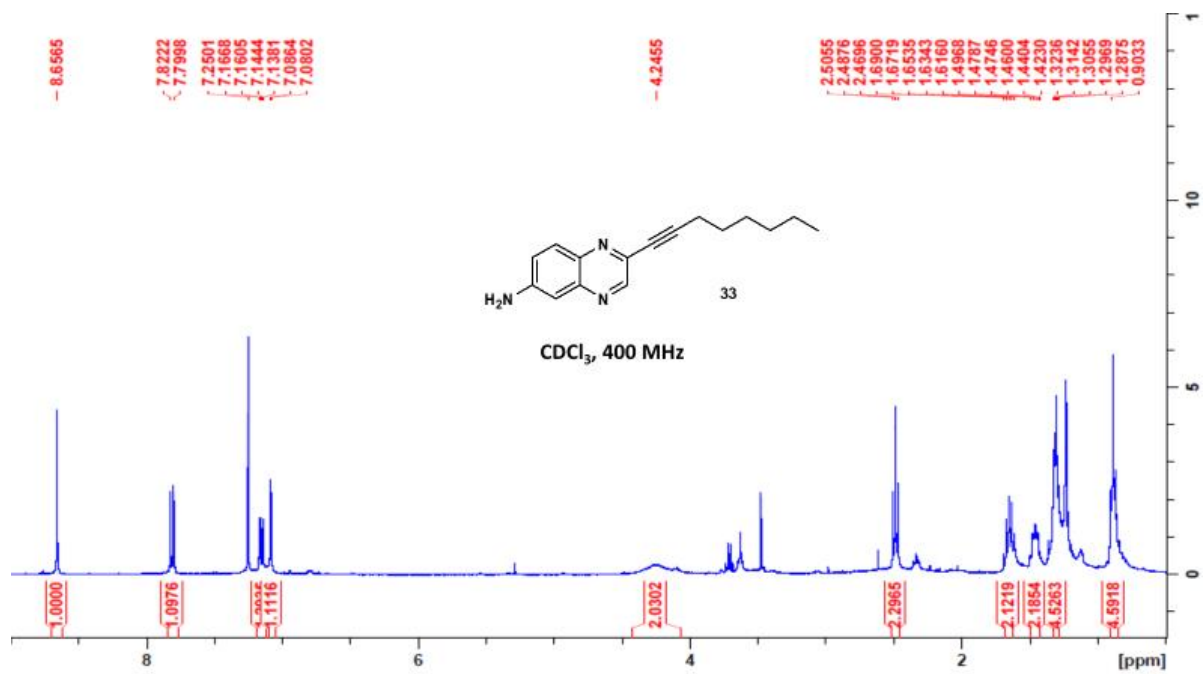


Figure 5.9: ^1H NMR spectrum of 2-(oct-1-ynyl)quinoxalin-6-amine **33**

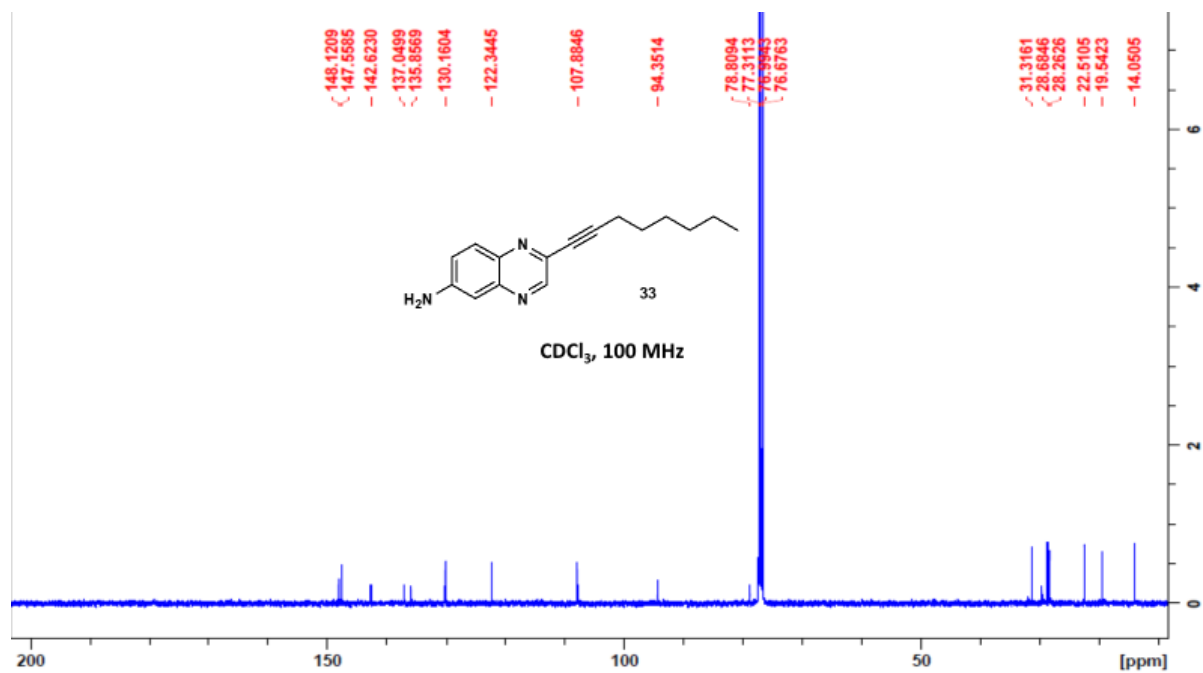


Figure 5.10: ^{13}C NMR spectrum of 2-(oct-1-ynyl)quinoxalin-6-amine **33**

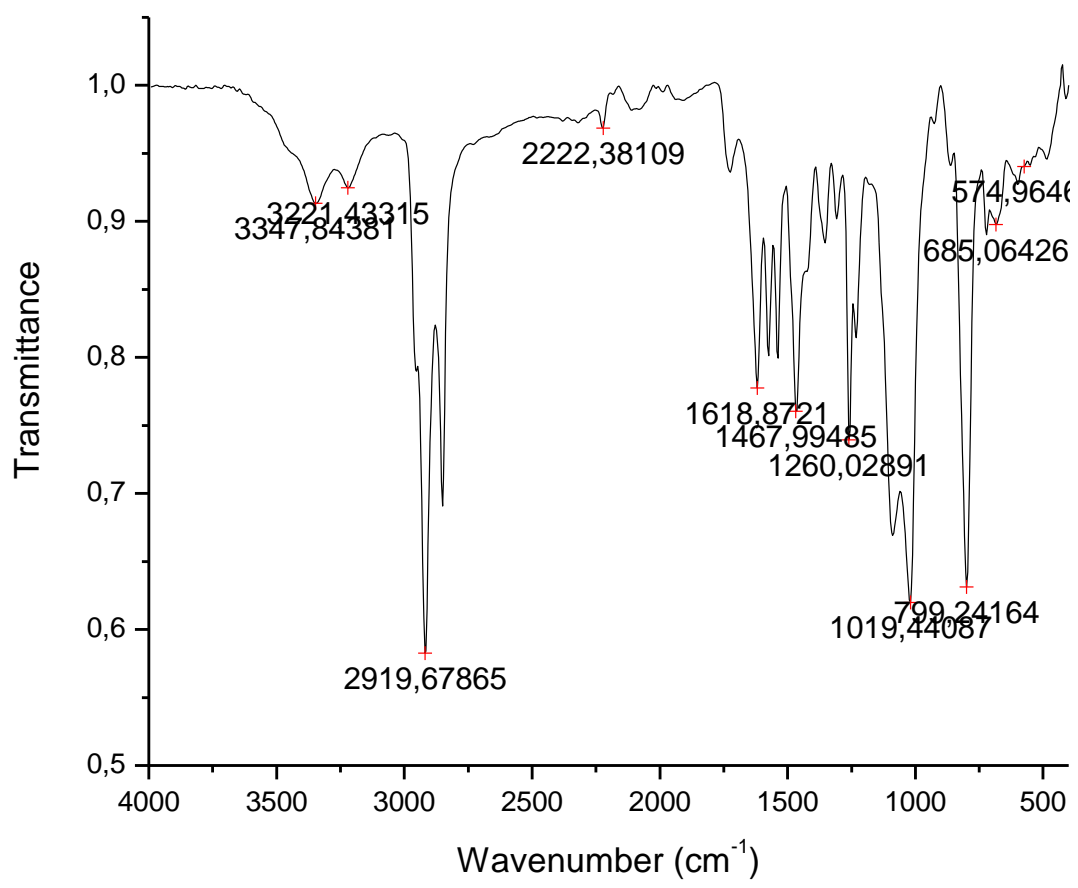


Figure 5.11: The FTIR spectrum of 2-(oct-1-ynyl)quinoxalin-6-amine **33**

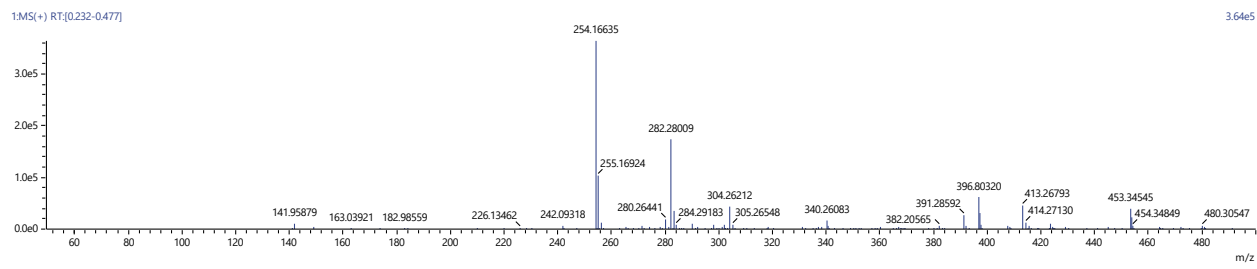


Figure 5.12: Mass spectrum of 2-(oct-1-ynyl)quinoxalin-6-amine **33**

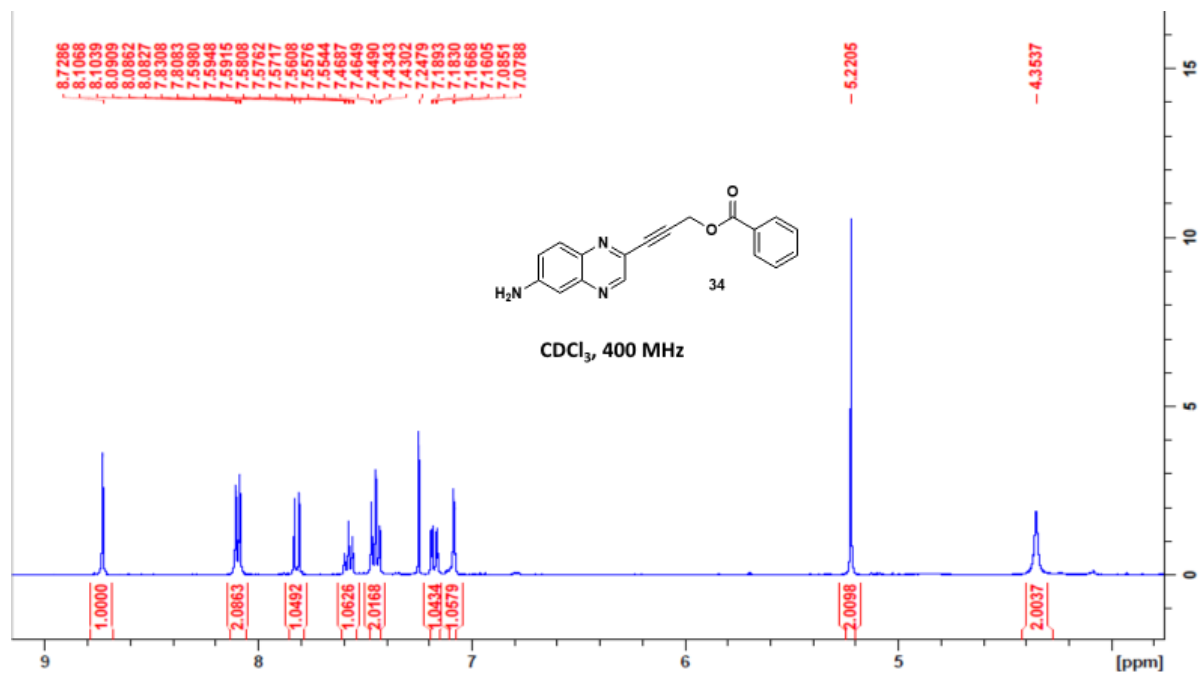


Figure 5.13: ^1H NMR spectrum of 3-(6-aminoquinoxalin-2-yl)prop-2-ynyl benzoate **34**

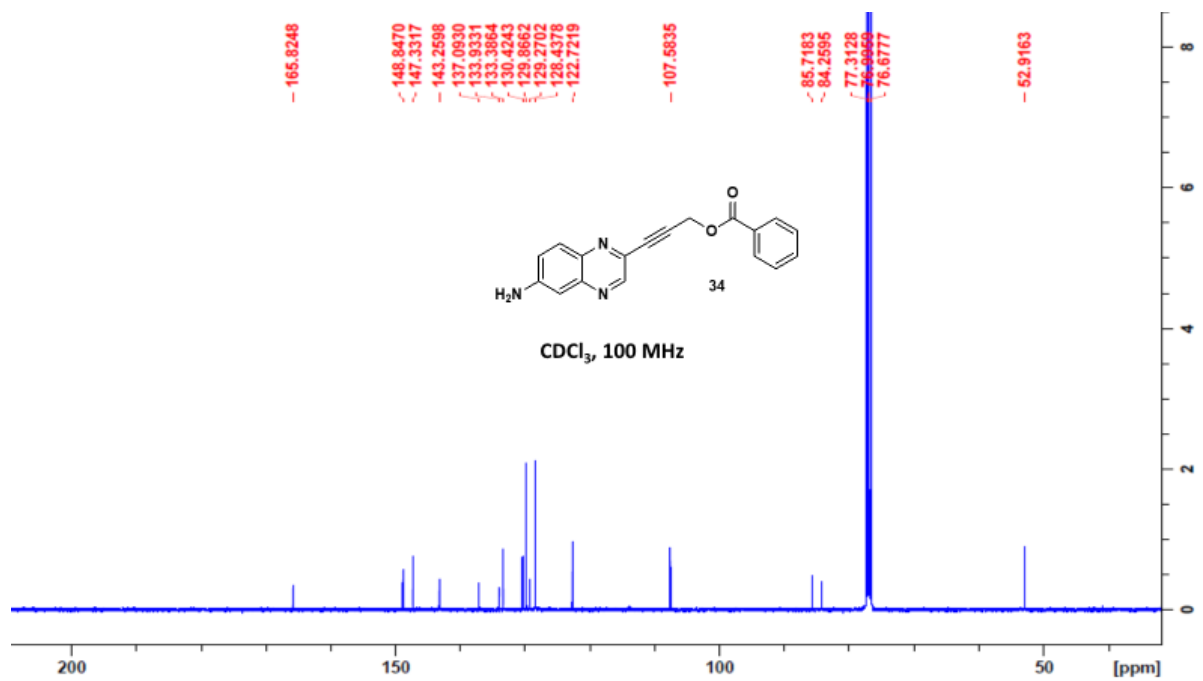


Figure 5.14: ^{13}C NMR spectrum of 3-(6-aminoquinoxalin-2-yl)prop-2-ynyl benzoate **34**

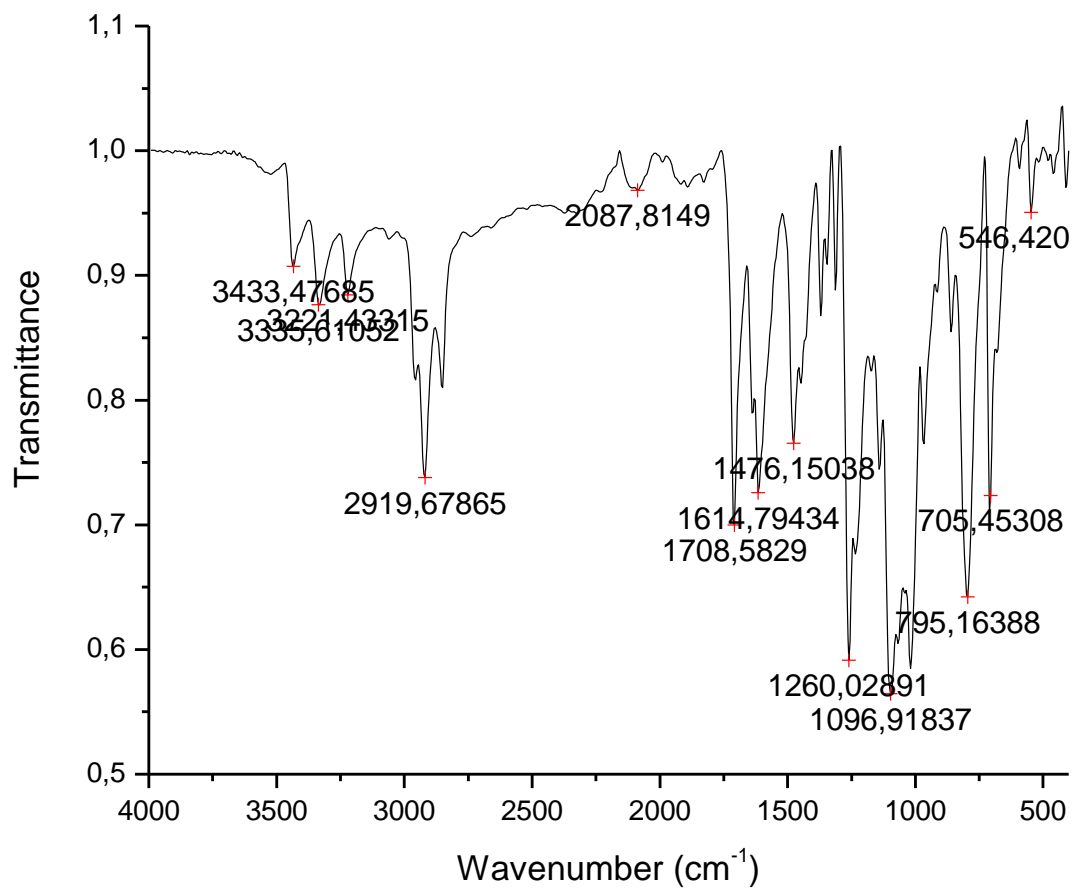


Figure 5.15: The FTIR spectrum of 3-(6-aminoquinoxalin-2-yl)prop-2-ynyl benzoate **34**

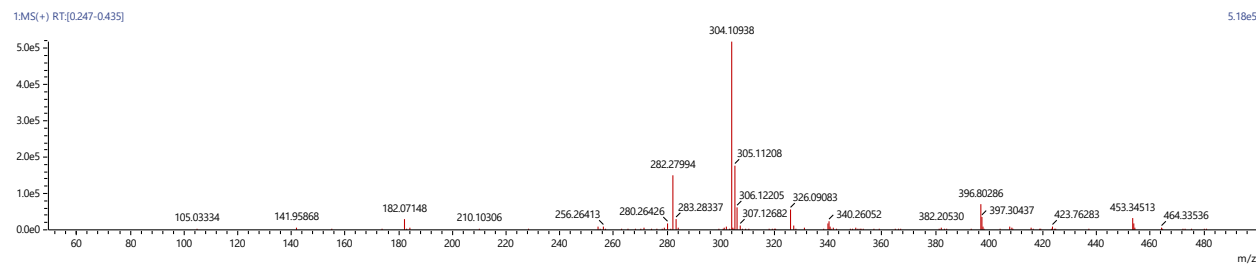


Figure 5.16: Mass spectrum of 3-(6-aminoquinoxalin-2-yl)prop-2-ynyl benzoate **34**

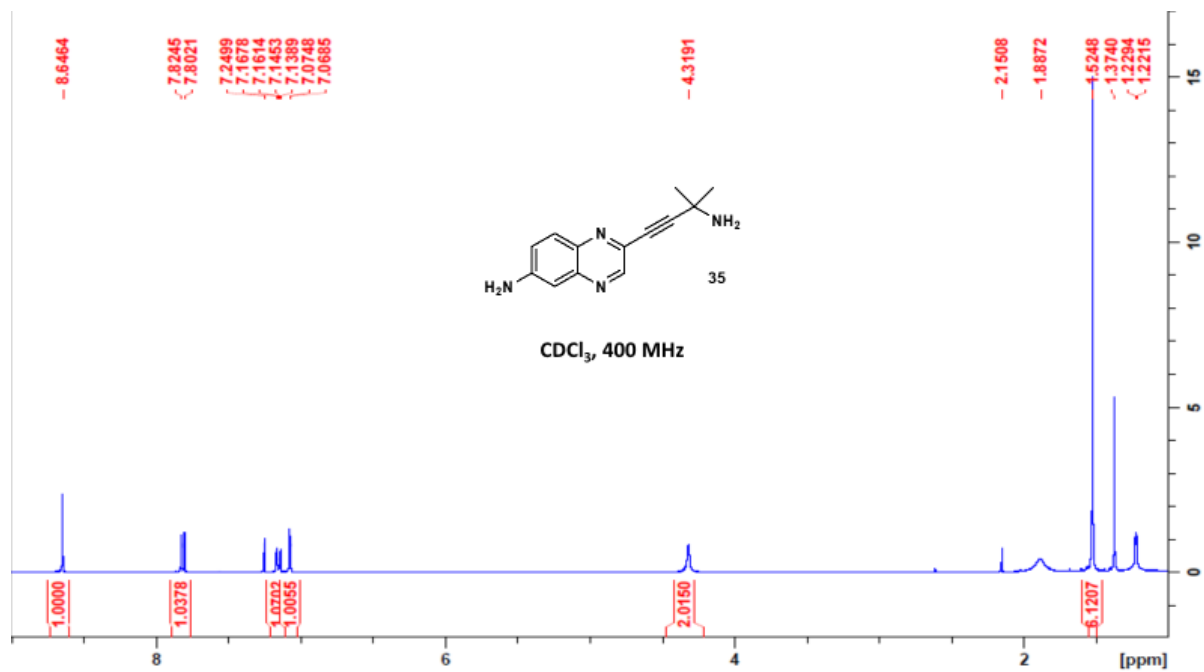


Figure 5.17: 1H NMR spectrum of 2-(3-amino-3-methylbut-1-ynyl)quinoxalin-6-amine **35**

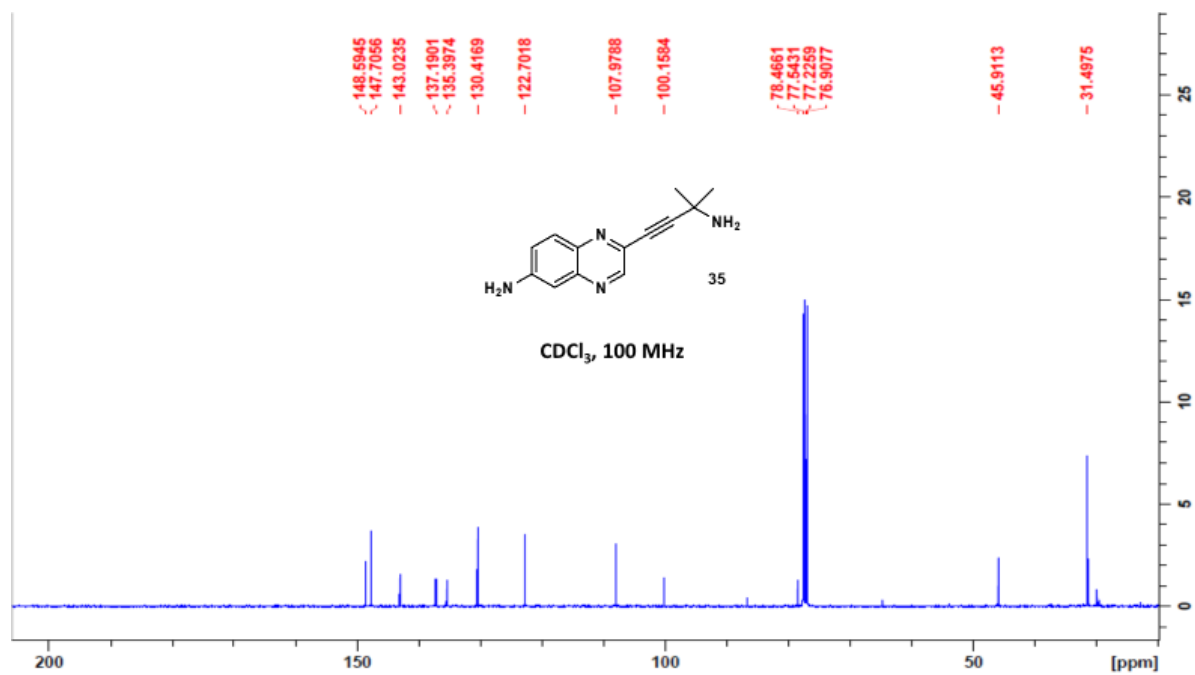


Figure 5.18: ^{13}C NMR spectrum of 2-(3-amino-3-methylbut-1-ynyl)quinoxalin-6-amine **35**

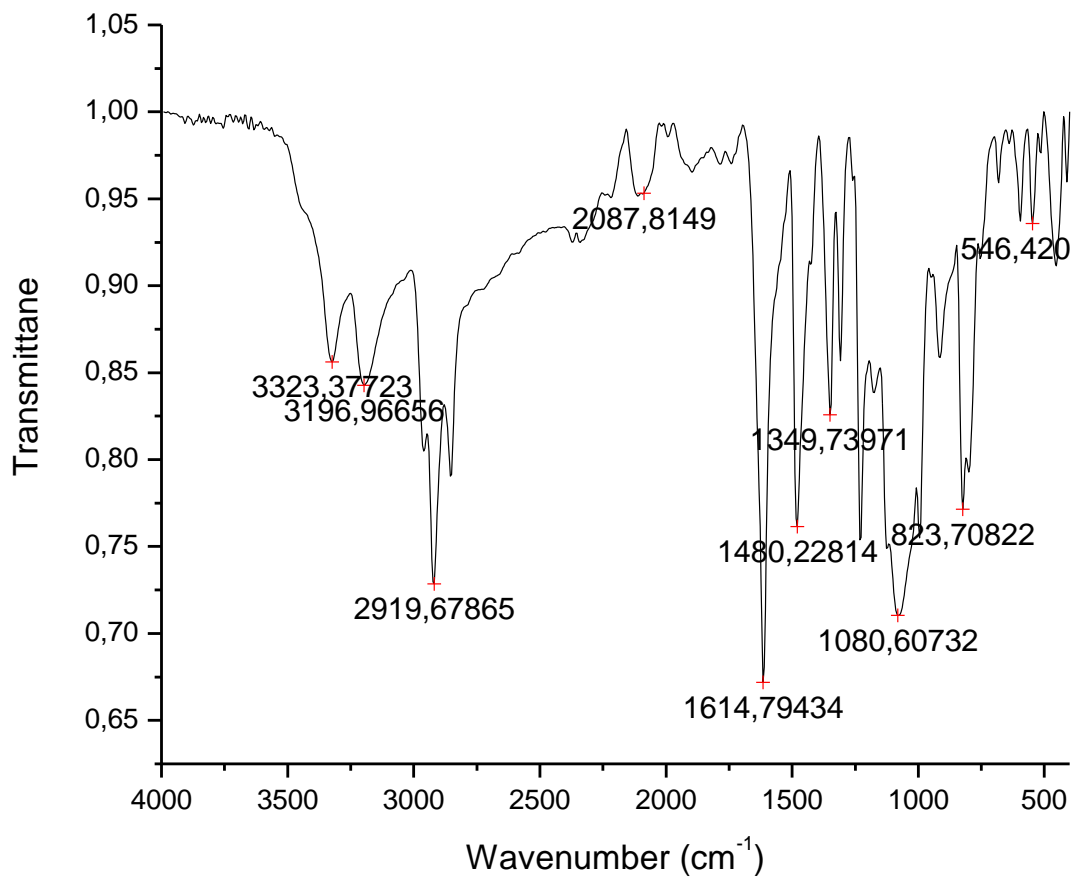


Figure 5.19: The FTIR spectrum of 2-(3-amino-3-methylbut-1-ynyl)quinoxalin-6-amine **35**

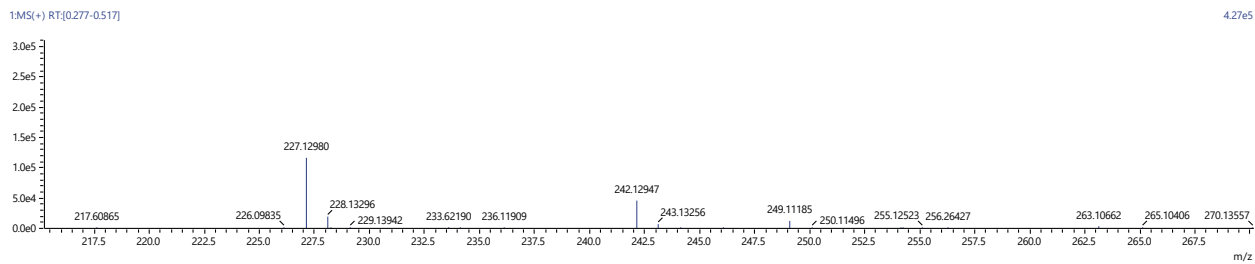


Figure 5.20: Mass spectrum of 2-(3-amino-3-methylbut-1-ynyl)quinoxalin-6-amine **35**

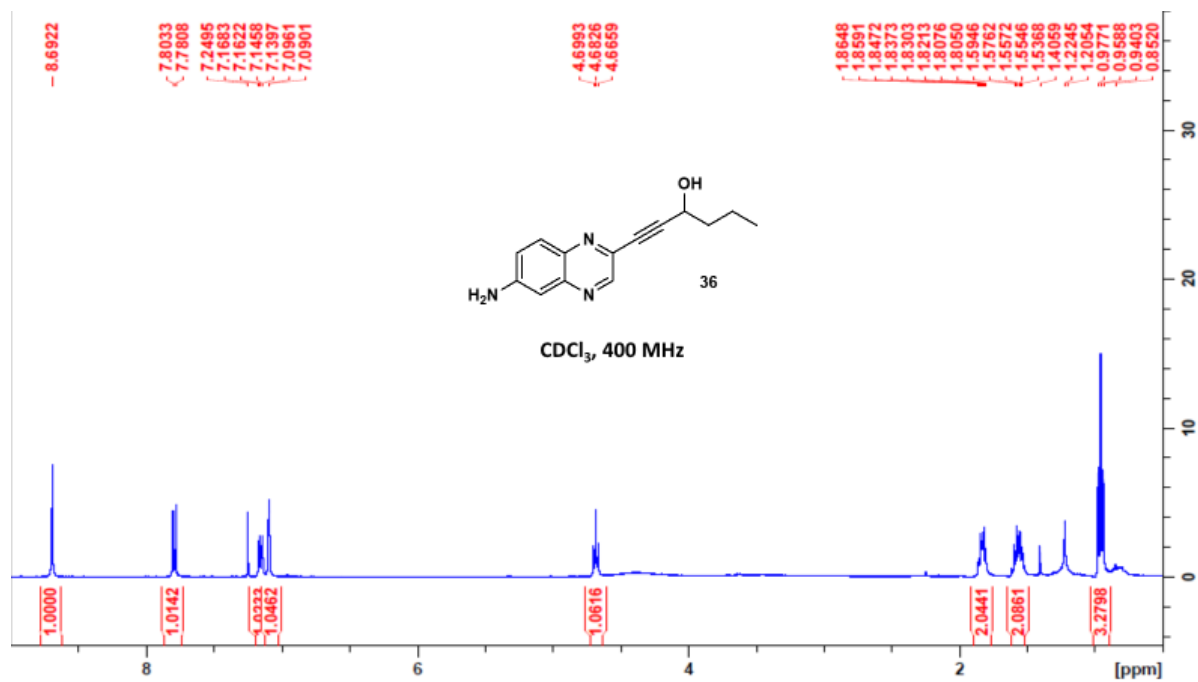


Figure 5.21: 1H NMR spectrum of 1-(6-aminoquinoxalin-2-yl)hex-1-yn-3-ol **36**

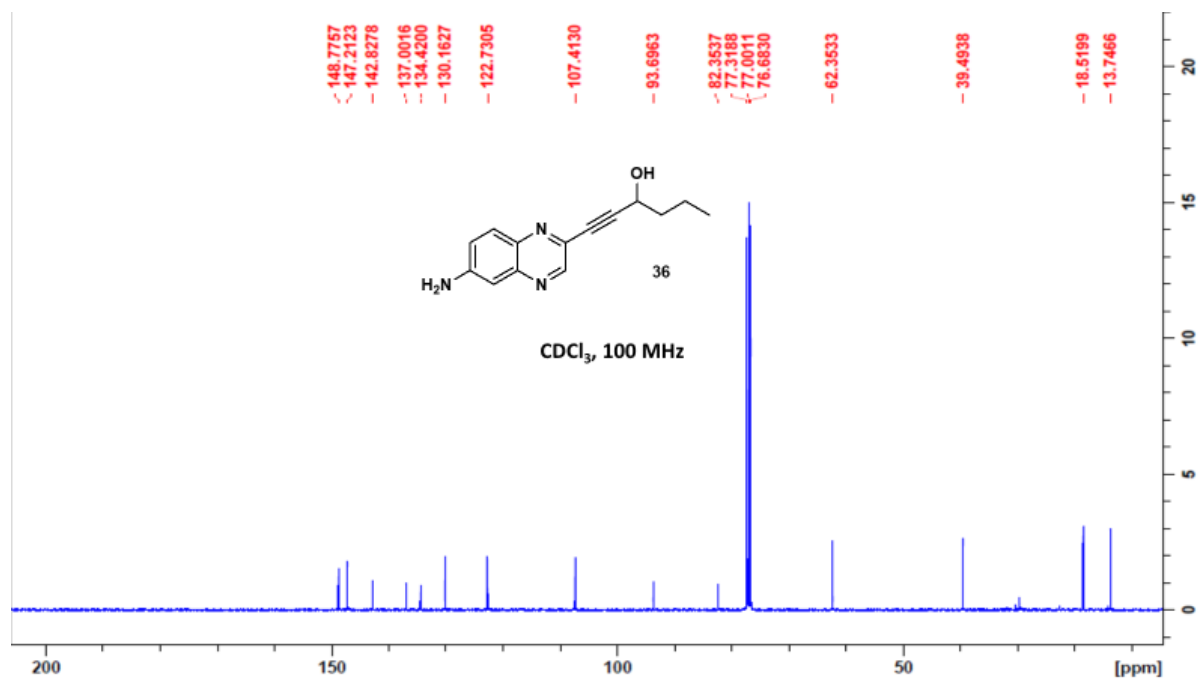


Figure 5.22: ^{13}C NMR spectrum of 1-(6-aminoquinoxalin-2-yl)hex-1-yn-3-ol **36**

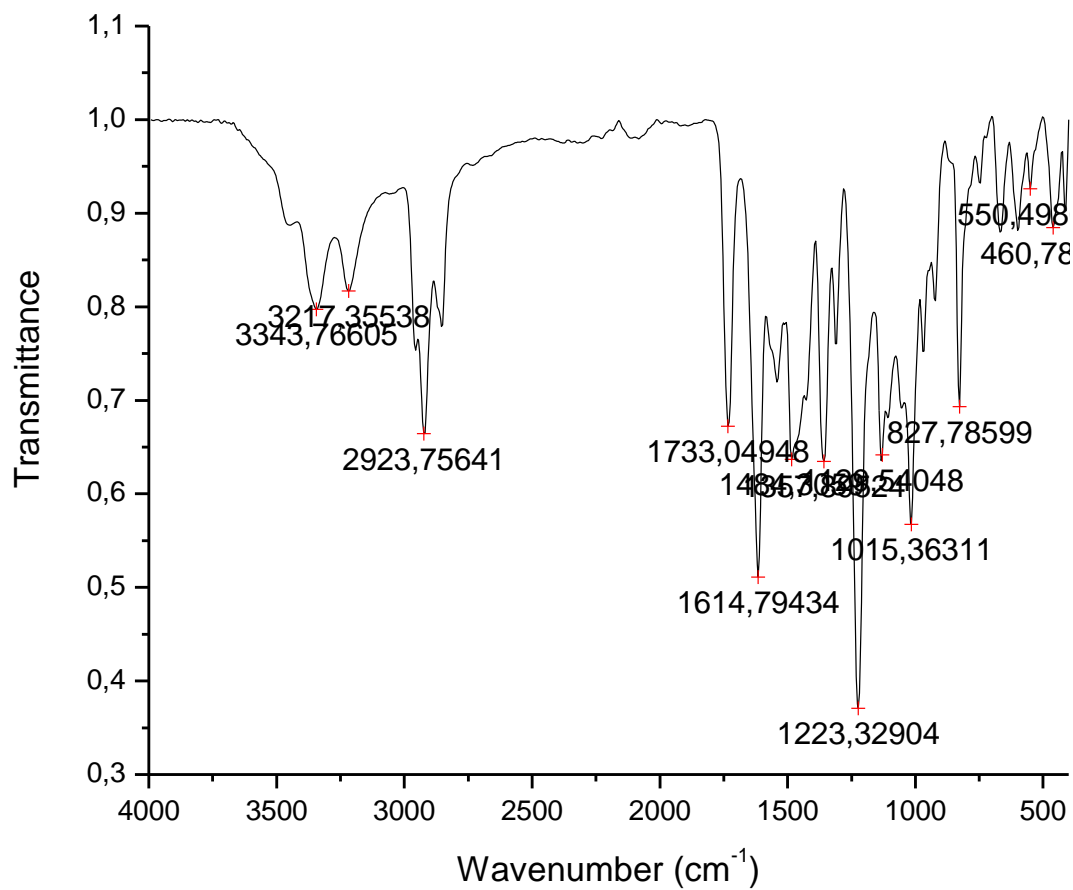


Figure 5.23: The FTIR spectrum of 1-(6-aminoquinoxalin-2-yl)hex-1-yn-3-ol **36**

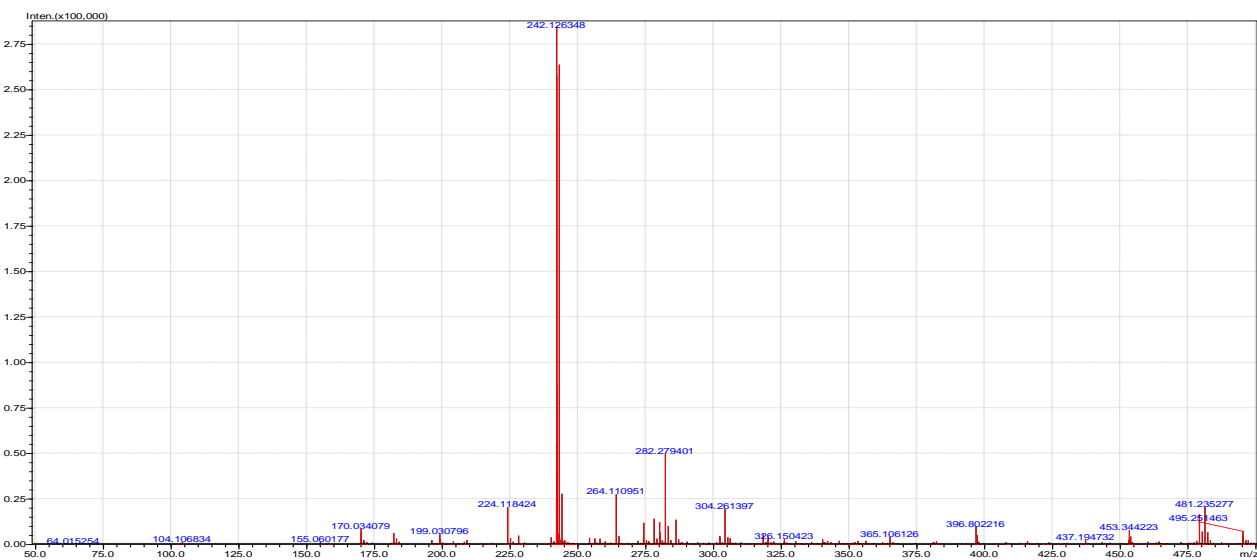


Figure 5.24: Mass spectrum of 1-(6-aminoquinoxalin-2-yl)hex-1-yn-3-ol **36**

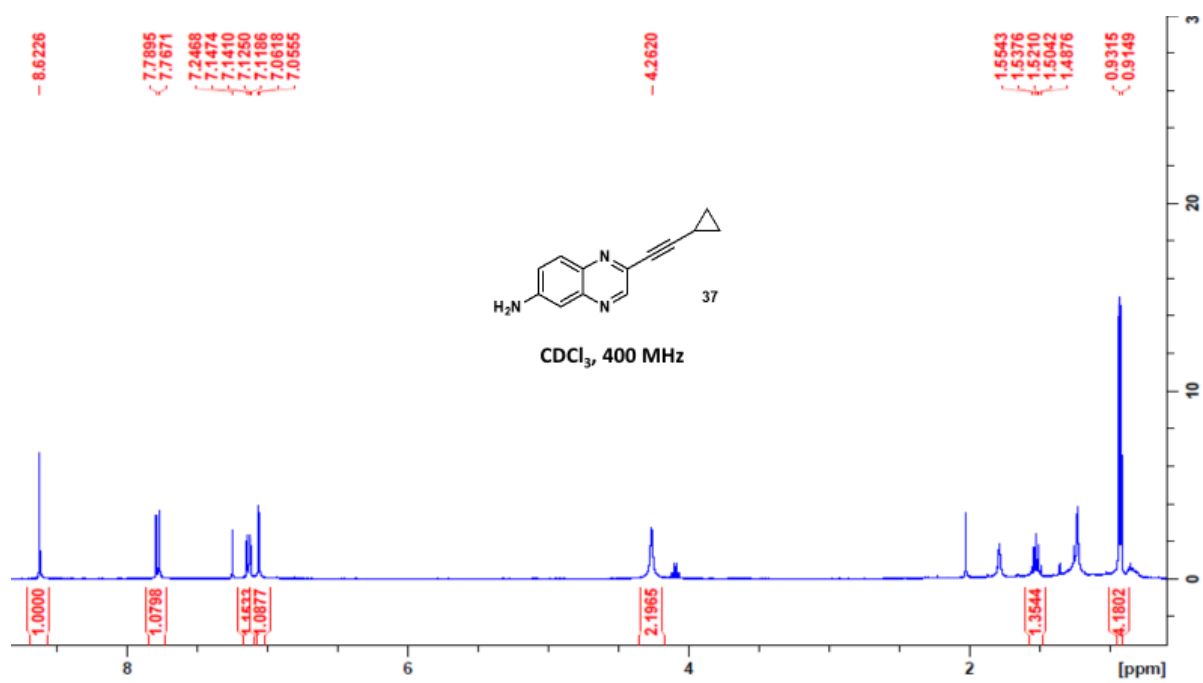


Figure 5.25: 1H NMR spectrum of 2-(2-cyclopropylethynyl)quinoxalin-6-amine **37**

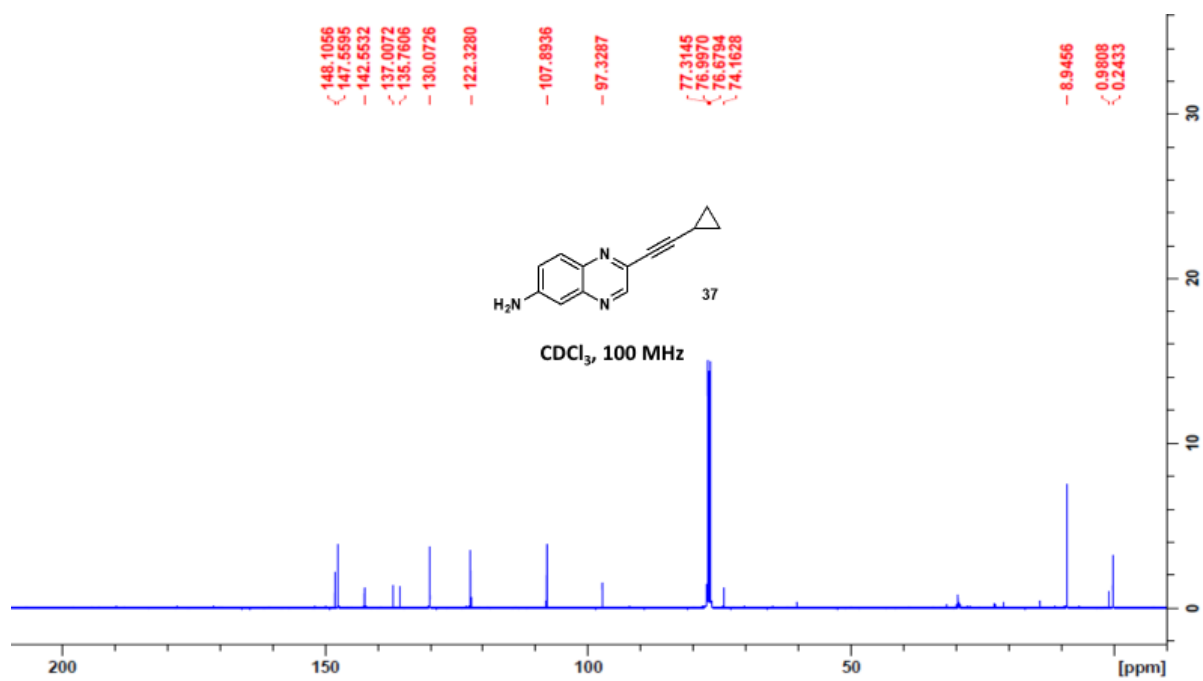


Figure 5.26: ^{13}C NMR spectrum of 2-(2-cyclopropylethynyl)quinoxalin-6-amine **37**

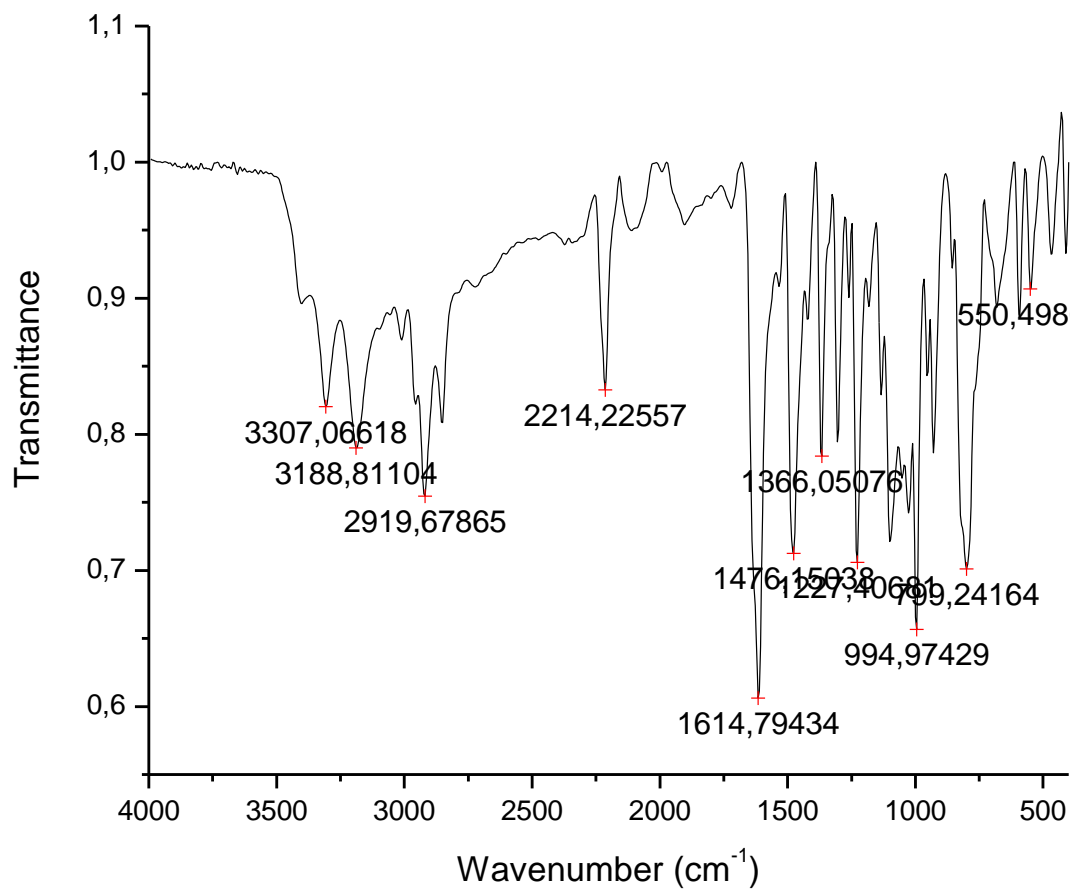


Figure 5.27: The FTIR spectrum of 2-(2-cyclopropylethynyl)quinoxalin-6-amine **37**

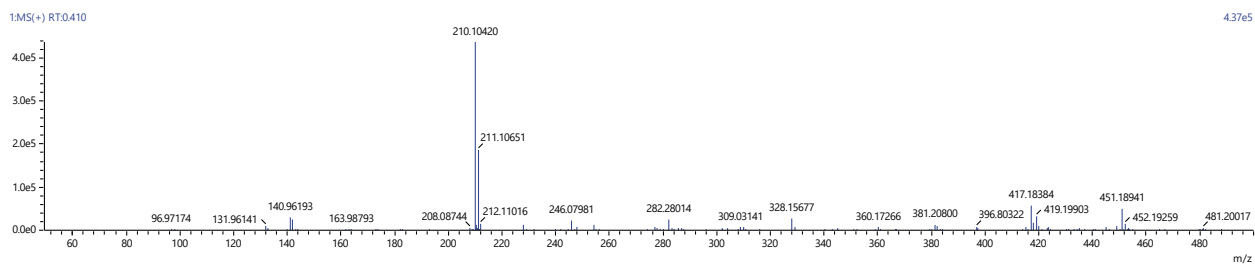


Figure 5.28: Mass spectrum of 2-(2-cyclopropylethynyl)quinoxalin-6-amine **37**

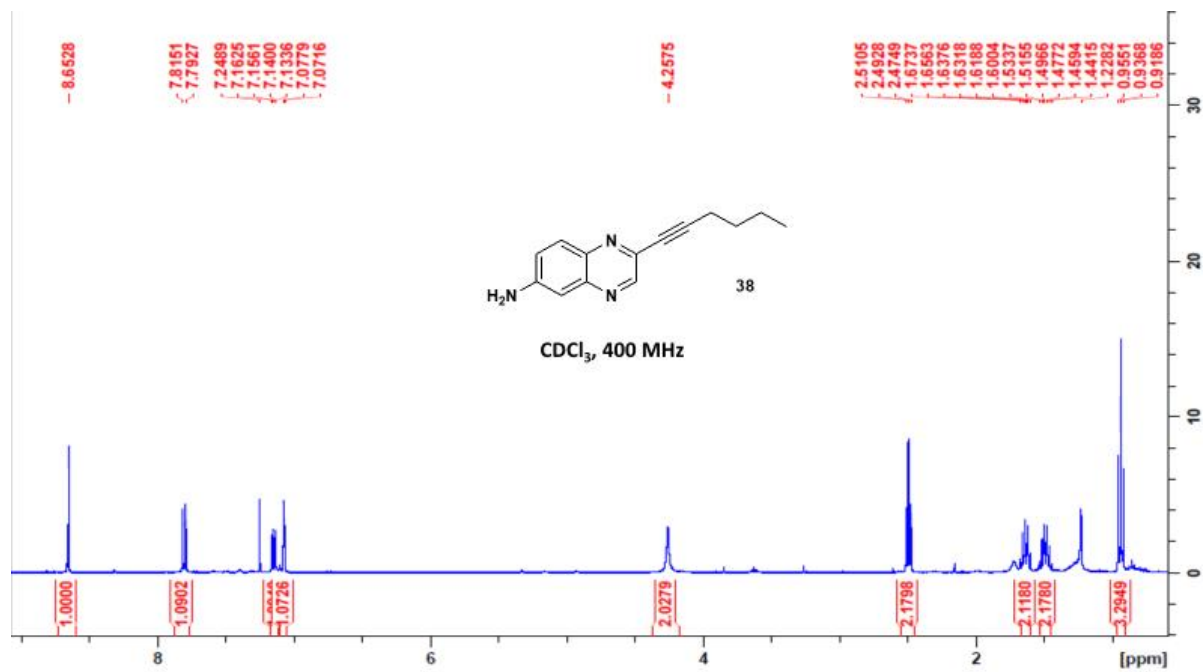


Figure 5.29: 1H NMR spectrum of 2-(hex-1-ynyl)quinoxalin-6-amine **38**

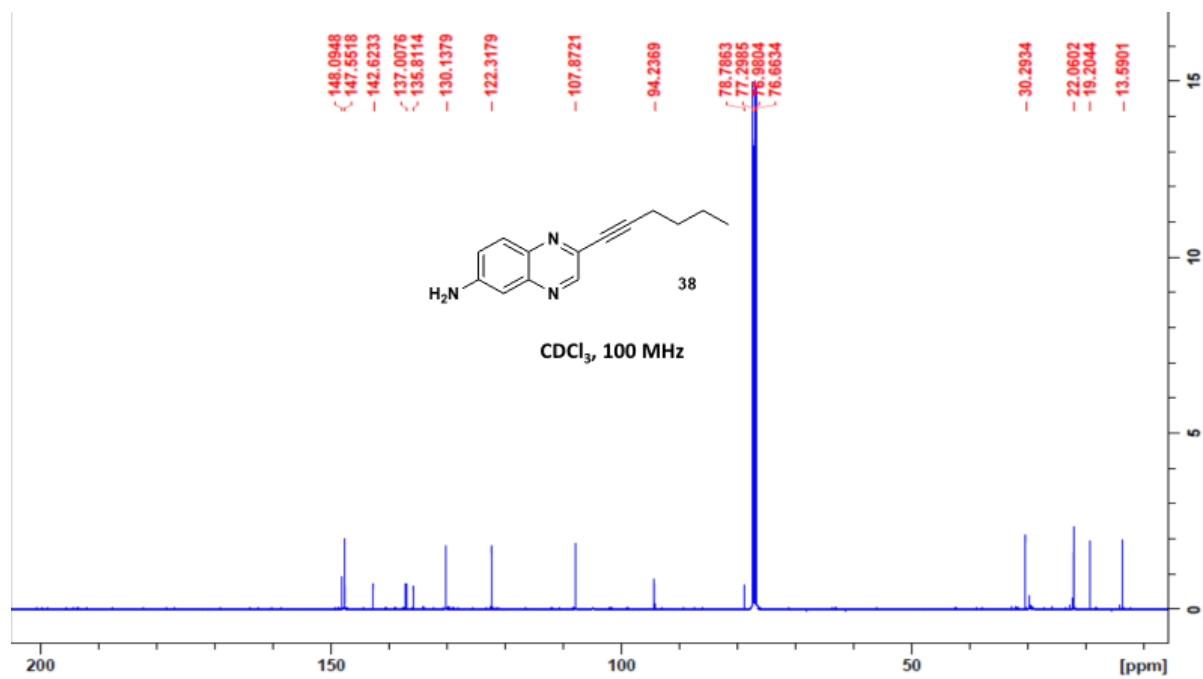


Figure 5.30: ^{13}C NMR spectrum of 2-(hex-1-ynyl)quinoxalin-6-amine **38**

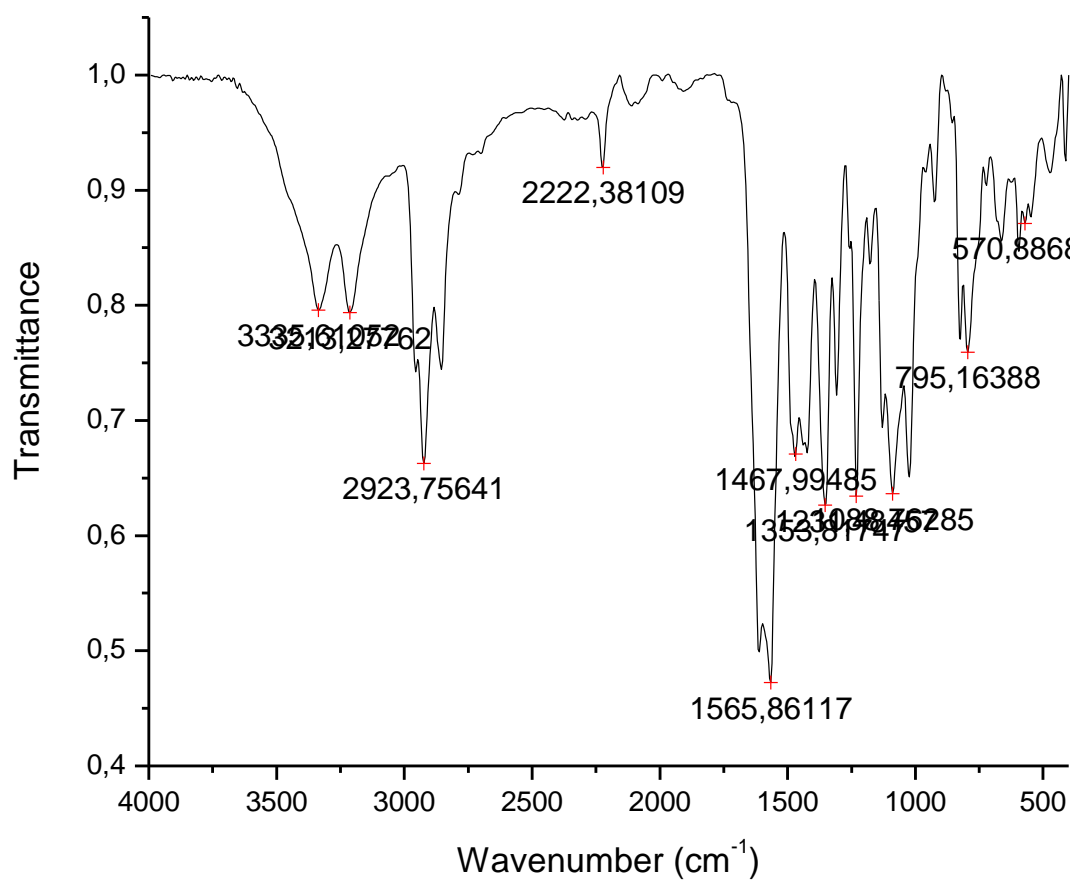


Figure 5.31: The FTIR spectrum of 2-(hex-1-ynyl)quinoxalin-6-amine **38**

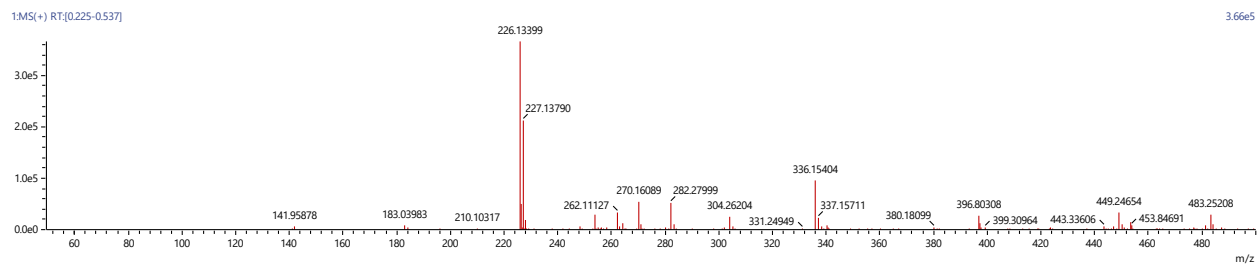


Figure 5.32: Mass spectrum of 2-(hex-1-ynyl)quinoxalin-6-amine **38**

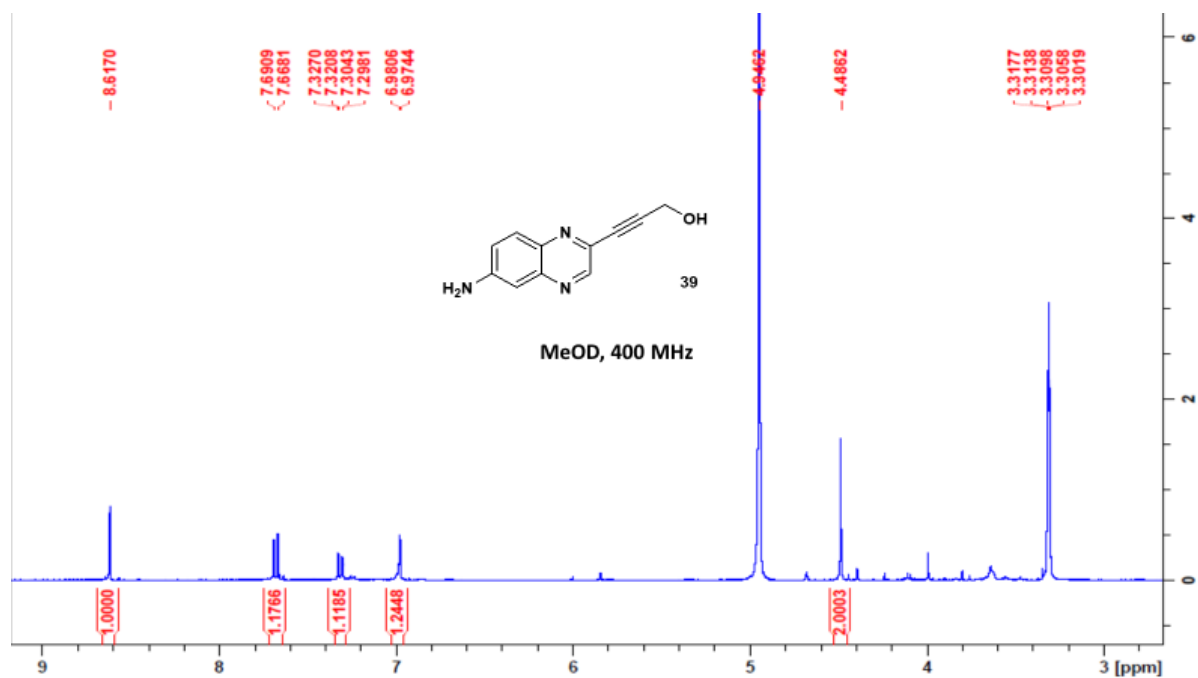


Figure 5.33: ^1H NMR spectrum of 3-(6-aminoquinoxalin-2-yl)prop-2-yn-1-ol **39**

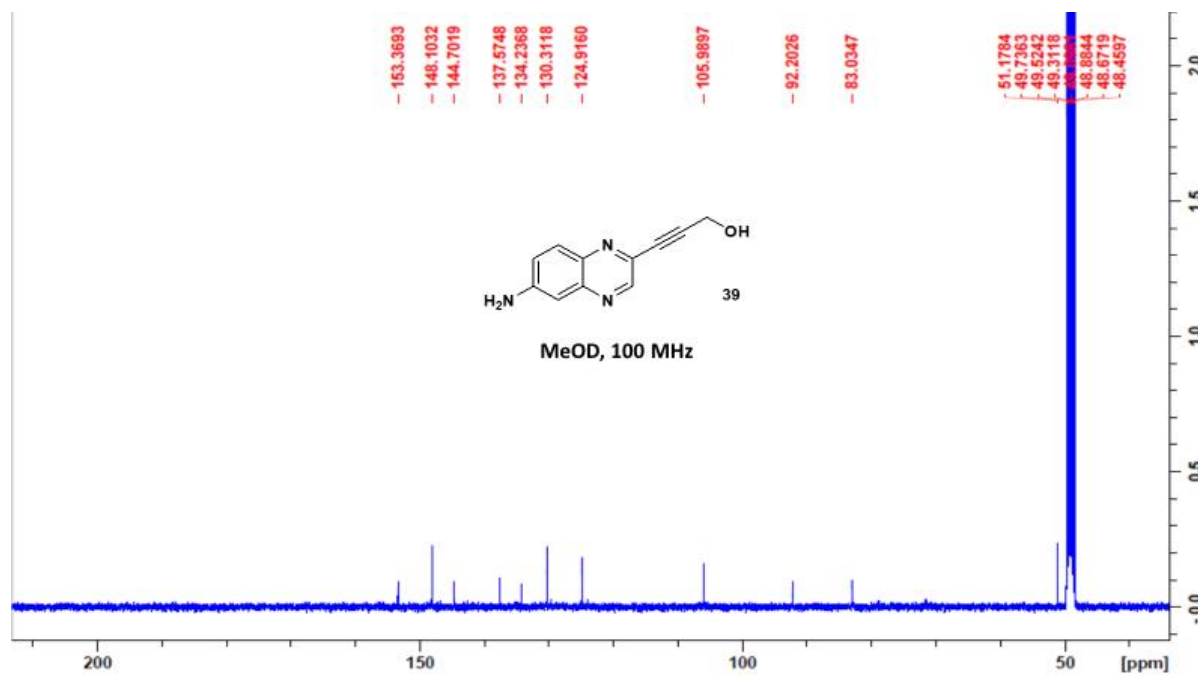


Figure 5.34: ^{13}C NMR spectrum of 3-(6-aminoquinoxalin-2-yl)prop-2-yn-1-ol **39**

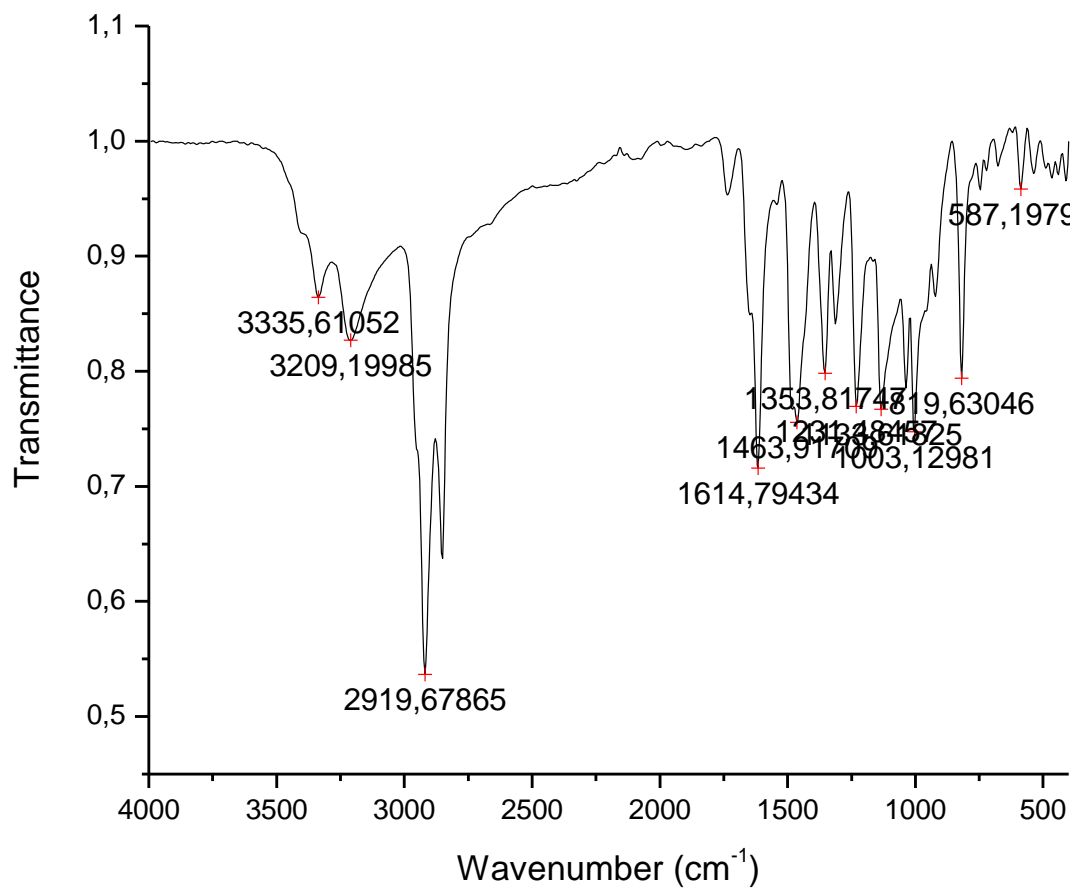


Figure 5.35: The FTIR spectrum of 3-(6-aminoquinoxalin-2-yl)prop-2-yn-1-ol **39**

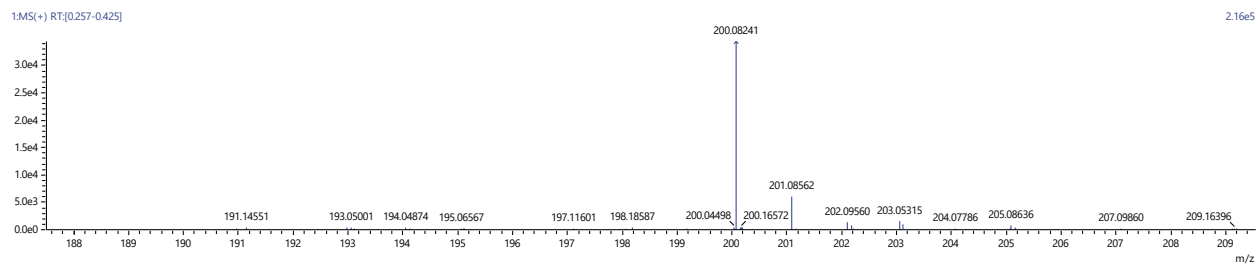


Figure 5.36: Mass spectrum of 3-(6-aminoquinoxalin-2-yl)prop-2-yn-1-ol **39**

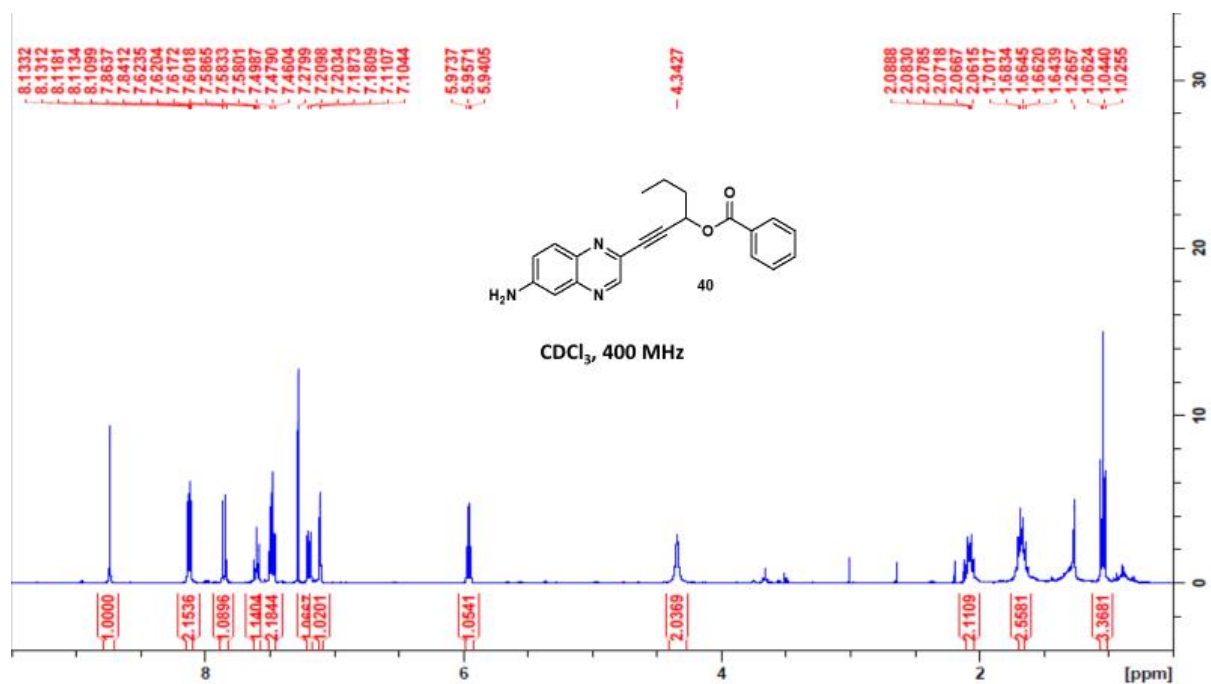


Figure 5.37: 1H NMR spectrum of 1-(6-aminoquinoxalin-2-yl)hex-1-yn-3-yl benzoate **40**

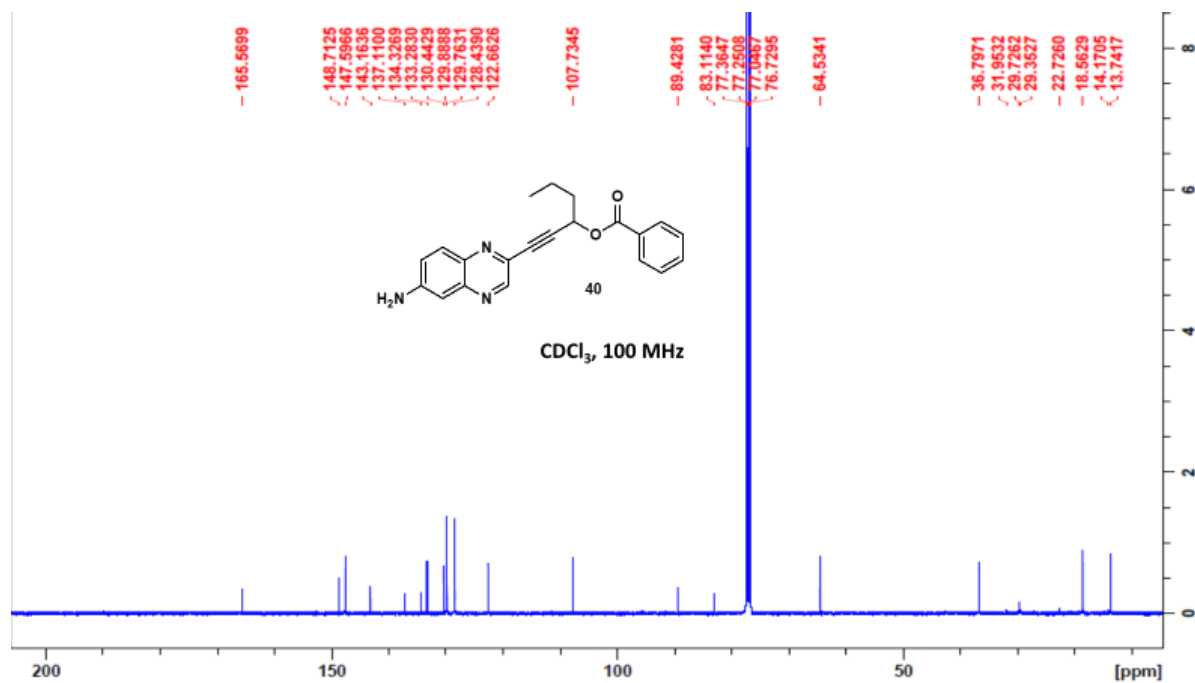


Figure 5.38: ^{13}C NMR spectrum of 1-(6-aminoquinoxalin-2-yl)hex-1-yn-3-yl benzoate **40**

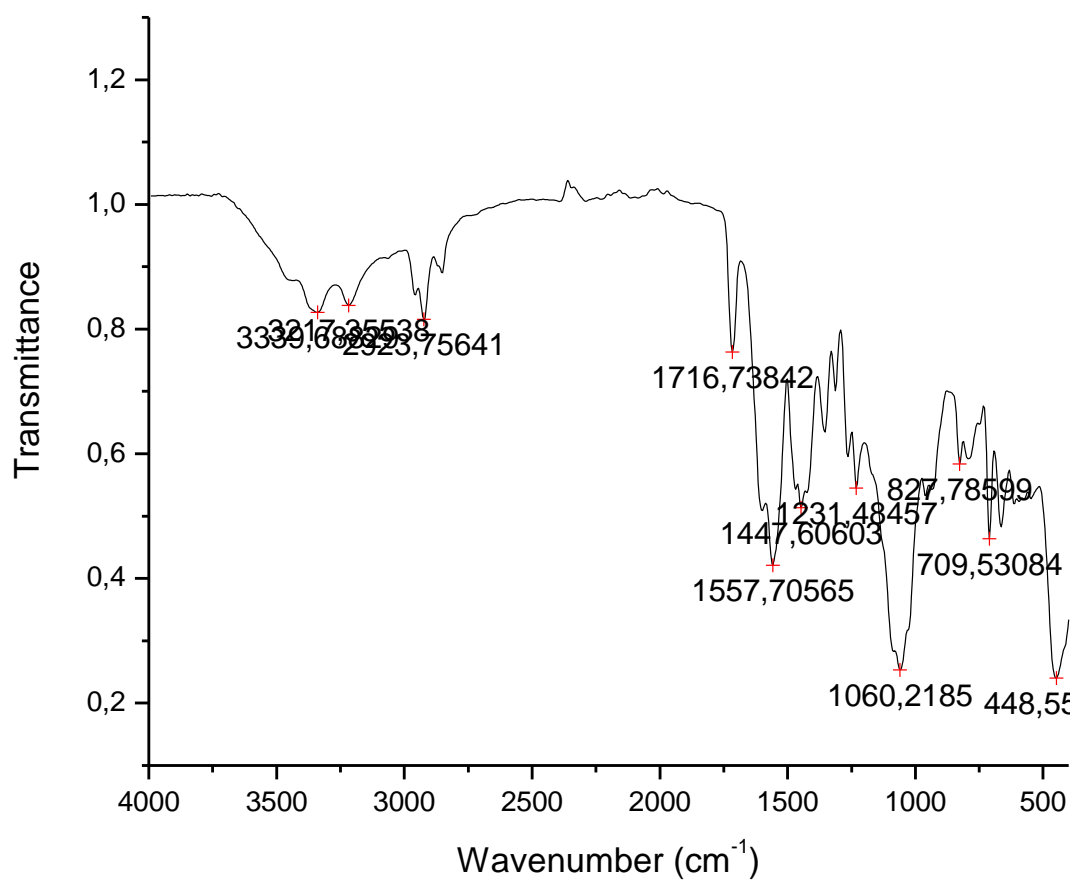


Figure 5.39: The FTIR spectrum of 1-(6-aminoquinoxalin-2-yl)hex-1-yn-3-yl benzoate **40**

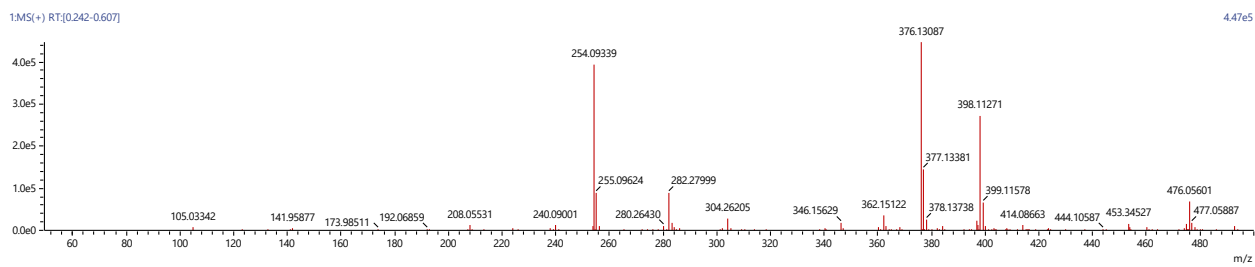


Figure 5.40: Mass spectrum of 1-(6-aminoquinoxalin-2-yl)hex-1-yn-3-yl benzoate **40**

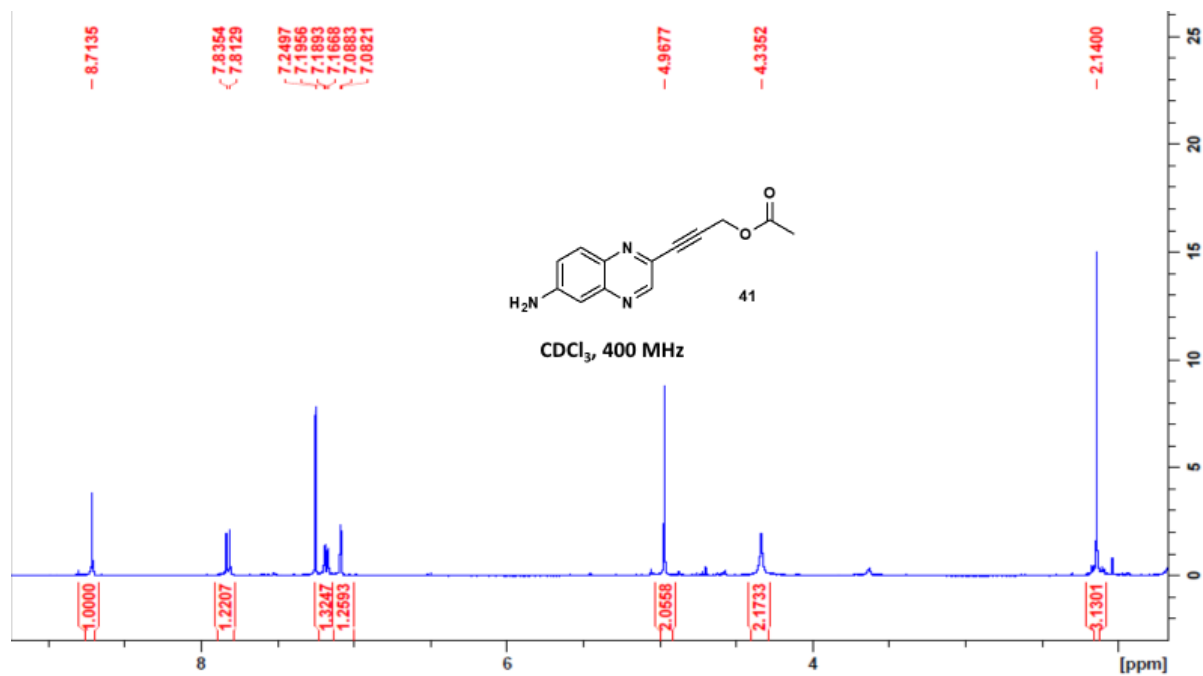


Figure 5.41: 1H NMR spectrum of 3-(6-aminoquinoxalin-2-yl)prop-2-ynyl acetate **41**

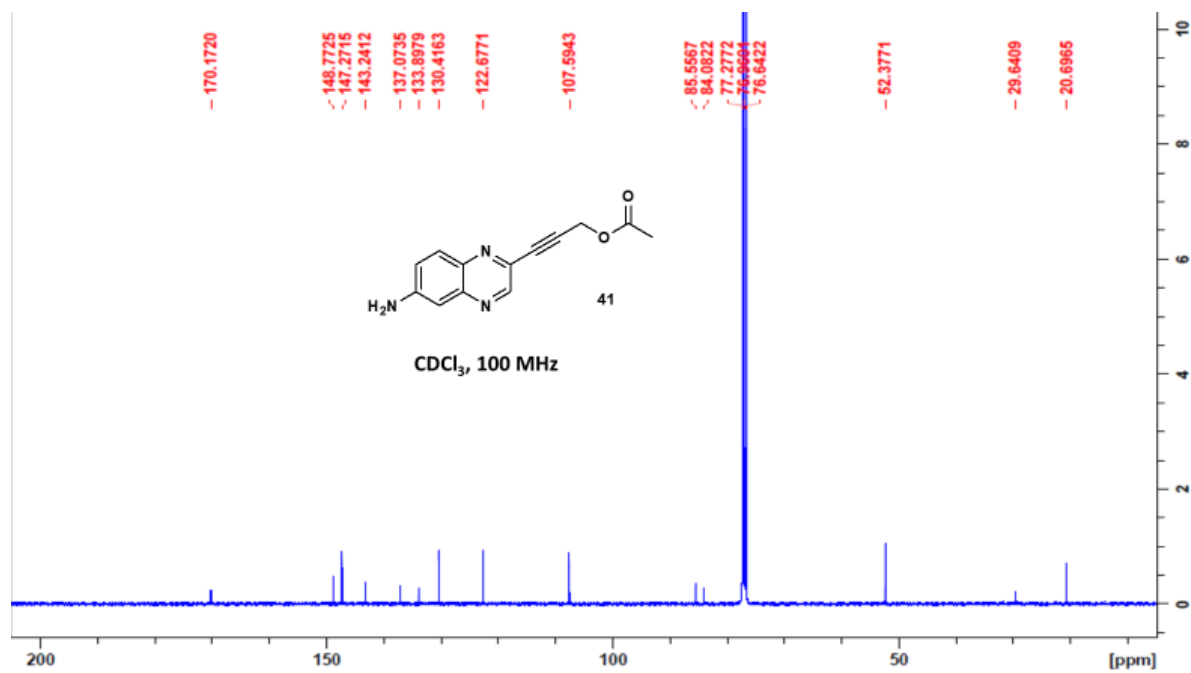


Figure 5.42: ^{13}C NMR spectrum of 3-(6-aminoquinoxalin-2-yl)prop-2-ynyl acetate **41**

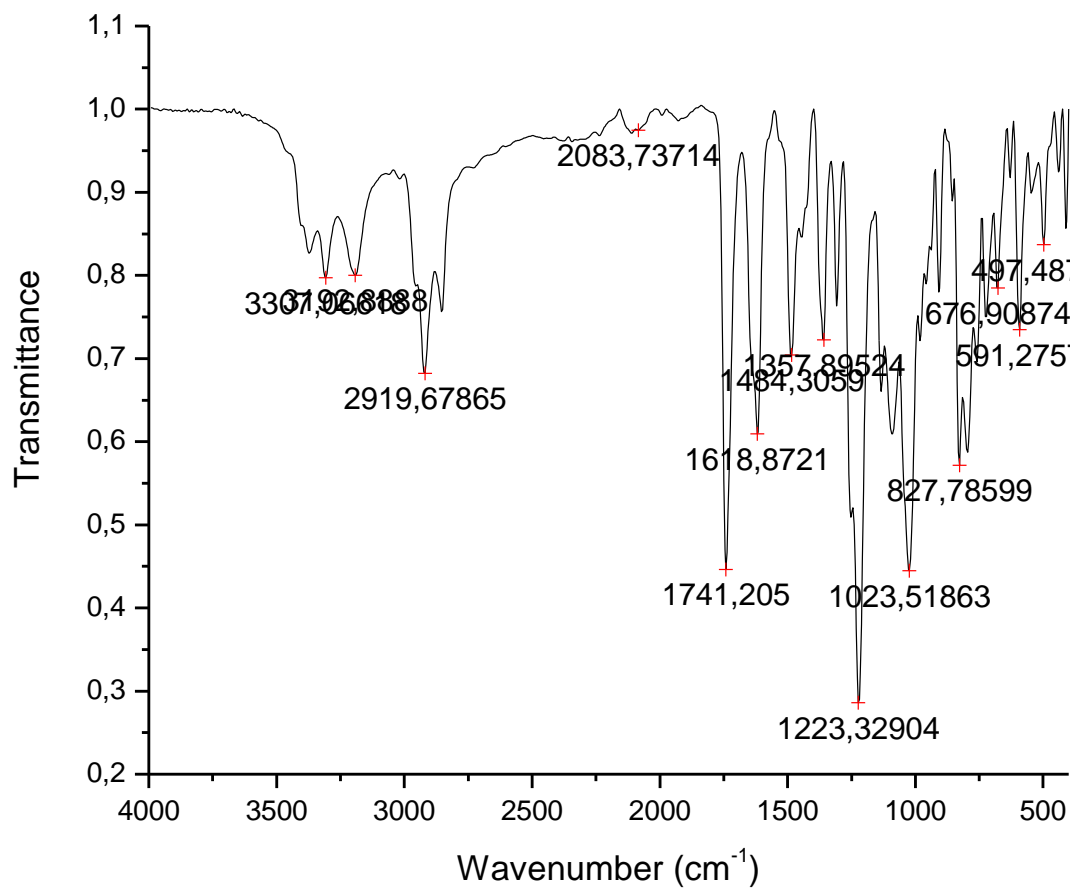


Figure 5.43: The FTIR spectrum of 3-(6-aminoquinoxalin-2-yl)prop-2-ynyl acetate **41**

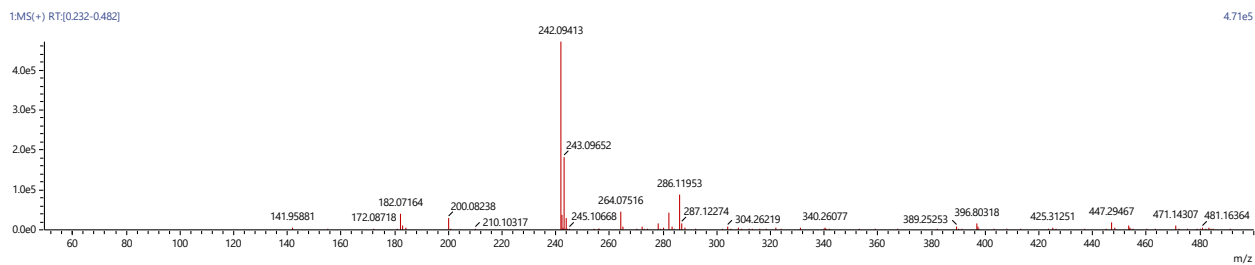


Figure 5.44: Mass spectrum of 3-(6-aminoquinoxalin-2-yl)prop-2-ynyl acetate **41**

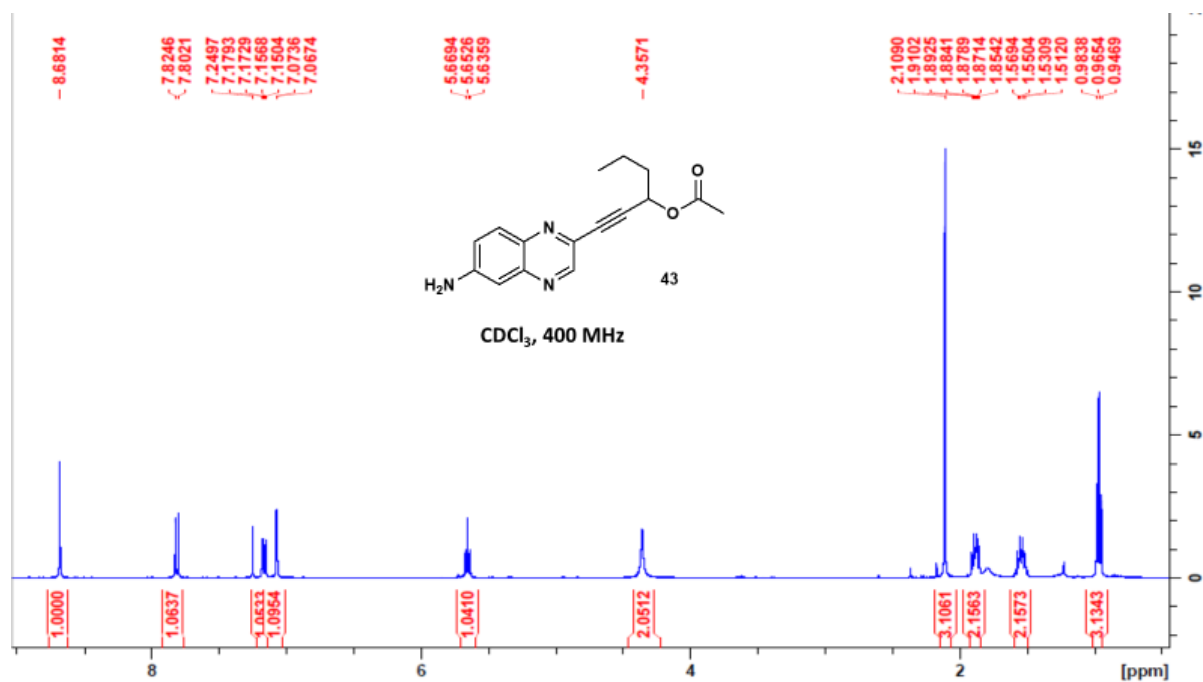


Figure 5.45: 1H NMR spectrum of 1-(6-aminoquinoxalin-2-yl)hex-1-yn-3-yl acetate **43**

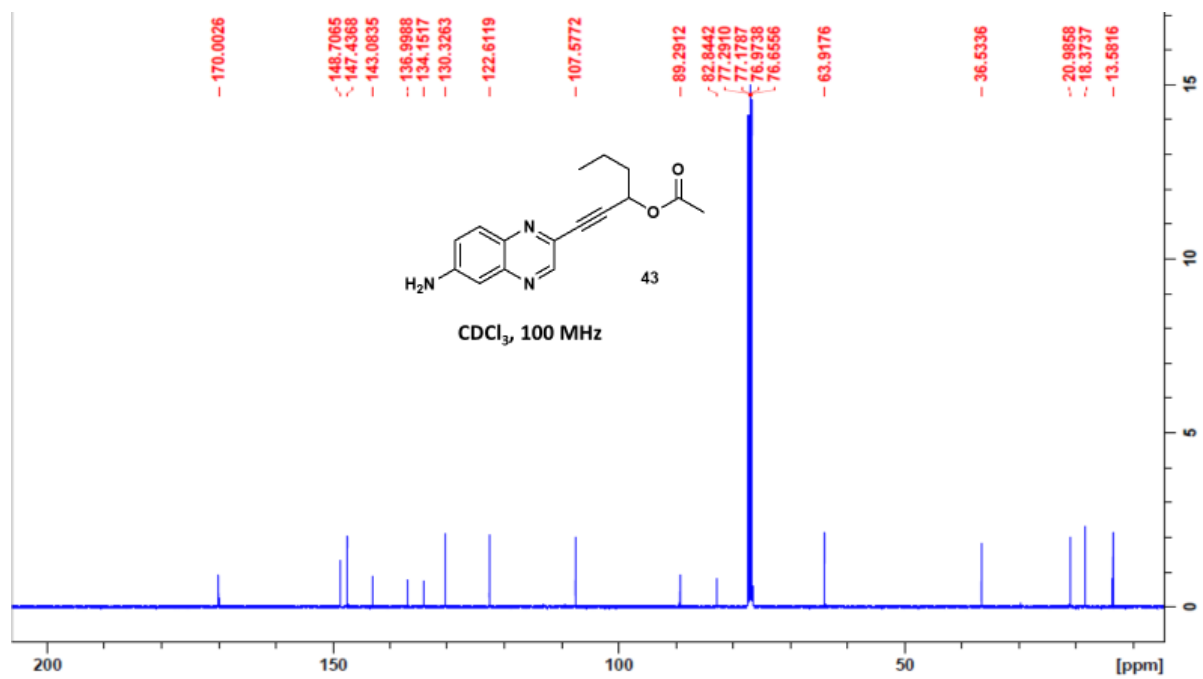


Figure 5.46: ^{13}C NMR spectrum of 1-(6-aminoquinoxalin-2-yl)hex-1-yn-3-yl acetate **43**

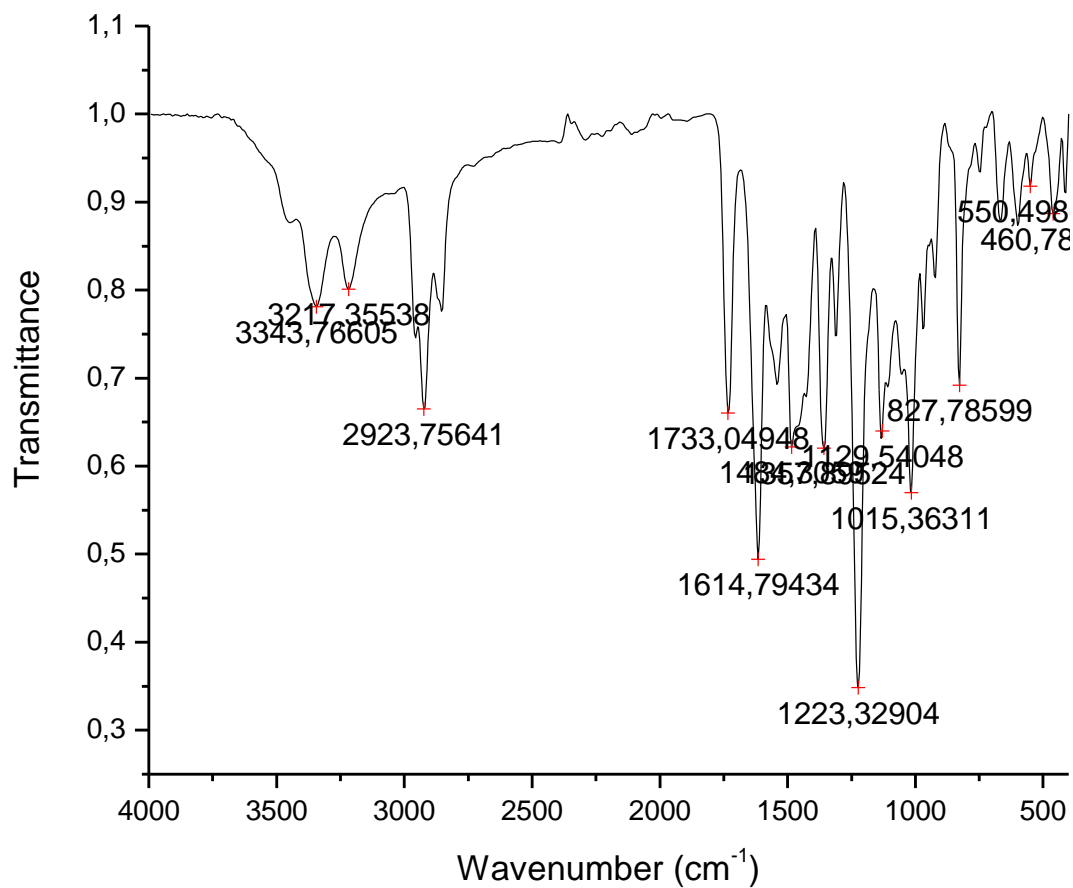


Figure 5.47: The FTIR spectrum of 1-(6-aminoquinoxalin-2-yl)hex-1-yn-3-yl acetate **43**

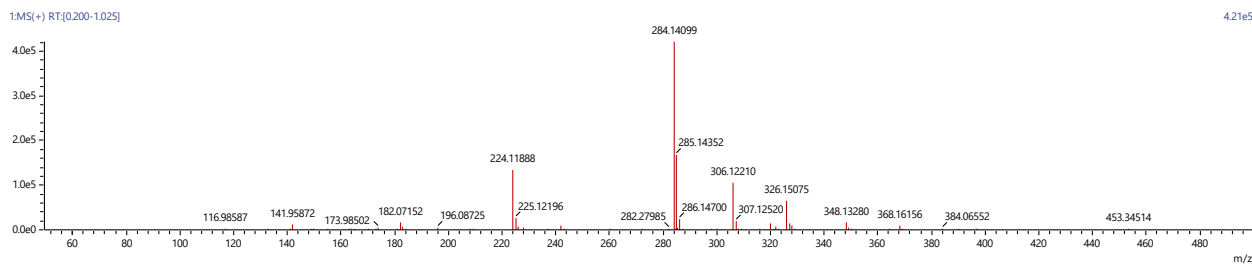


Figure 5.48: Mass spectrum of 1-(6-aminoquinoxalin-2-yl)hex-1-yn-3-yl acetate **43**

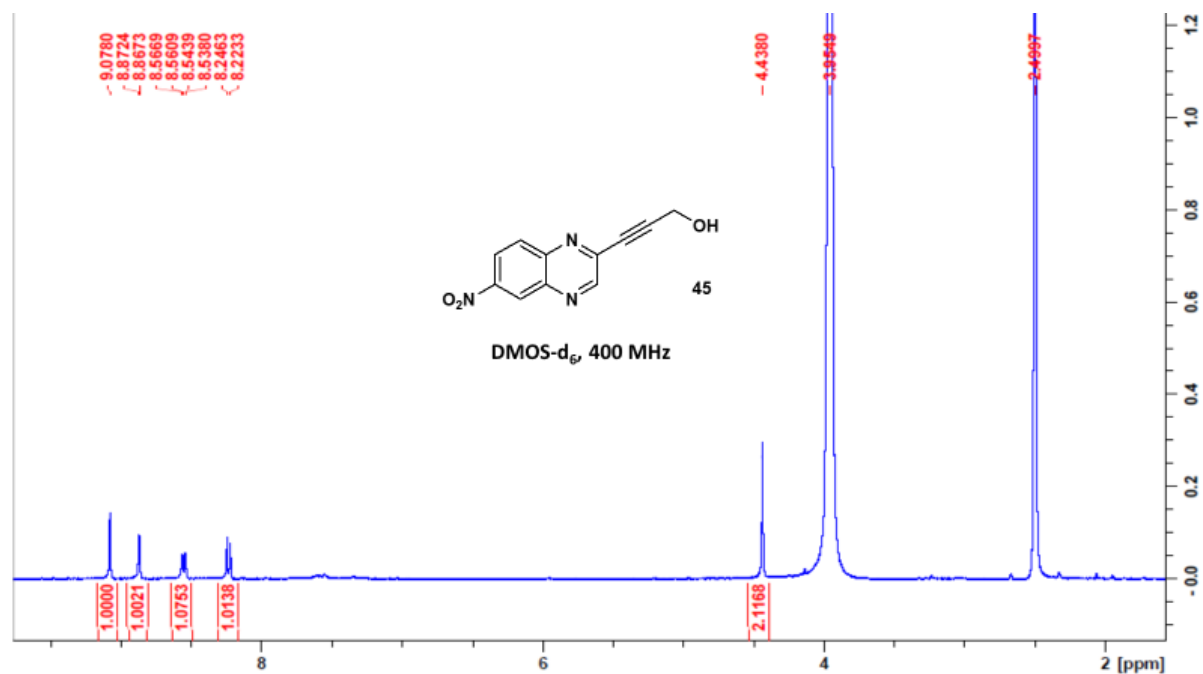


Figure 5.49: ¹H NMR spectrum of 3-(6-nitroquinoxalin-2-yl) prop-2-yn-1-ol **45**

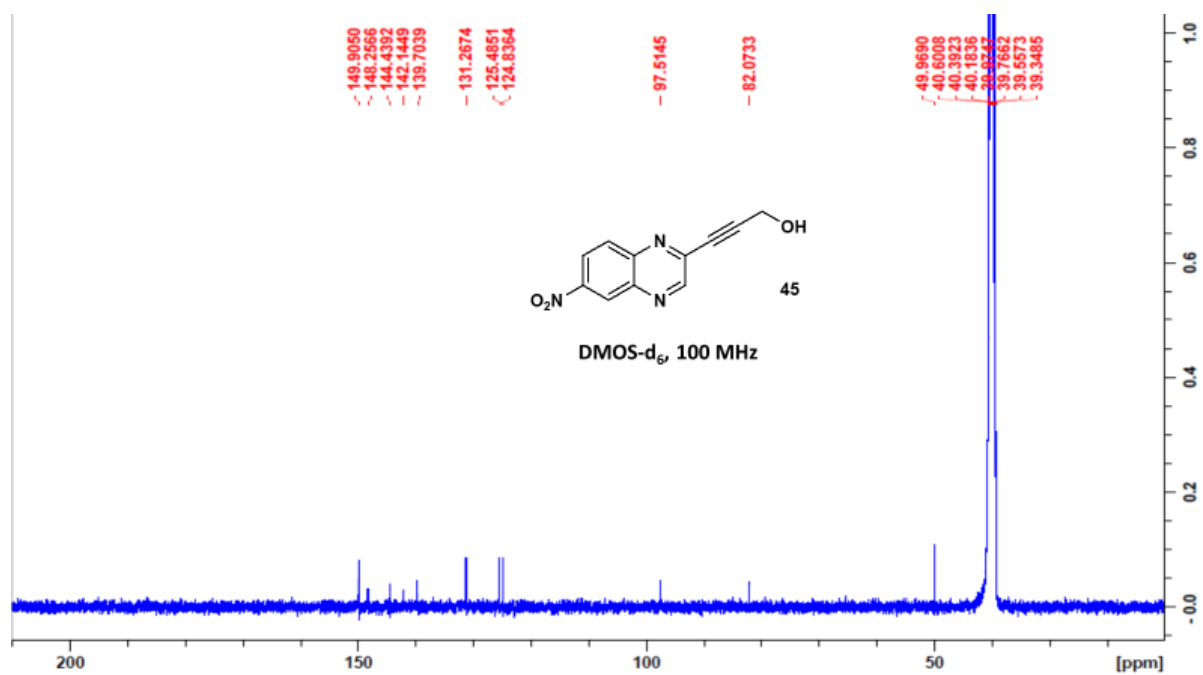


Figure 5.50: ¹³C NMR spectrum of 3-(6-nitroquinoxalin-2-yl) prop-2-yn-1-ol **45**

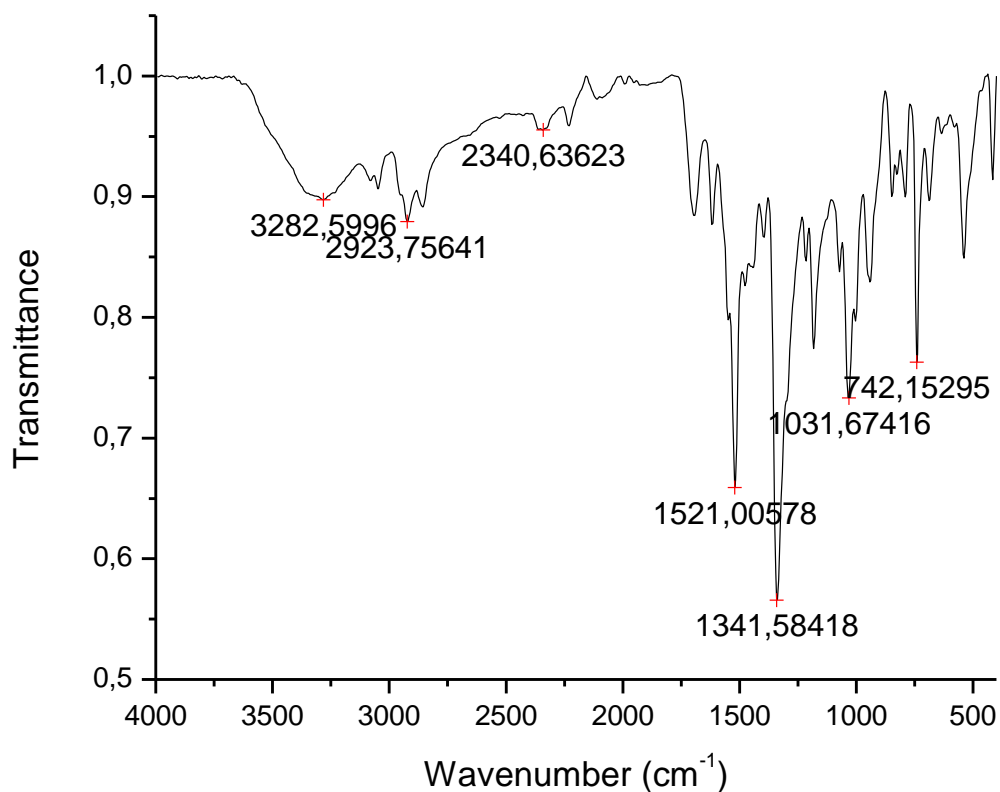


Figure 5.51: The FTIR spectrum of 3-(6-nitroquinoxalin-2-yl) prop-2-yl-1-ol **45**

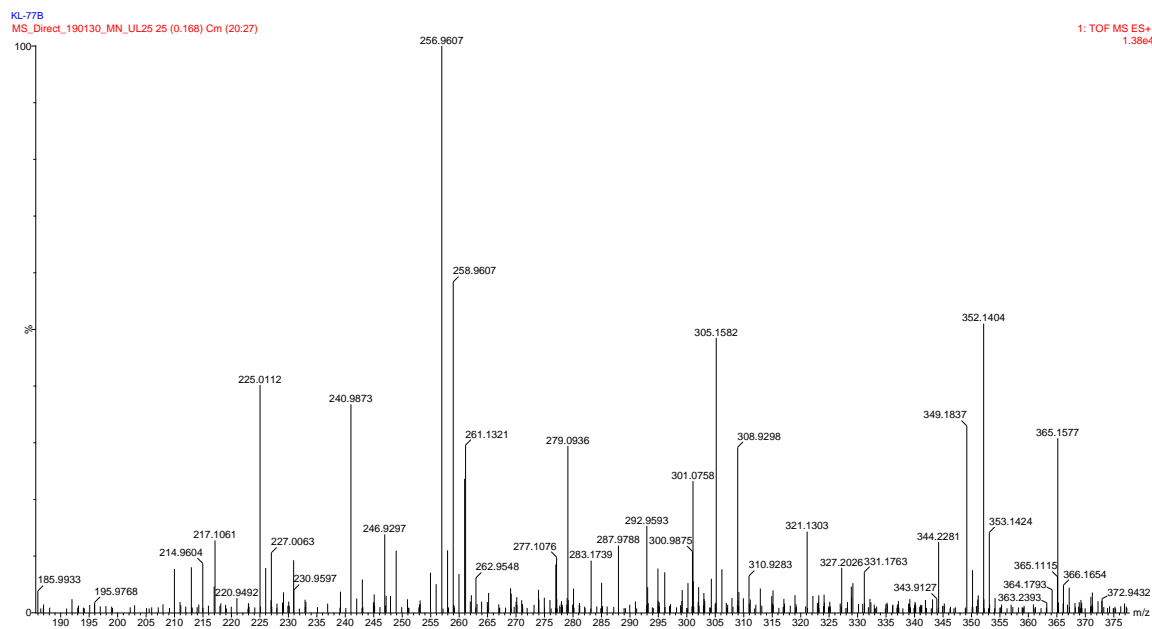


Figure 5.52: Mass spectrum of 3-(6-nitroquinoxalin-2-yl) prop-2-yl-1-ol **45**

Scientific contributions

Conference attended:

Oral presentation at:

10th Faculty of Sciences and Agriculture, University of Limpopo Research day

Date: 19-20 September 2019

Design and synthesis of quinoxaline derivatives for medicinal application against breast cancer cells

K Lekgau¹, TC Leboho¹, NJ Gumede² and W Nxumalo¹

¹ University of Limpopo, Department of Chemistry, Private Bag x1106, Sovenga, 0727

² Mangosuthu University of Technology, Department of Chemistry, PO Box 12363, Jacobs, 4026

E-mail address: u201401009@gmail.com

Breast cancer is a malignant tumour that starts in the cells of the breast. According to World Health Organisation (WHO), breast cancer is the second leading cause of death in women with 30% estimated new cases and 14% estimated death annually in female. Many studies revealed Aromatase as possible therapeutic targets regarding breast cancer treatment, because they play crucial roles in anti-apoptotic process during cell proliferation. Despite the advancement in development of chemotherapy agents, breast cancer remains the major challenge. Quinoxaline derivatives have attracted a great deal of attention due to their biological activities against fungi, virus, bacteria and cancer. Since the drug discovery process is expensive, time-consuming and involves

some risk, so visual screening technique (computer modelling) searches the library of molecules and identify those structures which are likely to bind to the drug target and several approved drugs such as Neuraminidase Inhibitors has heavily benefited from this technique. Visual screening was used to search a library of fifty alkyne-quinoxaline and six were identified to potentially inhibitors against aromatase, with the docking score ranging from -6,154 to -9,891 Kcal/mol representing the binding affinity. All six identified alkyne-quinoxaline were successfully and confirmed by NMR, FTIR and MS.

Keywords: Breast cancer, quinoxaline.

Frank Warren Conference 2019

7 – 11 July 2019

Student Lectures FW2019 Alpine Heath

SL06

Design and Synthesis of Quinoxaline Derivatives for Medicinal Application against Breast Cancer Cells

Karabo Lekgau¹, Tlabo C. Leboho¹, Njabulo J. Gumede², Winston Nxumalo¹

Department of Chemistry, University of Limpopo, Private Bag x1106, Sovenga, 0727, Polokwane, South Africa.¹; Department of Chemistry, Mangosuthu University of Technology, PO Box 12363, Jacobs, 4026, Kwa Zulu Natal, South Africa.²
*u201401009@gmail.com

Keywords: Breast cancer, CYP19A1, CDK2 and quinoxaline

Breast cancer is a malignant tumour that starts in the cells of the breast.¹ According to World Health Organisation (WHO), breast cancer is the second leading cause of death in women with 30% estimated new cases and 14% estimated death annually.² Many studies revealed Aromatase (CYP19A1) and Cyclin-dependent kinases (CDK2) as possible therapeutic targets regarding breast cancer treatment, because they play crucial roles in anti-apoptotic process during cell proliferation. Despite the advancement in development of chemotherapy agents, breast cancer remains the major challenge.^{3,4} Since the drug discovery process is complicated and time-consuming, Computer-aided drug design (CADD) offer an *in silico* (computer-based) approach which shortens time and expenses by predicting the activity of potential drug before synthesis and several approved drugs such as Neuraminidase Inhibitors and HIV protease inhibitors has heavily benefited from this technique.⁵ The computational technique, virtual screening work-flow was used to search a library of 100 amino- and nitro-quinoxaline with acetylene moiety in order to identify those structures which are likely to bind to the drug targets (CYP19A1 and CDK2), and it was found that 10 were likely to potentially inhibitors with the docking score ranging from -6,154 to -9,891 Kcal/mol representing the bonding affinity. The 10 identified compounds were successfully synthesised in the laboratory and confirmed by NMR, FTIR and MS.

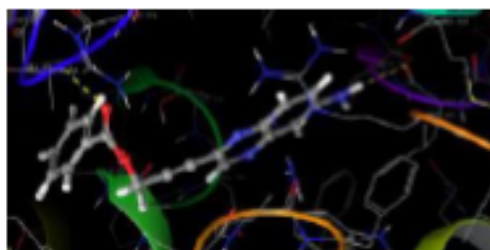


Figure 1. Docking model of compound 14

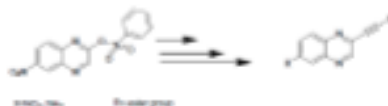


Figure 2. Typical reaction scheme

References:

1. De, A., Kuppasamy, G. and Kent, V. V. S. R. Antibody molecules for molecular imaging and targeted drug delivery in the management of breast cancer. *International Journal of Biological Macromolecules*, 107, 908–919 (2018).
2. Natal, C., Calcova, M., Prieto, M. and Tardón, A. Breast cancer incidence related with a population-based screening programme. *Medicina Clínica*, 144, 156–160 (2015).
3. Suvannang, N., Nantasenamat, C., Isarakura-na-ayudhya, C. and Prachayasittikul, V. Molecular Docking of Aromatase Inhibitors. *Molecules*, 16, 3597–3617 (2011).
4. Whitaker, S. R., Mellinger, A., Workman, P. and Clarke, P. A. Inhibitors of cyclin-dependent kinases as cancer therapeutics. *Pharmacology & Therapeutics Journal*, 173, 83–105 (2017).
5. Siedt, P. and Caffisch, A. Protein structure-based drug design: from docking to molecular dynamics. *Current Opinion in Structural Biology*, 48, 93–102 (2018).

46

Poster presentation at:

SACI Young chemists Symposium 2019

31st October 2019

Design and synthesis of quinoxaline derivatives for medicinal application against breast cancer cells

Karabo Lekgare^a, Njabulo J. Gumede^b, Tlabo C. Leboho^a, Winston Nxumalo^a

^aUniversity of Limpopo, Department of Chemistry, Private Bag #1106, Sovenga, 0727

e-mail: 021401201@unilim.ac.za

^bMangosuthu University of Technology, Department of Chemistry, PO Box 12363, Jacobs, 4026

Keywords: Breast cancer, quinoxaline

Breast cancer is a malignant tumour that starts in the cells of the breast. According to many studies revealed Aromatase as possible therapeutic targets regarding breast cancer treatment, because they play crucial roles in anti-apoptotic process during cell proliferation. Despite the advancement in development of chemotherapy agents, breast cancer remains the major challenge. Quinoxaline derivatives have attracted a great deal of attention due to their biological activities against fungi, virus, bacteria and cancer. Since the drug discovery process is expensive and time-consuming, so visual screening technique (computer modelling) searches the library of molecules and identify those structures which are likely to bind to the drug target and several approved drugs such as Neuraminidase Inhibitors. Visual screening was used to search a library of fifty nitro and amino quinoxaline alkyne and five were identified to be potentially inhibitors against aromatase, with the docking score ranging from -5.154 to -9.891 Kcal/mol representing the binding affinity. All five identified alkyne-quinoxaline were successfully synthesised and confirmed by NMR, FTIR and MS.

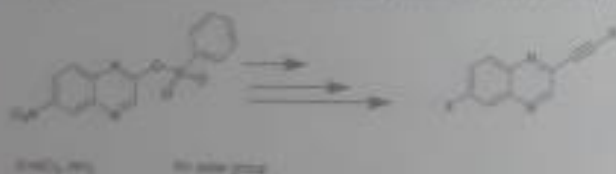


Figure 1 Typical reaction scheme

References:

1. Natal, C., Ceceyya, M., Prieta, M. and Tardón, A. Breast cancer incidence related with a population-based screening programme. *Medicina Clinica*, 2015, 144, 156-160.
2. Sovannang, N., Nantasenamat, C., Isarankura-na-ayudhya, C. and Pachayasittikul, V. Molecular Docking of Aromatase Inhibitors. *Molecules*, 2011, 16, 3597-3617.

Publication: Synthesis of novel quinoxaline-alkynyl derivatives and their anti-*Mycobacterium tuberculosis* activity.

Bioorg. Med. Chem. Lett. 35 (2021) 127784



Contents lists available at ScienceDirect

Bioorganic & Medicinal Chemistry Letters

journal homepage: www.elsevier.com/locate/bmcl



Synthesis of novel quinoxaline-alkynyl derivatives and their anti-*Mycobacterium tuberculosis* activity

Lerato A. Raphoko^a, Karabo Lekgau^a, Charity M. Lebepe^a, Tlabo C. Leboho^a,
Thabe M. Matsebalela^b, Winston Nxumalo^{a,*}

^a Department of Chemistry, Faculty of Science and Agriculture, University of Limpopo, Private Bag X1106, Sovenga 0727, South Africa

^b Department of Biochemistry, Microbiology and Biotechnology, Faculty of Science and Agriculture, University of Limpopo, Private Bag X1106, Sovenga 0727, South Africa

ARTICLE INFO

Keywords:
Mycobacterium tuberculosis
Quinoxaline-alkynyl derivatives
Sonogashira coupling
Esterification

ABSTRACT

The study report on the synthesis of a series of novel quinoxaline-alkynyl derivatives that were evaluated for their activity against *Mycobacterium tuberculosis* (*Mtb*) H37Rv strain. A total of 19 compounds bearing an alcohol, aldehyde, mesylate and ester groups on the alkynyl group, and also containing a chloro and nitro groups at the 6-position, were prepared. Seven compounds (3e, 4a-b, 5a, 5c, 6c and 6i), were found to have MIC₅₀ < 10 μM, while five compounds (3b, 6a, 6b, 6d and 6h) had MIC₅₀ in the range 10–20 μM. Compounds bearing a nitro substituent in the 6-position were generally more active and demonstrated a better safety profile, when compared to the unsubstituted and 6-chloro derivatives. Of the seven most active compounds, four contained nitro group at the 6-position.